POLITECNICO DI MILANO
Scuola di Ingegneria Industriale e dell'Informazione
Corso di Laurea Magistrale in Ingegneria Elettrica

Sequentially controlled two level inverters of multi-modular permanent magnet machines for wind energy systems

Supervisor: Prof. Roberto Perini

Tesi di Laurea Magistrale di:

Khaled ElShawarby, matricola 822525

Academic year 2015-2016


POLITECNICO
MILANO

Acknowledgment

I can't begin to express my sincerest appreciation to my advisor Professor Roberto Perini for his continuous support for my MSc study and research, for his patience, motivation, enthusiasm and immense knowledge. His care even extended more than the academic supervision.

Professor Perini, who was always a source of passion and motivation towards the work. He always pushed to me work better and harder. Whenever I needed any help, I would always find professor Perini helping me. I can't even begin to describe how much help and time he has given me.

I would also like to thank Professor Di Gerlando, who always offered the valuable insight to our work. His experience and knowledge were something to look up to.

I can say and without exaggeration that any student should consider himself lucky to work under the supervision of one of these professors. I count myself more than lucky to work with both professors, it has been an honor working with both of you. I know that for sure I had a guardian angel watching over me.

Thank you Professors.

I would like to thank Professor Marco Mauri for his assistance in the Simulink work.

I would like to express my gratitude to Politecnico Di Milano for financing my master degree and for giving me the opportunity to have this experience. I will never forget these two years.

To my parents, my guardian angels, I owe them everything. They supported me since I was a little boy, always by my side, encouraging me to do better and being two amazing role models to follow. They always offered guidance, advice and unconditioned love. Words are not enough to say how much they have done to me throughout the years.

Also, I have to express my gratitude to my brother who was always there for me, a true backbone to me. I am also grateful for having a lot friends whom I have known since forever. To me, they are more than my friends they are my brothers.


POLITECNICO
MILANO

Contents


POLITECNICO
MILANO

List of Figures

List of Tables

Abstract

Lower harmonic content is sometimes the attractive feature of some control systems. High power Axial flux Permanent Magnet Synchronous Generators for wind applications are often multi modular. Such system are often driven by a multilevel inverter due to its lower harmonic distortion compared to two level inverter. However a two level inverter has the advantage of a much simpler control system and lower cost. This thesis presents a particular system, each module of the machine is connected to a two level inverter; the inverters are paralleled on the dc side. The carrier signal of each inverter is shifted from its neighbouring inverter with an angle. The angles necessary are selected such to cancel out the least harmonic components in the dc side current. There are two types of modulation considered: square wave and pulse width modulation. We analysed the dc side current mathematically for both types of modulation; finding the full expression of the dc current ripple and finding the necessary angles to reduce the current ripple.

We have proven the effectiveness of the sequential control of the two level inverters in decreasing the dc current ripple through checking the mathematical calculations with some simulations. Decreasing the current ripple subsequently decrease the torque ripple of the shaft.

In chapter two gives a brief about wind energy systems and the illustration of the axial flux permanent magnet machine. In chapter three focuses on the most common topologies for multilevel inverters and a comparison between the multilevel inverter and the two level inverter. In chapter four presents the mathematical model for the dc current ripple and the verification of the equation on Matlab/Simulink. Finally chapter five includes the implementation of the control on the machine model on Simulink and a comparison between Simulink results and the mathematical results. Also includes the effect of changing some control parameters on the ripple components of both current and torque.

Chapter 1: Introduction

Wind systems comprise generally a wind turbine, which is installed on top of a tall tower, collects kinetic energy from the wind and converts it to electricity. The most important advantages of the wind systems are:

• They use clean and free energy

• They require no connection to an existing power source or fuel supply

• They could be combined with other power sources to increase system reliability

• They consume no fossil fuels

• They could be installed and upgraded as a wind form, more wind turbine could be added as power demand increases

The power price has considerably decreased since the last decade. This leads to a large-scale application of wind systems in several promising areas. Compared with conventional fossil energy sources, small wind energy systems are the best option for many isolated or rural areas applications around the world.

1.1 Aims of the Thesis

Many papers and researches have illustrated the attractive feature of multilevel inverters over the two level inverters. Basically they have better harmonic spectrum and lower THD than the conventional two level inverters despite the fact that they are more expensive and their control is complicated and need more switches than the 2 level inverters.

The main objective of the thesis is to introduce the so called “sequential control of the inverters”: we shift the carrier signals of different modules inverters in order to achieve a better harmonic spectrum as some harmonic components would cancel each other. And by achieving a better harmonic profile, the cost of the overall control system would eventually decrease by using 2 level inverters instead multilevel ones.

1.2 How the Book is organized?

The book is organized through five chapters as follows:

• Chapter 2 gives a brief about wind energy systems and components of such systems. Moreover it provides a comparison between geared and direct drive systems with detailed common structures of the direct drive machines, specifically the illustration of the axial flux permanent magnet machine because the case study used for thesis topic is an axial flux one

• Chapter 3 focuses on power electronics modeling and specifically the DC/AC inverters. Some brief explanation for the pulse width modulation PWM techniques applied to a three phase full bridge voltage source inverter is given. Moreover it exploits the most common topologies of the multilevel inverters with their advantages and disadvantages and at the end of the chapter a short comparison between the multilevel inverters and the conventional two level inverters.

• Chapter 4 presents the approach to find the function of the dc current ripple on the capacitor side of the 2 level inverter as a function of time in order to understand the nature of the harmonics in the dc side and to select the correct angles to exploit the sequential control of the inverters. Also includes the verification of the mathematical equation derived on Matlab/Simulink including the design of a PWM model.

• Chapter 5 includes the mathematical model for the permanent magnet machine and also presents our model of the machine on Matlab/Simulink and how to add modules to the machine in order to model a multimodular permanent magnet machine on Matlab. It also includes the PI controllers' design of both the current and speed loops with the methodology of the choice of the proportional and integral constants of the controller. Moreover, the simulation results of the actual drive system for the PMSG simulated on Matlab/Simulink which presents the single module machine, the two modules machine and the three modules machine with a comparison between their Total harmonic distortions. Also presents a comparison between the mathematical approach results and the Simulink results. Finally we show the effect of some control parameters change on the current and torque ripple components.

Chapter 2: Wind Energy Harvesting

Wind is a sustainable energy source since it is renewable, widely distributed, and plentiful. In addition, it contributes to reducing the greenhouse gas emissions since it can be used as an alternative to fossil-fuel-based power generation .Wind turbines capture the kinetic energy of winds and convert it into a usable form of energy.

Even though wind turbines currently provide only 1% of the worldwide power supply, wind energy is one of the fastest growing renewable energy technologies all over the world. In countries such as Denmark, Spain, Portugal, and Germany, wind power accounts for approximately 19%, 9%, 9%, and 6% of the required electric power, respectively. From 2000 to 2007, the global wind power generation increased to approximately five times of its previously recorded capacity.[1]

The kinetic energy of the wind can be expressed as [1]

$$E_k = \frac{1}{2}mv^2 = \frac{1}{2}\rho V v^2 = \frac{1}{2}\rho A d v^2 = \frac{1}{2}\rho R^2 \pi d v^2,$$

Where E_k is the wind kinetic energy, m is the wind mass, v is the wind speed, ρ is the air density, A is the rotor area, R is the blade length, and d is the thickness of the "air disc" shown in Figure 2-1.[1]

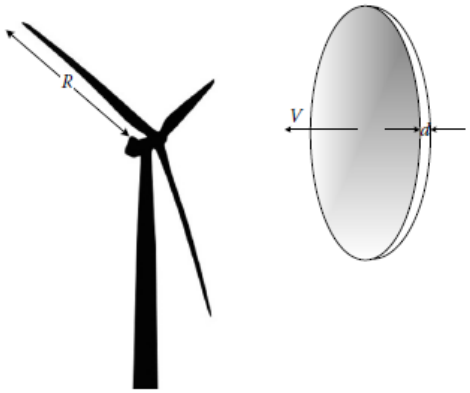

Figure 2-1: Kinetic Energy of the wind

Hence, the overall power of wind (P) is [1]

$$P = \frac{E_k}{t} = \frac{1}{2}\rho R^2 \pi \frac{d}{t} v^2 = \frac{1}{2}\rho R^2 \pi v^3,$$

$$P = \frac{1}{2}\rho R^2 \pi v^3. \qquad [2-1]$$

From [2-1], the power content of the wind varies with the cube (the third power) of the average wind speed (Figure 2-2) [1].

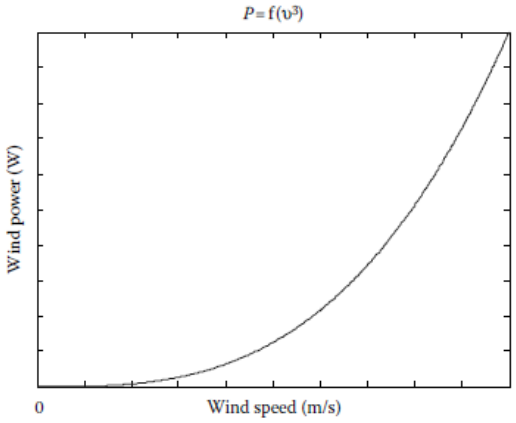

Figure 2-2: Specific wind power due to wind speed variation

Wind speed is one of the most important parameters in determining the available wind power. Therefore, it is important to accurately monitor and measure it.

2.1 Betz Law

Betz's law demonstrates the theoretical maximum power that can be extracted from the wind. The wind turbine extracts energy from the kinetic energy of the wind. Higher wind speeds result in higher extracted energy. It should be noted that the wind speed after passing through the turbine is much lower than before reaching the turbine (before energy is extracted). This means that there are two wind speeds: one before the wind approaches (in front of) the turbine and the other after (behind) the turbine. Figure 2-3 shows both speeds of the wind; after the turbine, the wind has a decreased speed.

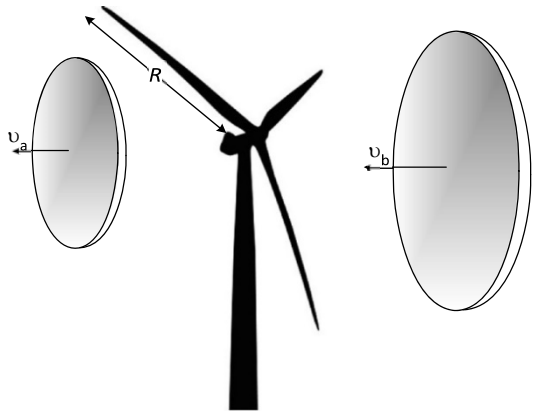

Figure 2-3 Wind speed before and after the turbine

The decreased wind speed, after the turbine, provides information on the amount of possible extracted energy from the wind. The extracted power from the wind can be calculated using equation [2-2]. [1]

$$P_{\text{extract}} = \frac{E_k}{t} = \frac{1}{2}\rho R^2 \pi \frac{d}{t}(v_b^2 - v_a^2) = \frac{1}{2}\rho R^2 \pi \frac{v_a + v_b}{2}(v_b^2 - v_a^2), \qquad [2-2]$$

Where P_{extract} is the maximum extracted power from the wind, v_a and v_b are wind speeds after and before passing through the turbine, ρ is the air density, and R is the radius of the blades.

According to [1] P_{extract} reaches its maximum value for (v_a/v_b) = 1/3.

$$\left.\frac{P_{\text{extract}}}{P_{\text{total}}}\right|_{\frac{v_a}{v_b}=\frac{1}{3}} \approx 59.3\%.$$

This equation shows that the maximum extracted power from the wind is 59.3% of the total available power. In other words, it is not possible to extract all 100% of wind energy since the wind speed after the turbine cannot be 0. The effect of v_a/v_b ratio on the $P_{\text{extract}}/P_{\text{total}}$ is shown in Figure 2-5. The maximum extracted power is approximately 2/3 of total wind power.

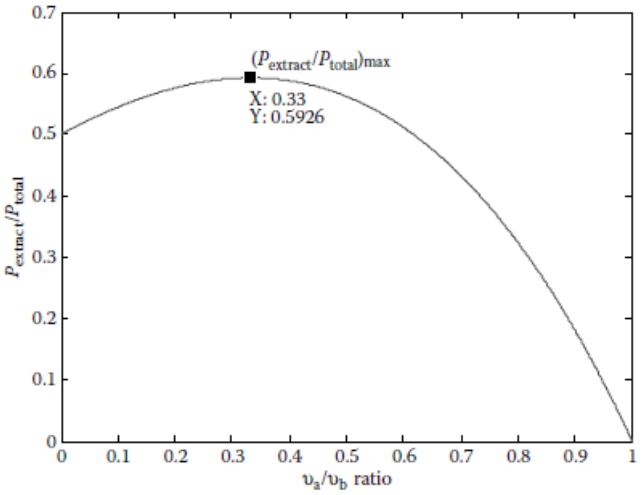

Figure 2-4: Maximum theoretical extracted power from wind

Betz's law indicates that the maximum theoretical extracted wind power is 59%.However, in practice, the real efficiency of the wind turbine is slightly different.

2.2 Wind Turbine Systems

Basically, a wind turbine consists of three main parts: a turbine, a nacelle, and a tower. The wind turbine presented in [1] demonstrates some other parts inside the tower and nacelle.

2.2.1: The Tower

The main purpose of the tower is to support the nacelle and resist vibration due to the wind speed variations. The cables that connect the generator (on top of the tower, inside the nacelle) and transmission line (down, in the basement of the tower) are inside the tower. The tower is the main component that carries most of the other components such as the turbine, nacelle, blades, generator, and so on.

2.2.2: Yaw Mechanism

The yaw mechanism is composed of the yaw motor and the yaw drive. The "yaw" mechanism turns the whole nacelle toward the wind direction in order to face the wind directly. Regardless of the direction of the wind, the yaw mechanism can help the turbine face the wind by changing the direction of the nacelle and the blades.

2.2.3: The Nacelle

The gearbox, generator, and the control electronics are all located inside of the nacelle. The nacelle is connected to the tower through the yaw mechanism. Inside the nacelle, two shafts connect the rotor of the turbine to the rotor of the electrical generator through the gearbox. The gearbox is the mechanical energy converter that connects the low-speed shaft of the turbine to the high-speed shaft of the electrical machine.

The electrical generator is the main part of the nacelle. It is the heaviest part and produces electrical energy, which is transferred through the cables to the grid. There are different types of generators that are used for wind turbines, and depending on the type of generator, wind turbines can operate with either fixed or variable speeds. Fixed speed (FS) turbines use synchronous machines, and operate at an FS that depends on the grid's frequency. These machines are not the best solution for the wind turbines, because the wind always changes its speed. Variable speed turbines use DC machines, brushless DC (BLDC) machines, and induction machines. DC machines are not commonly used due to the maintenance problems with the brushes. Induction and BLDC machines are more suitable for wind applications

2.2.4: The Turbine

The turbine, also called "low-speed rotor," usually has two to six blades. The most common number of blades is three since they can be positioned symmetrically, maintain the system's lightness, and ensure the stability of the wind power system (WPS). The radius of the blades is directly proportional to the amount of captured energy from the wind; hence an increased blade radius would result in a higher amount of captured energy. The blades can rotate around their longitudinal axis to control the amount of captured wind energy. This is called "pitch control." If the wind speed increases, the pitch control can be used to change the effective blade surface, hence keeping the turbine power constant. The pitch angle control is usually used for wind speeds above the nominal speed.

2.2.5: Permanent Magnet Synchronous Machines

Figure 2-5 shows a PMSG where the PWM rectifier is placed between the generator and the DC link, and the PWM inverter is connected to the utility. In this case, the back-to back converter can be used as the interface between the grid and the stator windings of the PMSG [1]. The turbine can be operated at its maximum efficiency and the variable speed operation of the PMSG can be controlled by using a power converter that is able to handle the maximum power flow.

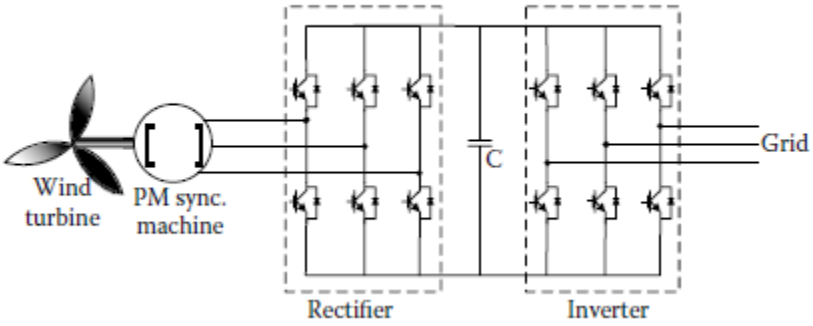

Figure 2-5: Basic Wind Turbine system

The main advantages of PM excitation in comparison with electrical excitation are lower losses (no excitation losses) and lower weight (roughly a factor of 2 in active generator material), which results in lower cost. The disadvantage is that the excitation is not controllable. Usually, PM machines are designed as radial flux machines. Therefore, magnets are magnetized in a radial axis, but there are some examples of PM machines of different designs such as axial flux and transverse flux generators [1].

Axial flux generators (where flux is positioned along the axial axis) are smaller, but heavier and more expensive than radial flux machines [1]. This is mainly due to the fact that in axial flux machines, the force intensity is not optimal for all radii, and the radius where the force works is not maximum everywhere.

2.3 Comparison of Direct – Drive and Geared Generator Systems

Different direct-drive and geared generator systems of the wind turbines have been discussed by a number of authors.

According to the comparison of different direct-drive and geared generator systems discussed in literature [2] [3], the features of the systems can be summarized as the following.

Considering the energy yield and reliability, the direct drive generator systems seem to be more powerful. The comparisons of different generator systems for wind turbines can be summarized as the following. The direct-drive generator system, especially direct-drive permanent magnet generator system, is superior in terms of the energy yield, reliability, and maintenance problem. The geared generator system has the advantages in terms of the cost, size, and weight. The geared drive system has been mostly used on the market of wind turbines, even though the direct-drive system is superior in performance. According to the review of different generator systems in literature and on the market, it can be expected that the direct-drive PM generator system with both light construction and low cost could be the most suitable system. Consequently that generator system could be defined as the most suitable generator concept with the maximum energy yield and the minimum cost.

Compared to geared drive systems: [2]

- The permanent magnet synchronous generator with one stage gearbox has the highest ratio of the annual energy yield to cost.
- The direct-drive permanent magnet synchronous generator system (PMSG DD) is superior compared to other systems in terms of losses and energy yield.
- The doubly-fed induction generator system with three stage gearbox (DFIG 3G) seems lightweight and low cost solution.
- Different generator systems can be arranged in the order of high cost as direct-drive electrically generator system can be the most suitable generator concept, because the energy yield of this system is the maximum. Therefore reducing the cost of direct-drive generator systems will be the most important issue in both the electromagnetic design and the mechanical design.

The necessity of new wind power system comes from recent studies which have shown that gearboxes are responsible for the greatest percentage of outage time

Wind turbine manufacturers are turning away from the industry-standard gearboxes and generators in a bid to boost the reliability and reduce the cost of wind power.

In conventional wind turbines, the gearbox increases the speed of the wind-driven rotor several hundred fold, which radically reduces the size of the generator required. In the direct-drive generator for wind turbine, the rotor is directly connected to the rotor hub. Direct-drive generators operate at the same speed as the turbine's blades and must therefore be much bigger.

Even for a large direct-drive generator, with a diameter of several meters, the air-gap should not exceed a few millimeters, to avoid excessive magnetization requirements. This means that the

mechanical construction has to be very rigid, in order to maintain the air-gap against the powerful force of attraction between the rotor and the stator. This stiffness requirement applies to the load path through the rotor, the shaft, the bearings and the stator. Thus the stiffness places a practical and economical limit on the diameter of a conventionally built generator.

Because of that, the direct-drive concept is operated in low speed. When scaling up the wind turbine, the rotational speed is decreased more and more considering the tip speed limitation. In order to scale up the power of the direct-drive generator, the torque T, must be thus increased in inverse proportion to the decrease of the mechanical angular speed ω_m by [2]

$$P = T \cdot \omega_m$$

The generator power P can be also defined as a function of the tangential force density, F_d, the air gap diameter, D_g, the axial length l_s and the mechanical angular speed ω_m as shown in [2]

$$P = \frac{\pi}{2} F_d \cdot D_g^2 \cdot l_s \cdot \omega_m$$

Direct-drive generator has a larger diameter to produce higher torque because the torque is proportional to the air gap diameter squared. Thus higher torque demands large air gap diameter of the generator and high tangential force. This results in the increase of materials to maintain the air gap in proper deflection against the normal stress between the rotor and stator. Therefore the concept of direct-drive generator is operated in low speed and has the disadvantages such as high large diameter, heavy mass, torque rating and high cost compared to the concept of geared generator. That is why the concept of direct-drive generator is designed with a large diameter and small pole pitch to increase the efficiency, to reduce the active material and to keep the end winding losses small.

Direct-drive permanent magnet machines have several advantages compared to the electrically excited machines. They can be listed as:

- Higher power to weight ratio
- Improvement in the efficiency
- High energy yield and light weight
- No additional power supply for the field excitation,
- Higher reliability without slip rings

Because of those advantages, permanent magnet machines are considered as the promising electromagnetic structure for direct-drive generator.

2.4 Electromagnetic Structures for Direct drive

The PM machines can be classified by both the direction of flux path and the structure as the following.

- The longitudinal and the transverse flux machine (TFPM)
- The radial (RFPM) and the axial flux machine (AFPM)
- The slotted and the slotless machine
- The surface mounted and the flux concentrating machine

2.4.1: Radial-flux PM machines

RFPM synchronous machines are the most conventional PM machines. Figure 2-6 shows two views of a RFPM machine with the direction of the flux and current. The flux flows radially through the air gap of the machine while the current circulates in the axial direction.

RFPM machines are the easiest and cheapest to manufacture among the PM ma- chines. However, they are much larger than the axial-flux and transverse-flux machines in terms of active weight and axial length [2]. Different rotor configurations of RFPM machines are shown in Figure 2-7.

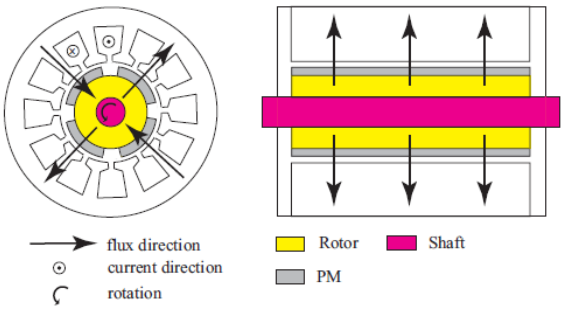

Figure 2-6: RFPM machine with flux and current directions

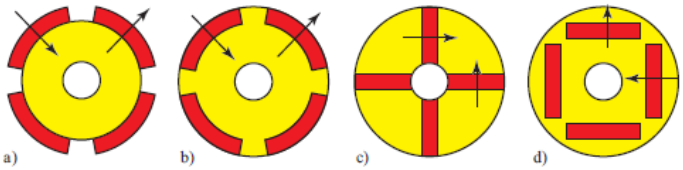

Figure 2-7: Rotor Configurations: (a) Surface mounted PM; (b) Inset PM; (c) tangentially-magnetized buried PM; (d) Radially magnetized buried PM

2.4.2: Axial-flux PM machines

AFPM machines feature a large diameter and a relatively short axial length compared to RFPM machines. As suggested by its name and Figure 2-8, the flux flows axially through the air gap while the current flows in the radial direction. It will be explained in depth in 2.5.

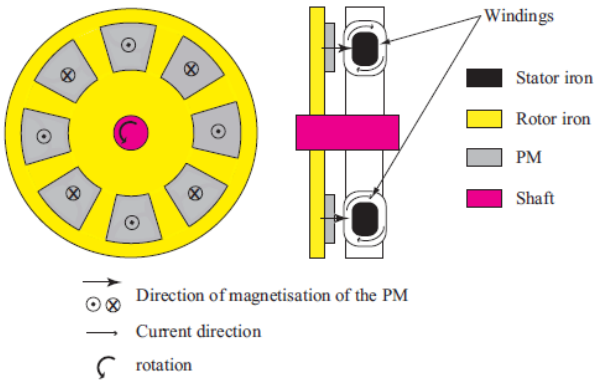

Figure 2-8: AFPM machine with flux and current directions

2.4.3: Transverse-flux PM machines

The basic arrangement of a TFPM machine is shown in Figure 2-9. This type of machine suits well for low-speed direct-drive applications because of a small pole pitch. Nevertheless, it is not very common yet.

The advantage of the TFPM machine is the high specific torque that allows the compactness of the machine. The major drawbacks are the poor power factor at high specific torque and the complexity of the structure which leads to high manufacturing cost.

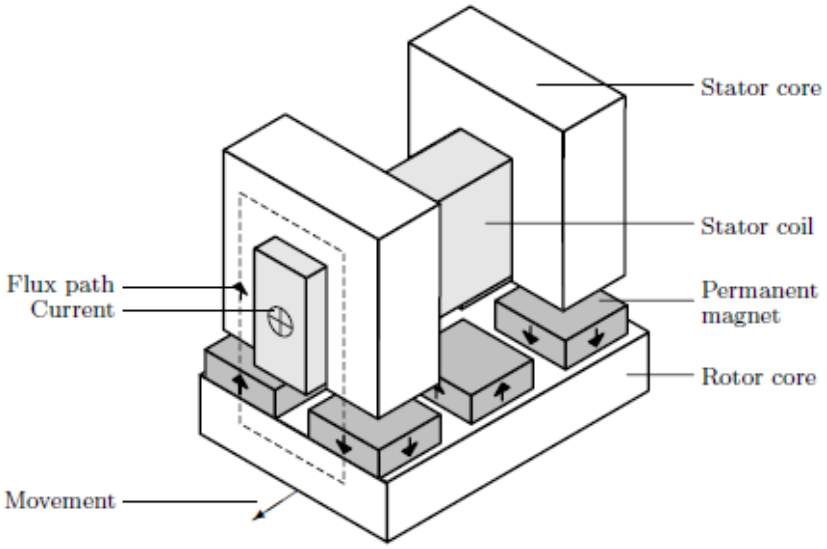

Figure 2-9: Basic Single Phase transverse flux topology with PM excitation

Most of the RFPM machines have a conventional inner rotor design. The design of RF machines is simple and widely used. The structural stability of RF machines is easy to make sufficient. Most of the low speed megawatts wind generators are RF machines and these RF machines seem to be the most interesting machine type for the large scale direct drive wind turbines. When using permanent magnets (PM) for the direct-drive generators, the generators can operate with good and reliable performance over a wide range of speeds. In manufacture, the simple way of constructing the machine with high number of poles is gluing PMs on the rotor surface. In RFPM machines, the length of the stator and the air gap diameter can be chosen independently. If necessary, the radial flux machine can be made with a small diameter by using a long stator.

RFPM machines (PMSG) have the advantages such as a better torque density than the RF electrically excited synchronous machine (EESG), so that these machines have been discussed in a number of literature. However, the presence of PMs makes the assembly more difficult and the structure stronger, especially in large machines. RFPM machines with general topology have been almost optimized in the electromagnetic design, so that it seems hard to reduce the active material and the cost of the machines significantly.

The AFPM machine is a machine producing magnetic flux in the axial direction with permanent magnets. Fig. 2-10 depicts different AFPM machines such as slotless, toroidal-stator, slotted, coreless machines.

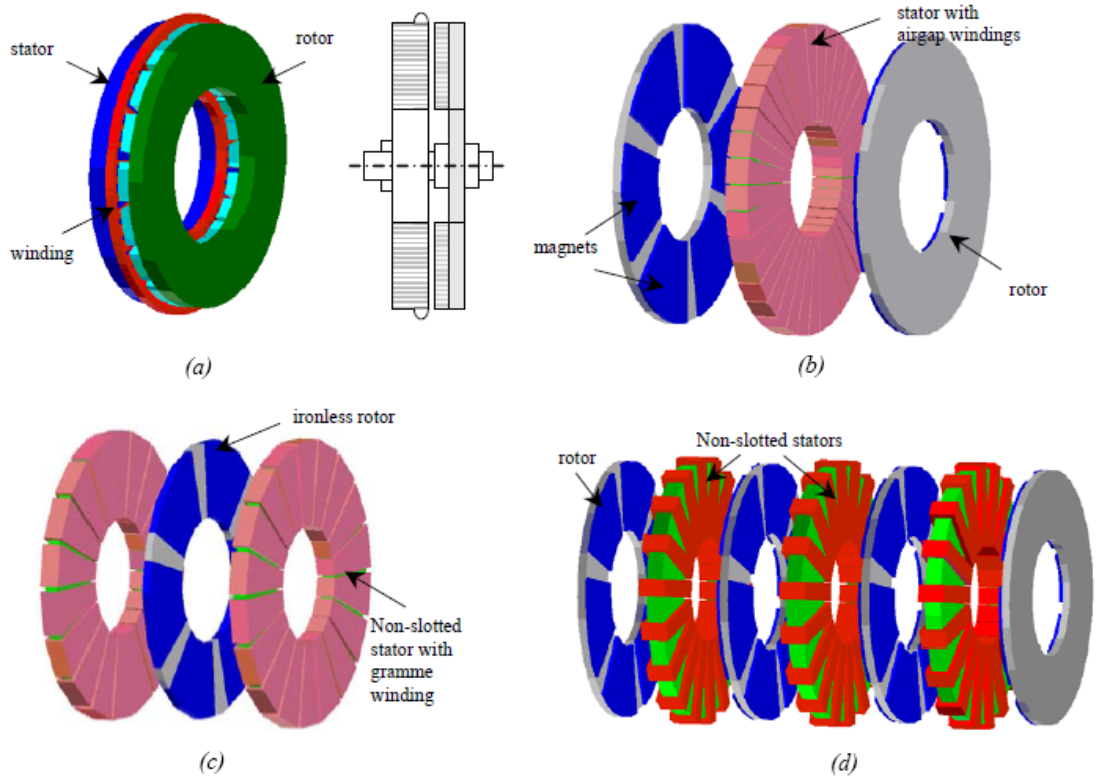

Figure 2-10: Different Axial Flux Permanent magnet machines: (a) single rotor single stator AFPM structure, (b) AF TORUS type non-slotted surface mounted PM motor configuration, (c) AF internal rotor type non-slotted surface mounted PM motor configuration, (d) slotless Multi stage PM machine with N=3 (where N is the number of stages or stators)

According to [3], AFPM machine has the advantages compared to RFPM machines as the following:

- simple winding
- low cogging torque and noise (in slotless machine)
- short axial length of the machine
- higher torque/volume ratio

However, the disadvantages of AFPM machines have been also discussed compared to RFPM machines as the following.

- Lower torque/mass ratio
- Larger outer diameter, large amount of PM, and structural instability (in slotless machine)
- Difficulty to maintain air gap in large diameter (in slotted machine)
- Difficult production of stator core (in slotted machine)

Permanent Magnet Direct-Drive turbines are the future of wind energy generation. It's a smart technology that can sense variable load demands and automatically adjust power output. By eliminating gearbox maintenance and most importantly, failure, all of our nearly 100 permanent magnet solutions provide increased up-time with 75% less upkeep and repair.

2.5 Axial-flux permanent-magnet machines

Regardless of the success of radial-flux permanent-magnet machines, axial-flux permanent magnet machines have also been under research interest particularly due to special-application limited geometrical considerations.

Several axial-flux machine configurations can be found regarding the stator(s) position with respect to the rotor(s) positions and the winding arrangements giving freedoms to select the most suitable machine structure into the considered application. Possible configurations are: Figure 2-11 [4]

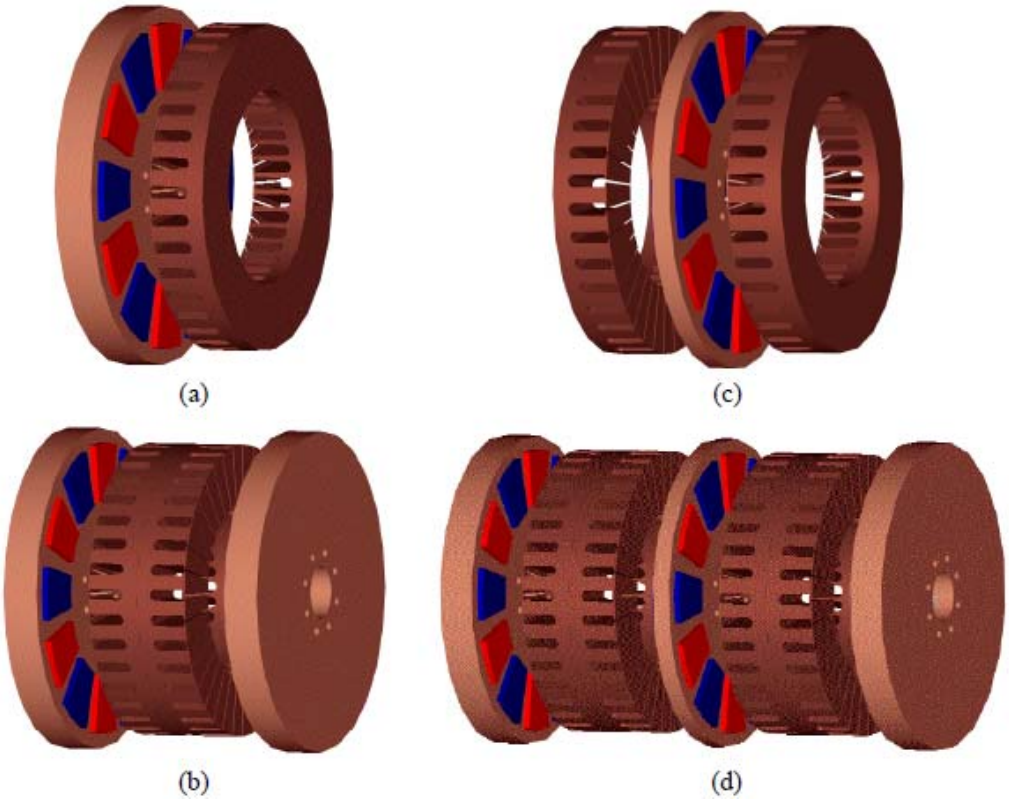

Figure 2-11: Axial Flux machine configurations: (a) single rotor single stator structure (b) Two rotors single stator structure (c) Single rotor two stators structure called "Axial Flux Interior rotor Permanent Magnet machine" (AFIPM) (d) Multistage structure including two stator and three rotor blocks

The single-rotor – single-stator structure, shown in Fig. 2-11 (a),

It is the simplest axial-flux permanent-magnet machine configuration (Campbell, 1974; Kurronen, 2003). This structure suffers, however, from an unbalanced axial force between the rotor and the stator; as a consequence more complex bearing arrangements and a thicker rotor disk are needed, compared to structures in which the axial forces are balanced.

The one stator – two rotors structure, illustrated in Fig. 2.11 (b), is a "TORUS" type axial-flux machine that has its phase coils wound around the slotted stator or non-slotted stator. The first "TORUS" type

permanent-magnet machine, with non-slotted stator, was introduced in the late 1980's (Spooner and Chalmers, 1988). The toroidally wound phase winding has short end-windings, which improves the machine efficiency and power density. As a drawback, the fixing of the stator to the frame is more complex; compared to the opposite structure, in which the rotor is located between the stators the AFIPM Fig 2-11 (c), less space is left for the winding. More complex arrangements can be found by assembling several machines lined up on the same shaft and by forming a multistage axial-flux machine according to Fig. 2-11 (d). Such machines may be considered for ship propulsion drive, pump and high-speed permanent-magnet generator applications.

2.5.1: Torque production

Considering an idealized axial-flux machine structure with double air-gaps, according to Fig. 2-11, the expression for the electromagnetic torque produced by the machine may be derived [4]. In the analysis, it is assumed that the permanent magnets produce a square wave flux density distribution into the air-gap with maximum value B_{max}. It is also assumed that all the winding conductors carry constant current with RMS value I, and the current is appropriately timed and perpendicularly oriented with the flux density distribution in the air gaps. The conductors are located as closely together as possible on the inner radius of the stator core r_{in}. Therefore, the linear current density A on radius r can be written as [4]:

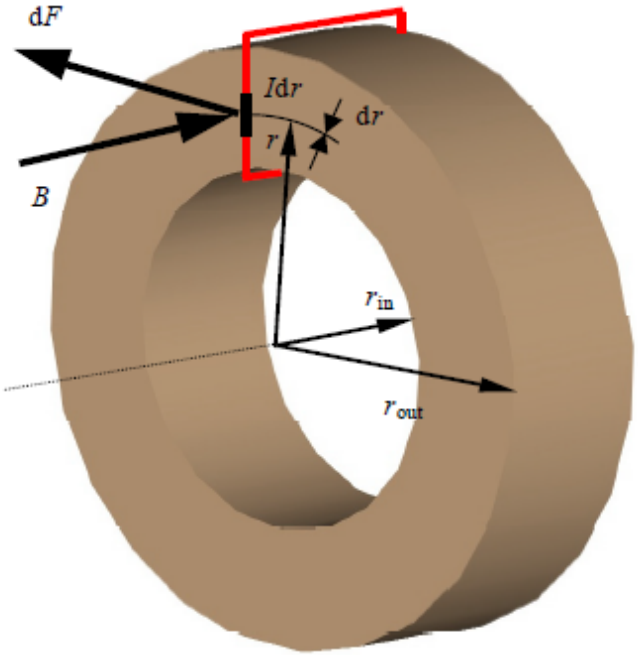

Figure 2-12: Illustration of torque production in axial flux machines

$$A(r) = \frac{A_{in} r_{in}}{r},$$

Where, A_{in} is the linear current density on the inner radius, r_{in}, of the machine and is defined as

$$A_{in} = \frac{m N_{ph} I}{\pi r_{in}},$$

Where, m is the number of phases, N_{ph} is the number of coil turns in series per stator phase winding

With the given assumptions, the machine torque can be calculated from the elementary forces dF acting on the surface of the stator core. The elementary torque component dT_{em} on radius r takes the form

$$dT_{em} = 2\pi r_{in} A_{in} B_{max} r dr ,$$

Where, B_{max} is the maximum value of the air-gap flux density produced by the permanent magnet.

Integrating dT_{em} equation over the machine radius gives the electromagnetic torque for the ideal double sided axial-flux machine

$$T_{em} = 2\pi B_{max} A_{in} 2 \int_{r_{in}}^{r_{out}} r_{in} r dr = 2\pi B_{max} A_{in} r_{out}^3 k_D (1 - k_D^2) ,$$

Where, k_D is the diameter ratio and is defined as

$$k_D = \frac{r_{in}}{r_{out}} .$$

The electromagnetic torque produced by a real machine is somewhat reduced due to the actual distribution of the flux density in the air-gaps and in the current waveform. This is investigated in detail in [4]. According to [4] the optimal diameter ratio for the idealized axial-flux machine, which is

$$k_{D,opt} = \frac{1}{\sqrt{3}} \approx 0.58 .$$

Note that, as axial-flux machines are concerned, the diameter ratio is an important design parameter. The torque production capability of the machine, as a function of k_D, is described in Fig. 2-12. The curve is scaled for the maximum torque to be equal to value 1.

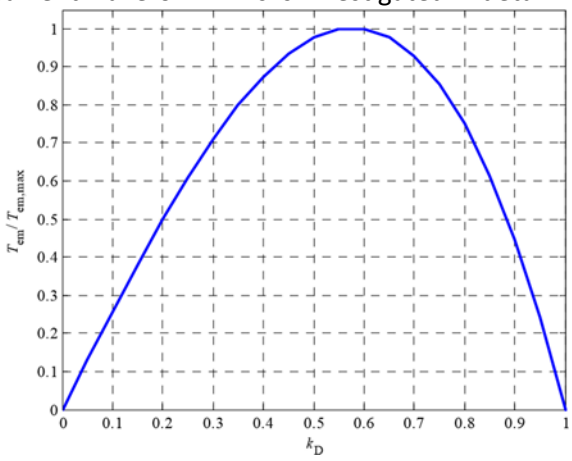

Figure 2-13: Electromagnetic torque of an ideal axial-flux machine as a function of the machine diameter ratio.

Chapter 3: Pulse Width-Modulated DC/AC Inverters

DC/AC inverters are quickly developed with knowledge of the power switching circuits applied in industrial applications in comparison with other power switching circuits. In the past century, plenty of topologies of DC/AC inverters have been created. DC/AC inverters are mainly used in AC motor adjustable speed drives (ASDs). Power DC/AC inverters have been widely used in other industrial applications since the late 1980s. Semiconductor manufacture development allowed high-power devices such as IGBTs and MOSFETs to operate at higher switching frequencies (e.g., from tens of kHz up to a few MHz). [5]

Square waveform DC/AC inverters were used well before the 1980s and the thyristor, GTO, and triac could be used in low-frequency switching operations.Nowadays, most DC/AC inverters are still PWM DC/AC inverters in different prototypes.

DC/AC inverters are used for converting a DC power source into AC power applications. They are generally used in the following applications:

1. Variable voltage/variable frequency AC supplies in adjustable speed drive (ASD), devices such as induction motor drives, synchronous machine drives, and so on
2. Constant regulated voltage AC power supplies, such as uninterruptible power supplies (UPSs)
3. Static variability (reactive power) compensations
4. Passive/active series and parallel filters
5. Flexible AC transmission systems (FACTSs)
6. Voltage compensations

3.1 Parameters Used in PWM Operation

Some parameters specially used in PWM operation are introduced in this section.

3.1.1: Modulation Ratios

The modulation ratio is usually obtained from a uniform amplitude triangle (carrier) signal with amplitude V_c. The maximum amplitude of the input signal is assumed to be V_m. We define the amplitude modulation ratio M for a single-phase inverter as follows:

$$M = \frac{V_m}{V_c}$$

We also define the frequency modulation ratio m_f as follows:

$$m_f = \frac{f_c}{f_m}$$

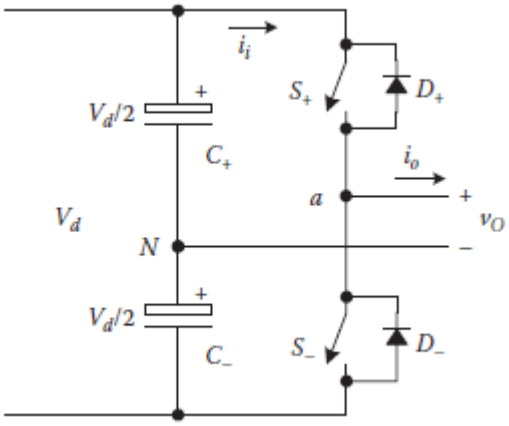

Figure 3-1 Single Leg switch mode converter

A single-leg switch-mode inverter is shown in Figure 3.1 [5]. The DC-link voltage is V_d. Two large capacitors are used to establish the neutral point N. The AC output voltage from point a to N is V_{AO}, and its fundamental component is $(V_{AO})_1$.

Notes on the amplitude modulation ratio *M: Fig. 3-2*

- $(V_{Ao})_1 = M\frac{V_d}{2}$ $for\ M \leq 1$, is valid in the linear range for.
- $\frac{V_d}{2} < (V_{Ao})_1 < \frac{4}{\pi}\frac{V_d}{2}$ $for\ 1 < M \leq 3.24$ That's the overmodulation region. Overmodulation causes the output voltage to contain many more harmonics in the sidebands compared with the linear range.
- $(V_{Ao})_1 > \frac{4}{\pi}\frac{V_d}{2}$ $for\ M > 3.24$ That's square wave production. Each switch of the inverter leg is on for half cycle of the desired output frequency

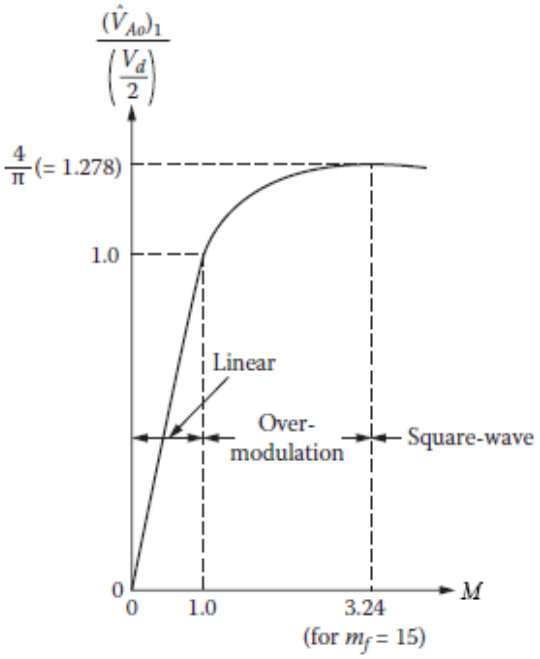

Figure 3-2 Voltage control by varying m_a

Notes on the amplitude modulation ratio m_f:

- m_f can be an integer (called synchronous PWM) or a non-integer (called asynchronous PWM). However, asynchronous PWM is undesirable because it produces sub harmonics (of the fundamental frequency)

3.2 Three-Phase Full-Bridge VSI

3.2.1: SPWM Spectra:

Although the SPWM waveform has harmonics of several orders in the phase voltage waveform, the dominant ones other than the fundamental are of order m_f and $m_f \pm 2$. This is evident for the spectrum for m_f=15 and m_a = 0.8 shown in Fig.3-3 [6]. Note that if the other two phases are identically generated but 120^o apart in phase, the line-line voltage will not have any *3k* harmonics. Hence it is advisable to choose $m_f = 3k, (k \in N)$, as then the dominant harmonic will be eliminated. It is evident from Fig 3-3b, that the dominant 15th harmonic in Fig. 3-3a is effectively eliminated in the line voltage. Choosing a multiple of 3 is also convenient as then the same triangular

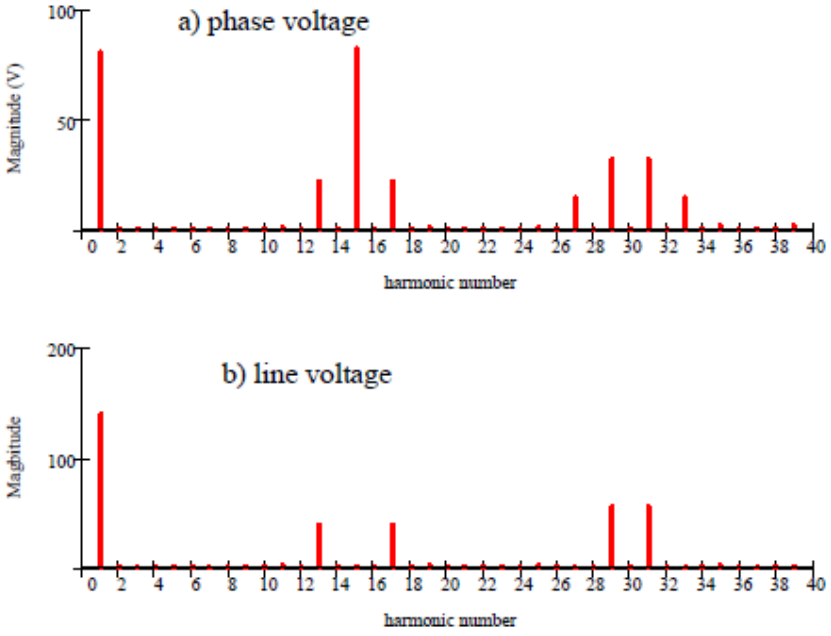

Figure 3-3 SPWM harmonic Spectra for n=15, m=0.8

waveform can be used as the carrier in all three phases, leading to some simplification in hardware.

A three-phase full-bridge VSI is shown in Figure 3.4[5]. The carrier-based pulse width modulation (PWM) technique is applied in this single-phase full-bridge VSI. Two large capacitors may be used to provide a neutral point N, but one maybe enough. Six switches $S_1 - S_6$ in three legs are applied and switched by the PWM signal. Figure 3-5[5] shows the ideal waveforms associated with the full-bridge VSI.
We can find out the phase delay between the output current and voltage.

The modulation indication of a three-phase VSI is different from that of single-phase half-bridge VSI as noted in [5]. It is shown in Figure 3-6.

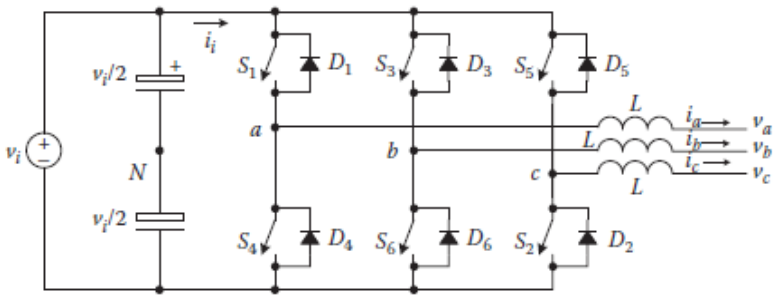

Figure 3-4 Three Phase full bridge VSI

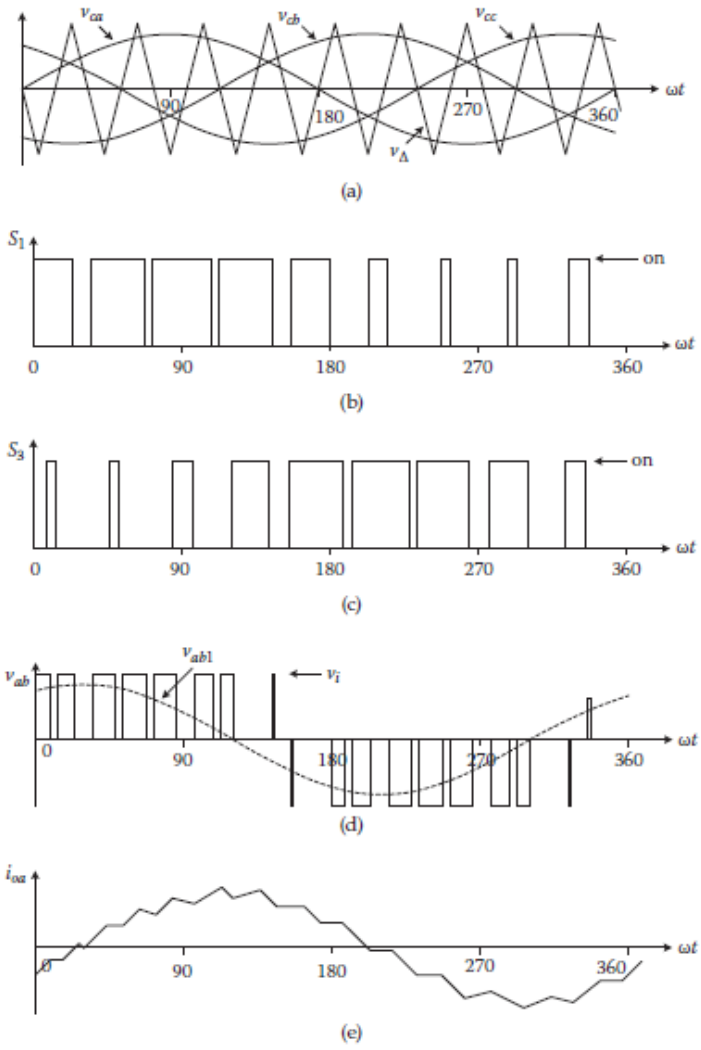

Figure 3-5: Three Phase full bridge VSI (m_a=0.8,m_f=9): (a) carrier & modulating signals (b) switch s1 state (c)switch s3 state (d) AC output voltage (e) AC output current

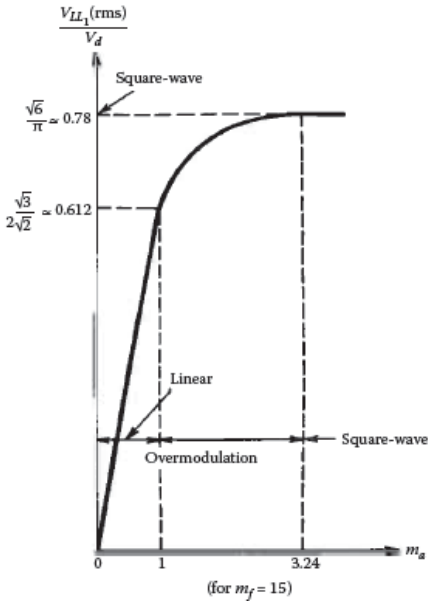

Figure 3-6 Function of modulation for three phase inverter

3.3 Multilevel inverters

Some types of multilevel inverters are shown in the following [7]:

3.3.1 Cascaded H-Bridges

A single-phase structure of an *m*-level cascaded inverter is illustrated in Figure 3-7[7], Each separate dc source (SDCS) is connected to a single-phase full-bridge, or H-bridge, inverter. Each inverter level can generate three different voltage outputs, $+V_{dc}$, *0*, and $-V_{dc}$ by connecting the dc source to the ac output by different combinations of the four switches, S_1, S_2, S_3, and S_4. To obtain $+V_{dc}$, switches S_1 and S_4 are turned on, whereas $-V_{dc}$ can be obtained by turning on switches S_2 and S_3. By turning on S_1 and S_2 or S_3 and S_4, the output voltage is *0*. The ac outputs of each of the different full-bridge inverter levels are connected in series such that the synthesized voltage waveform is the sum of the inverter outputs. The number of output phase voltage levels *m* in a cascade inverter is defined by $m = 2s+1$, where *s* is the number of separate dc sources. An example phase voltage waveform for an 11-level cascaded H-bridge inverter with 5 SDCSs and 5 full bridges is shown in Figure 3-8.

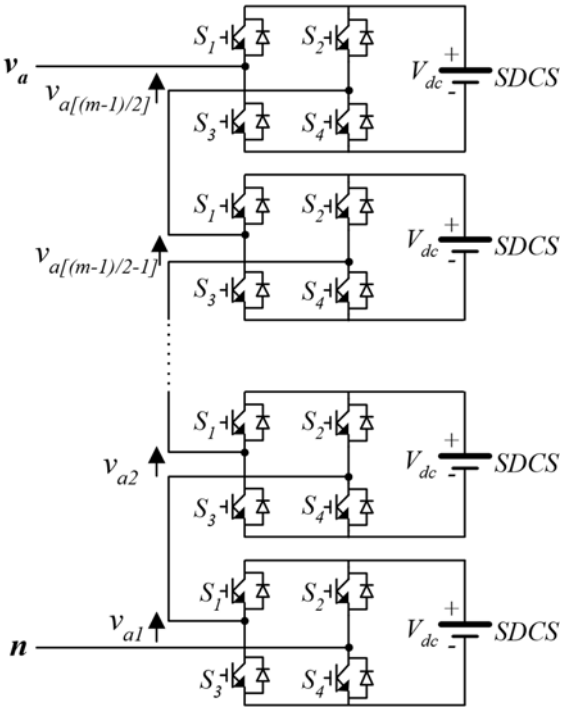

Figure 3-7: Single phase structure of multilevel cascaded H Bridges inverter

The phase voltage $v_{an} = v_{a1} + v_{a2} + v_{a3} + v_{a4} + v_{a5}$.

The main advantages and disadvantages of multilevel cascaded H-bridge converters are as follows [7].

<u>Advantages:</u>

- The number of possible output voltage levels is more than twice the number of dc sources ($m = 2s + 1$).
- The series of H-bridges makes for modularized layout and packaging. This will enable the manufacturing process to be done more quickly and cheaply.

<u>Disadvantages:</u>

- Separate dc sources are required for each of the H-bridges. This will limit its application to products that already have multiple SDCSs readily available.

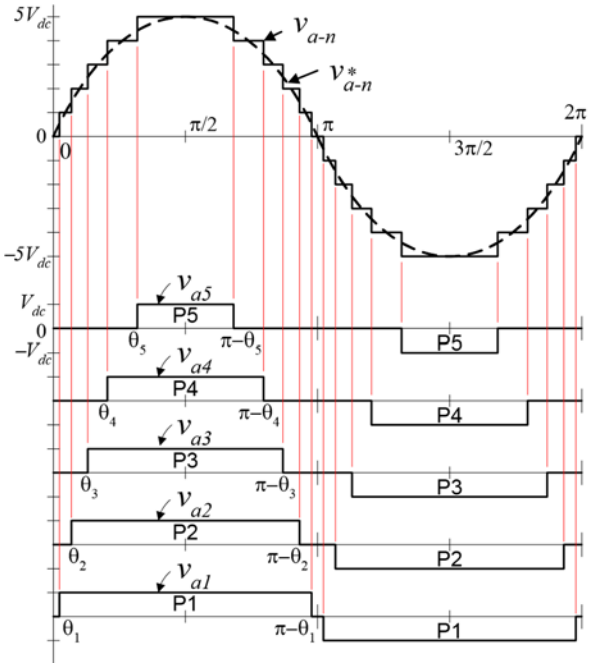

Figure 3-8 Output phase voltage waveform of an 11 level cascade inverter with 5 separate dc sources.

3.3.2: Diode-Clamped Multilevel Inverter

A three-phase six-level diode-clamped inverter is shown in Figure 3-9. Each of the three phases of the inverter shares a common dc bus, which has been subdivided by five capacitors into six levels. The voltage across each capacitor is V_{dc}, and the voltage stress across each switching device is limited to V_{dc} through the clamping diodes. Table 3.1 lists the output voltage levels possible for one phase of the inverter with the negative dc rail voltage V_O as a reference. State condition 1 means the switch is on, and 0 means the switch is off. Each phase has five complementary switch pairs such that turning on one of the switches of the pair requires that the other complementary switch be turned off. The complementary switch pairs for phase leg a are (S_{a1}, $S_{a'1}$), (S_{a2}, $S_{a'2}$), (S_{a3}, $S_{a'3}$), (S_{a4}, $S_{a'4}$), and (S_{a5}, $S_{a'5}$). Table 3.1 also shows that in a diode-clamped inverter, the switches that are on for a particular phase leg are always adjacent and in series. For a six-level inverter, a set of five switches is on at any given time.

Voltage V_{a0}	Switch State									
	S_{a5}	S_{a4}	S_{a3}	S_{a2}	S_{a1}	$S_{a'5}$	$S_{a'4}$	$S_{a'3}$	$S_{a'2}$	$S_{a'1}$
$V_5 = 5Vdc$	1	1	1	1	1	0	0	0	0	0
$V_4 = 4Vdc$	0	1	1	1	1	1	0	0	0	0
$V_3 = 3Vdc$	0	0	1	1	1	1	1	0	0	0
$V_2 = 2Vdc$	0	0	0	1	1	1	1	1	0	0
$V_1 = Vdc$	0	0	0	0	1	1	1	1	1	0
$V_0 = 0$	0	0	0	0	0	1	1	1	1	1

Table 3-1 Diode-clamped six-level inverter voltage levels and corresponding switch states

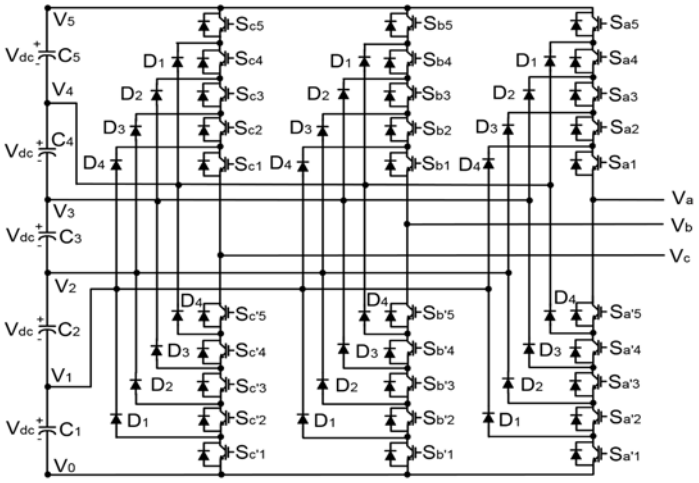

Figure 3-9 Three phase six level structure of diode clamped inverter

Figure 3-10 shows one of the three line-line voltage waveforms for a six-level inverter. The line voltage V_{ab} consists of a phase-leg a voltage and a phase-leg b voltage. The resulting line voltage is an 11-level staircase waveform. This means that an m-level diode-clamped inverter has an m-level output phase voltage and a (2m-1)-level output line voltage.

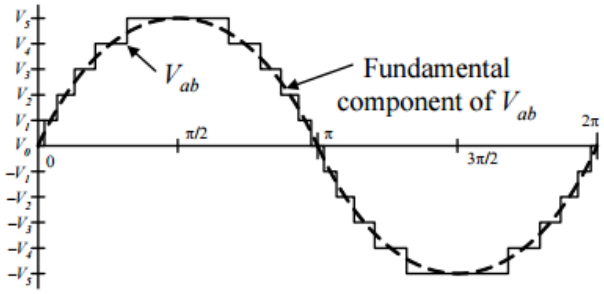

Figure 3-10 Line voltage waveform for a six level diode clamped inverter

Although each active switching device is required to block only a voltage level of V_{dc}, the clamping

diodes require different ratings for reverse voltage blocking. Using phase *a* of Figure 3.9 as an example, when all the lower switches $S_{a'1}$ through $S_{a'5}$ are turned on, D_4 must block four voltage levels, or $4V_{dc}$. Similarly, D_3 must block $3V_{dc}$, D_2 must block $2V_{dc}$, and D_1 must block V_{dc}. If the inverter is designed such that each blocking diode has the same voltage rating as the active switches, D_n will require *n* diodes in series; consequently, the number of diodes required for each phase would be (*m*-1) × (*m*-2). Thus, the number of blocking diodes is quadratically related to the number of levels in a diode-clamped converter

Advantages:

- All of the phases share a common dc bus, which minimizes the capacitance requirements of the converter. For this reason, a back-to-back topology is not only possible but also practical for uses such as a high-voltage back-to-back inter-connection or an adjustable speed drive.
- The capacitors can be pre-charged as a group.
- Efficiency is high for fundamental frequency switching.

Disadvantages:

- Real power flow is difficult for a single inverter because the intermediate dc levels will tend to overcharge or discharge without precise monitoring and control.
- The number of clamping diodes required is quadratically related to the number of levels, which can be cumbersome for units with a high number of levels.

3.4 Two level inverter versus multilevel inverters

The attractive features of a multilevel converter can be briefly summarized as follows. [7]

- Staircase waveform quality: Multilevel converters not only can generate the output voltages with very low distortion, but also can reduce the dv/dt stresses; therefore electromagnetic compatibility (EMC) problems can be reduced.
- Common-mode (CM) voltage: Multilevel converters produce smaller CM voltage; therefore, the stress in the bearings of a motor connected to a multilevel motor drive can be reduced.
- Input current: Multilevel converters can draw input current with low distortion.

Unfortunately, multilevel converters do have some disadvantages. One particular disadvantage is the greater number of power semiconductor switches needed. Although lower voltage rated switches can be utilized in a multilevel converter, each switch requires a related gate drive circuit. This may cause the overall system to be more expensive and complex.
The cost of inverters is mainly dependent on the IGBT and DC-link capacitor. In addition, the cost of three-level inverter includes the clamped diode. A cost comparison is done in [8] and shows how 2 level inverters are cheaper than 3 level inverters

The two-level configuration is 27% cheaper than the three-level configuration. The difference is mostly due to the cost of diodes, which are not needed in two-level configuration.

Chapter 4: Derivation of the instantaneous DC current ripple

In this chapter, we are set to find an expression to the current ripple on the dc side, so that we are able to visualize the current harmonics on the dc side. Eventually, after finding the expression of the current ripple, we will be able to choose the correct angles of displacement between the carrier waveforms; so that we can obtain the elimination of some of the harmonic contents.

4.1: Square wave modulation

The equivalent circuit of our system can be modelled as in figure 4-1; the generator is modelled as R-L in series with the internal emf of the PMSM "e_A, e_B, e_C"

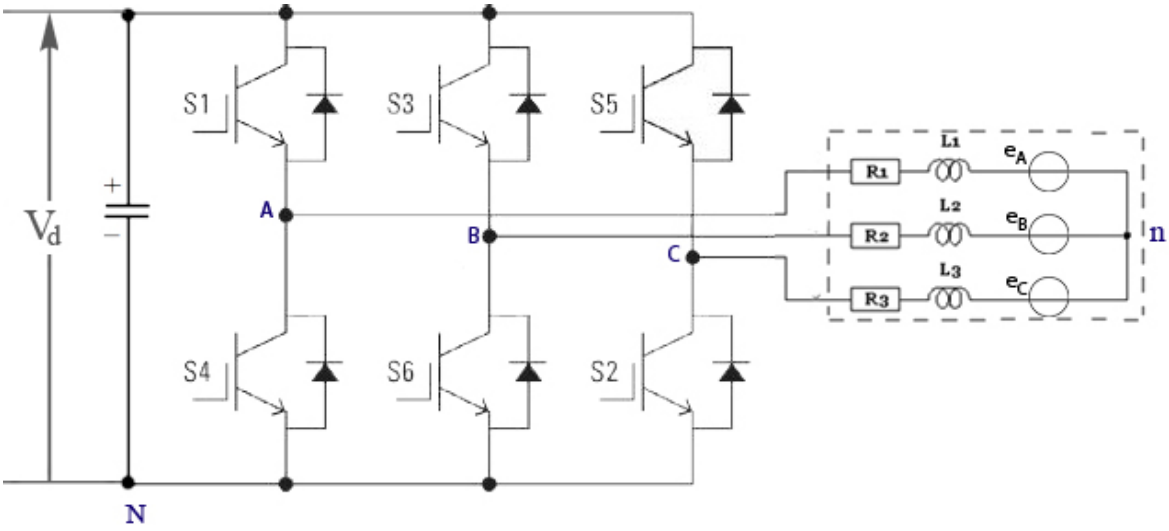

Figure 4-1 Equivalent circuit of our system

The voltage of the dc bus V_d is applied to each phase for a period of π and shifted by 120° (Figure 4-2a)

We can deduce the Line to line voltages which are shown in figure 4-2b :

$$v_{AB} = v_{AN} - v_{BN}$$
$$v_{BC} = v_{BN} - v_{CN}$$
$$v_{CA} = v_{CN} - v_{AN}$$

Applying KVL:

$V_{AN} = V_{nN} - V_{An}$ And $\mathcal{V}_{An} = R_S\, i_A + L_S \frac{dl_A}{dt} + e_A =$

$R_S l_A + L_S\, p i_A + e_A$

$V_{BN} = V_{nN} - V_{Bn}$ And $\mathcal{V}_{Bn} = R_S i_B + L_S\, p\, i_B + e_B$

$V_{CN} = V_{nN} - V_{Cn}$ And $\mathcal{V}_{Cn} = R_S i_C + L_S\, p\, i_C + e_C$

Summing up v_{An}, v_{Bn}, v_{Cn} we get

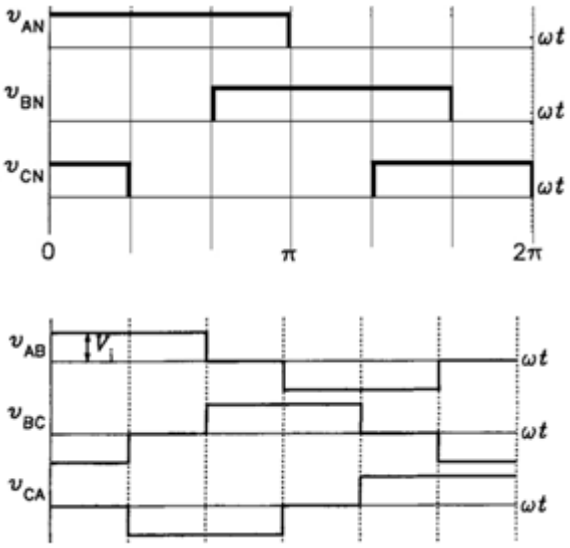

Figure 4-2 a) voltages applied to the 3 phases, (b) line to line voltages

$$v_{An} + v_{Bn} + v_{Cn} = R_S(i_A + i_B + i_C) + L_S\, p(i_A + i_B + i_C) + (e_A + e_B + e_C)$$

Because we assumed that our machine is a star connected machine which means that $i_A + i_B + i_C = 0$ and moreover because it's a symmetric balanced three phase machine (displaced by 120 degrees) thus $e_A + e_B + e_C = 0$

We can deduce that

$$\mathcal{V}_{An} + \mathcal{V}_{Bn} + \mathcal{V}_{Cn} = 0$$

Thus $\mathcal{V}_{AN} + \mathcal{V}_{BN} + \mathcal{V}_{CN} = 3V_{nN}$ which translates into $V_{nN} = \frac{\mathcal{V}_{AN} + \mathcal{V}_{BN} + \mathcal{V}_{CN}}{3}$ and the waveform of V_{nN} can be seen in Figure 4-3a. it can be seen that the amplitudes are oscillating between $\frac{Vd}{3}$ and $\frac{2Vd}{3}$.

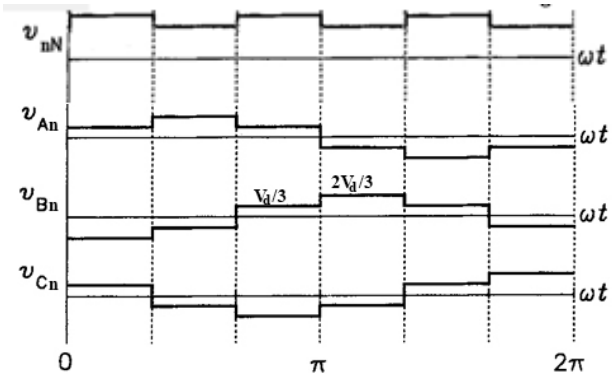

Figure 4-3 a) the voltage waveform between the star point of the machine "n" and the neutral "N", (b) the waveforms of the phase voltages

We can now easily find the voltages across the machine of each phase V_{An}, V_{Bn}, V_{Cn}. Figure (4-3b) where the amplitudes are $\frac{Vd}{3}$, $\frac{2Vd}{3}$, $\frac{-Vd}{3}$ and $\frac{-2Vd}{3}$.

If we consider the waveform of $\mathcal{V}_{An}(t)$ to apply the Fourier series expansion, we can deduce that it is an odd function ($\mathcal{V}_{An}(-\theta) = -\mathcal{V}_{An}(\theta)$) and also the function has quarter wave symmetry ($\mathcal{V}_{An}(\pi - \theta) = \mathcal{V}_{An}(\theta)$). These two properties mean that only odd harmonics exist.

Therefore,

$$V_{An}(h) = \frac{4}{\pi}\int_0^{\pi/2} \mathcal{V}_{An}(\theta)\sin h\theta\, d\theta = \frac{4}{\pi}\left(\int_0^{\pi/3} \frac{Vd}{3}\sin h\theta\, d\theta + \int_{\pi/3}^{\pi/2} \frac{2Vd}{3}\sin h\theta d\theta\right) =$$

$$= \frac{4Vd}{3\pi h}\left(1 - \cos\frac{h\pi}{3} + 2\cos\frac{h\pi}{3}\right) = \frac{4}{\pi} * \frac{Vd}{3h} * \left(1 + \cos\frac{h\pi}{3}\right) \qquad (4-1)$$

And applying the trigonometric function $1 + cos\, x = 2cos^2\left(\frac{x}{2}\right)$ on (4-1) we get,

$$\mathcal{V}_{An}(h) = \frac{8}{\pi} * \frac{Vd}{3h} * cos^2\left(\frac{h\pi}{6}\right) \qquad (4-2)$$

This equation is valid for $h = 1,5,7,11, \dots etc$ not for the third harmonics and its multiples because their waveforms are 120 degrees apart and the machine is star connected so their sum is zero.

4.1.1: For the fundamental frequency (h=1):

An equivalent circuit is presented in Figure 4-4,

We can draw the phasor diagram Figure 4-5 and apply the Euler formula to obtain the magnitudes of the current, voltage and impedence for h=1 which can be found in table 4-1.

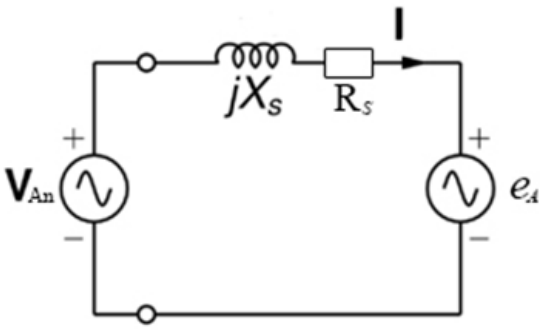

Figure 4-4 Equivalent circuit for the fundamental frequency

Table 4-1 Magnitudes for fundamental frequency h=1

$$\boldsymbol{i(t) = \frac{V'}{Z}\sin(\omega t - \phi)}$$
$$\boldsymbol{V' = \sqrt{(V_{An} - E\cos\delta)^2 + (E\sin\delta)^2}}$$
$$\boldsymbol{\phi = \tan^{-1}\left(\frac{\omega_1 L}{R}\right) - \tan^{-1}\left(\frac{E\sin\delta}{V_{An} - E\cos\delta}\right)}$$
$$\boldsymbol{Z' = \sqrt{R^2 + (\omega_1 L)^2}}$$

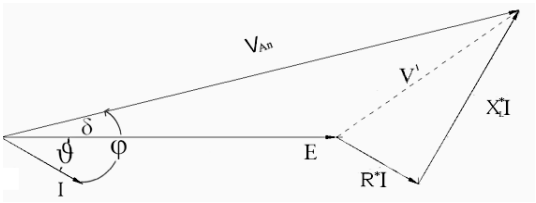

Figure 4-5 Phasor diagram for fundamental frequency

where ϕ is the angle between the fundamental voltage and the current.

4.1.2: For the generic harmonic h:

The equivalent circuit will not have the emf of the machine as it is shown in figure 4-6

From equation (4-2) we can find that the fundamental voltage amplitude is

$$\hat{V}_{An}(1) = \frac{2 * Vd}{\pi}$$

And the amplitude for any generic harmonic "h" is

$$\hat{V}_{An}(h) = \frac{2 * V_d}{h * \pi} = \frac{\hat{V}_{An}(1)}{h}$$

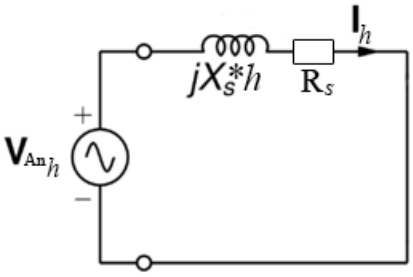

Figure 4-6 Equivalent circuit for generic harmonic h

As for the reactance it will vary with the frequency such that $X_{s(h)} = h * X_{s1}$. Thus the generic formulas for the amplitudes will be in table 4-2

Table 4-2 Amplitudes for generic harmonic h

$\boldsymbol{i_h(t) = \frac{\hat{V}_{An}(h)}{Z_h}\sin(h * \omega_1 t - \theta_h)}$
$\boldsymbol{\hat{V}_{An}(h) = \frac{2 * Vd}{h * \pi}}$
$\boldsymbol{\theta_h = \tan^{-1}\left(\frac{h * \omega_1 L}{R}\right)}$
$\boldsymbol{Z_h = \sqrt{R^2 + (h * \omega_1 L)^2}}$

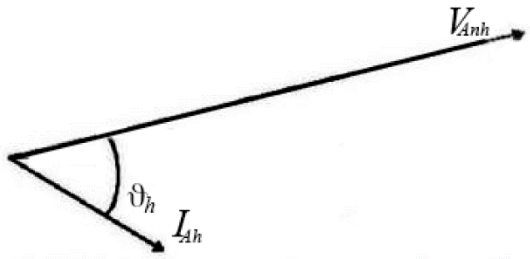

Figure 4-7 Phasor diagram for generic harmonic h

Therefore, Equations can be written in the following manner for the phases a, b and c:

$$v_{An}(t) = \frac{2V_d}{\pi}.\sin(\omega_1 t) + \sum_{h\neq 1} V_h \sin*(h(\omega_1 t - \psi))$$

$$i_A(t) = \hat{I}_1.\sin(\omega_1 t - \phi) + \sum_{h\neq 1} \hat{I}_h \sin(h * (\omega_1 t - \psi) - \theta_h)$$

$$v_{Bn}(t) = \frac{2V_d}{\pi}\sin(\omega_1 t - 120°) + \sum_{h\neq 1} V_h \sin(h * (\omega_1 t - \psi - 120))$$

$$i_B\ (t) = \hat{I}_1.\sin(\omega_1 t - \phi - 120°) + \sum_{h\neq 1} \hat{I}_h \sin(h * (\omega_1 t - \psi - 120) - \theta_h)$$

$$v_{Cn}(t) = \frac{2V_d}{\pi}\sin(\omega_1 t - 240°) + \sum_{h\neq 1} V_h \sin(h * (\omega_1 t - \psi - 120))$$

$$i_c(t) = \hat{I}_1.\sin(\omega_1 t - \phi - 240°) + \sum_{h\neq 1} \hat{I}_h \sin(h * (\omega_1 t - \psi - 240) - \theta_h) \qquad (4-3)$$

Where ψ is the shift between the voltages of different inverter.

4.1.3: Power balance across the inverter

We will start the procedure of finding the expression of the instantaneous current ripple by performing a power balance across the inverter.

Assuming a constant dc voltage V_d and an ideal inverter Figure 4-8 we can perform a power balance across the inverter as the following:

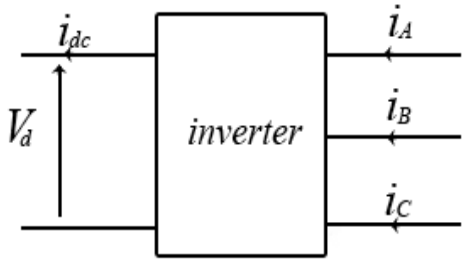

Figure 4-8 Power balance across an ideal inverter

$$V_d.i_{dc}(t) = i_A(t).v_{An}(t) + i_B(t).v_{Bn}(t) + i_C(t).v_{Cn}(t)$$

The multiplication between the components of the voltages and currents will be in three forms; either in the form $i_x.v_x$ or $i_y.v_x$ or $i_x.v_y$ (where x and y are generic harmonic orders). The result of $i_x.v_x$ will be the direct component because when we multiply the current and voltage of the same harmonic order that results of constant value (three phase system) in the form of $3.I_x.V_x.\cos(\vartheta_x)$. While the interaction between two different harmonic orders in the form of $i_y.v_x$ or $i_x.v_y$ won't produce a constant value anymore, but will produce a sinusoidal component (ripple component). Such ripples are in fact the dc current ripple, because we have assumed earlier a constant dc voltage V_d.

4.1.4: Instantaneous dc current ripple expression development

In our derivation we will consider the 5th and 7th harmonics only by expanding equations (4-3), such that;

$$v_{An}(t) = \hat{V}_{An(1)}\sin(\omega_1 t - \psi) + \hat{V}_{An(5)}\sin(5\omega_1 t - 5\psi) + \hat{V}_{An(7)}\sin(7\omega_1 t - 7\psi)$$
$$v_{Bn}(t) = \hat{V}_{An(1)}\sin(\omega_1 t - \psi - 120°) + \hat{V}_{An(5)}\sin(5\omega_1 t - 5\psi + 120°) + \hat{V}_{An(7)}\sin(7\omega_1 t - 7\psi - 120°)$$
$$v_{cn}(t) = \hat{V}_{An(1)}\sin(\omega_1 t - \psi - 240°) + \hat{V}_{An(5)}\sin(5\omega_1 t - 5\psi - 120°) + \hat{V}_{An(7)}\sin(7\omega_1 t - 7\psi - 240°)$$

Where the amplitudes are $\hat{V}_{An1} = \frac{2Vd}{\pi}$, $\hat{V}_{An(5)} = \frac{2Vd}{5\pi}$, $\hat{V}_{An(7)} = \frac{2Vd}{7\pi}$

$$i_A(t) = \hat{I}_1\sin(\omega_1 t - \psi - \phi) + \hat{I}_5\sin(5\omega_1 t - 5\psi - \theta_5) + \hat{I}_7\sin(7\omega_1 t - 7\psi - \theta_7)$$
$$i_B(t) = \hat{I}_1\sin(\omega_1 t - \psi - \phi - 120°) + \hat{I}_5\sin(5\omega_1 t - 5\psi - \theta_5 + 120°) + \hat{I}_7\sin(7\omega_1 t - 7\psi - \theta_7 - 120°)$$
$$i_c(t) = \hat{I}_1\sin(\omega_1 t - \psi - \phi - 240°) + \hat{I}_5\sin(5\omega_1 t - 5\psi - \theta_5 - 120°) + \hat{I}_7\sin(7\omega_1 t - 7\psi - \theta_7 - 240°)$$

Where the amplitudes are $\hat{I}_1 = \frac{\hat{V}_{An1}}{\sqrt{R^2+(\omega_1 L)^2}}$, $\hat{I}_5 = \frac{\hat{V}_{An5}}{\sqrt{R^2+(5\omega_1 L)^2}}$, $\hat{I}_7 = \frac{\hat{V}_{An7}}{\sqrt{R^2+(7\omega_1 L)^2}}$

Therefore if we perform the power balance we will get:

$$V_d.i_{dc}(t) = i_A(t).v_{An}(t) + i_B(t).v_{Bn}(t) + i_c(t).v_{cn}(t) =$$
$$i_{A_1}.v_{An_1} + i_{B_1}v_{Bn_1} + i_{C_1}v_{Cn_1} +$$
$$i_{A_5}v_{An_5} + i_{B_5}v_{Bn_5} + i_{C_5}v_{Cn_5} +$$
$$i_{A_7}v_{An_7} + i_{B_7}v_{Bn_7} + i_{C_7}v_{Cn_7} +$$
$$i_{A_1}v_{An_5} + i_{A_5}v_{An_1} + i_{B_1}v_{Bn_5} + i_{B_5}v_{Bn_1} + i_{C_1}v_{Cn_5} + i_{C_5}v_{Cn_1}$$
$$i_{A_7}v_{An_5} + i_{A_5}v_{An_7} + i_{B_7}v_{Bn_5} + i_{B_5}v_{Bn_7} + i_{C_7}v_{Cn_5} + i_{C_5}v_{Cn_7}$$
$$i_{A_1}v_{An_7} + i_{A_7}v_{An_1} + i_{B_1}v_{Bn_7} + i_{B_7}v_{Bn_1} + i_{C_1}v_{Cn_7} + i_{C_7}v_{Cn_1}$$

The direct component contribution from the multiplication of voltages and currents of the same harmonic

The dc current ripple production due to the multiplication between voltages and currents of different harmonic orders

$$(4-4)$$

Thus we can now write the expression for both the dc component and the ripple component of $i_{dc}(t)$

Dc component I_{dc}:

$$V_d I_{dc} = \frac{3\hat{I}_1 V_d(2)}{\pi.(2)}\cos\phi + \frac{3\hat{I}_5(2V_d)}{(2)5\pi}\cos\theta_5 + \frac{3\hat{I}_7(2V_d)}{(2)7\pi}\cos\theta_7 \qquad (4-5)$$

$$I_{dc} = \frac{3}{\pi}\hat{I}_1.\cos\phi + \frac{3}{5\pi}\hat{I}_5\ \cos\theta_5 + \frac{3}{7\pi}\hat{I}_7\ \cos\theta_7$$

Ripple component $i_r(t)$:

$$V_d.i_r(t) = i_{A_1}v_{An_5} + i_{A_5}v_{An_1} + i_{B_1}v_{Bn_5} + i_{B_5}v_{Bn_1} + i_{C_1}v_{Cn_5} + i_{C_5}v_{Cn_1} + i_{A_7}v_{An_5} + i_{A_7}v_{An_1} + i_{B_7}v_{Bn_5} + i_{B_7}v_{Bn_1} + i_{C_7}v_{Cn_5} + i_{C_7}v_{Cn_1} + i_{A_1}v_{An_7} + i_{A_5}v_{An_7} + i_{B_1}v_{Bn_7} + i_{B_5}v_{Bn_7} + i_{C_1}v_{Cn_7} + i_{C_5}v_{Cn_7} \quad (4-6)$$

Let's consider the interaction between the first and fifth harmonic:

$$\frac{i_{A_1}v_{An_5}}{V_d} = [\frac{1}{V_d}][\hat{I}_1\sin((\omega_1 t - \psi) - \phi)] * [\frac{2V_d}{5\pi}\sin 5 * (\omega_1 t - \psi)]$$

We should notice that when we introduce a shift between the phases (120 degrees shift) or when we introduce a generic shift angle ψ (that we are going to use to shift between various modules), the shift angle is associated with $\omega_1 t$. In other words, the shift angle will be multiplied by the harmonic order h in the higher order harmonic components.

From the trigonometric function $\sin a \sin b = \frac{1}{2}(\cos(a-b) - \cos(a+b))$ we can expand the expression as follows:

$$\frac{i_{A_1}v_{An_5}}{V_d} = \frac{\hat{I}_1}{5\pi}.(\cos(4\omega_1 t - 4\psi + \phi) - \cos(6\omega_1 t - 6\psi - \phi))$$

And similarly,

$$\frac{i_{A_5}v_{An_1}}{V_d} = \frac{\hat{I}_5}{\pi}.(cos(4\omega_1 t - 4\psi - \theta_5) - cos(6\omega_1 t - 6\psi - \theta_5))$$

$$\frac{i_{B_1}v_{Bn_5}}{V_d} = \frac{\hat{I}_1}{5\pi}(cos(4\omega_1 t - 4\psi + \phi + 240) - cos(6\omega_1 t - 6\psi - \phi))$$

$$\frac{i_{B_5}v_{Bn_1}}{V_d} = \frac{\hat{I}_5}{\pi}(cos(4\omega_1 t - 4\psi - \theta_5 + 240°) - cos(6\omega_1 t - 6\psi - \theta_5))$$

$$\frac{i_{C_1}v_{Cn_5}}{V_d} = \frac{\hat{I}_1}{5\pi}(cos(4\omega_1 t - 4\psi + \phi + 120°) - cos(6\omega_1 t - 6\psi - \phi))$$

$$\frac{i_{C_5}v_{Cn_1}}{V_d} = \frac{\hat{I}_5}{\pi}(cos(4\omega_1 t - 4\psi - \theta_5 + 120) - cos(6\omega_1 t - 6\psi - \theta_5)) \quad (4-7)$$

Looking closely to the equations of (4-7) we can find that two harmonic components co-exist; the fourth and the sixth harmonics.

Fourth harmonic:

$$i_{r4}(t) = \frac{\hat{I}_1}{5\pi}[\cos(4\omega_1 t - 4\psi + \phi) + \cos(4\omega_1 t - 4\psi + \phi + 240°) + \cos(4\omega_1 t - 4\psi + \phi + 120°)]$$
$$+ \frac{\hat{I}_5}{\pi}[\cos(4\omega_1 t - 4\psi - \theta_5)$$
$$+ \cos(4\omega_1 t - 4\psi - \theta_5 + 240°) + \cos(4\omega_1 t - 4\psi - \theta_5 + 120°)] \qquad (4-8)$$

As it can be fairly noticed from (4-8) the components of the three phases are displaced by 120 degrees. Due to our earlier assumption it's a balanced three phase, the summation of the contributions of the three phases is equal to zero; $i_{r4}(t) = 0$

Sixth harmonic:

$$i_{r6}(t) = \frac{-3\hat{I}_1}{5\pi}\cos(6\omega_1 t - 6\psi - \phi) - \frac{3\hat{I}_5}{\pi}\cos(6\omega_1 t - 6\psi - \theta_5) \qquad (4-9)$$

The summation of the three phases isn't equal to zero because the sixth harmonic components from all phases has no shift between them, hence it's a contribution to the dc current ripple.

The interaction between the first – seventh harmonic and the fifth – seventh harmonic are mentioned in the Appendix A1.

Some harmonics (like the second and the eighth harmonics) appear but cancel out in the same manner of the fourth harmonic.

After the summation we end up with the instantaneous dc side current ripple: (see App. A-1)

$$i_r(t) = -\frac{3\hat{I}_7}{5\pi}\cos(12\omega_1 t - \theta_7 - 12\psi) - \frac{3\hat{I}_5}{7\pi}\cos(12\omega_1 t - \theta_5 - 12\psi) - \frac{3\hat{I}_1}{5\pi}\cos(6\omega_1 t - \phi - 6\psi)$$
$$- \frac{3\hat{I}_5}{\pi}\cos(6\omega_1 t - \theta_5 - 6\psi) + \frac{3\hat{I}_1}{7\pi}\cos(6\omega_1 t + \phi - 6\psi) + \frac{3\hat{I}_7}{\pi}\cos(6\omega_1 t - \theta_7 - 6\psi)$$

We see the presence of two kinds of harmonics, the sixth and the twelfth harmonics, in the instantaneous equation of the dc current ripple.

Adding two sinusoidal waveforms shifted in time by half of its cycle will result in the elimination of such harmonic content Figure 4-9. Also adding three sinusoidal waveforms shifted from each other by 120 degrees will have a null summation. From these two facts we build the shifting strategy which in general is to eliminate the most significant harmonic.

Hence we can find the following results:

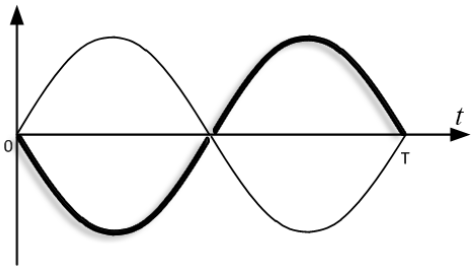

Figure 4-9 two sinusoidal waveforms shifted by 180 degrees

Using two inverter modules (or its multiples)

We choose to eliminate the sixth harmonic because it's the lower order harmonic. So we will use a displacement angle for the first inverter that's $6\psi = 0\ that\ \psi = 0$ and displacement angle for the second inverter $6\psi = 180°\ that\ \psi = 30°$ .Thus, we will only have the twelfth harmonic in our dc current because the shift angle will be $12\psi = 12 * 30° = 360° = 0$ so the harmonics of the first inverter and the second inverter will add up.

$$i_r(t)_{two-modules} = -\frac{6\hat{I}_7}{5\pi}\cos(12\omega_1 t - \theta_7) - \frac{6\hat{I}_5}{7\pi}\cos(12\omega_1 t - \theta_5)$$

Using three inverter modules (or its multiples)

We will follow the same procedure to have 120 degrees shift in between the sixth harmonic components between the three inverters. So we will use a displacement angle for the first inverter that's $6\psi = 0\ that\ \psi = 0$ and displacement angle for the second inverter $6\psi = 120°\ that\ \psi = 20°$ displacement angle for the third inverter $6\psi = 240°\ that\ \psi = 40°$. An interesting result will appear that the twelfth harmonic is eliminated as well

$$\begin{aligned} i_r(t)_{three-modules} &= -\frac{3\hat{I}_7}{5\pi}\cos(12\omega_1 t - \theta_7) - \frac{3\hat{I}_7}{5\pi}\cos(12\omega_1 t - \theta_7 - 240) - \frac{3\hat{I}_7}{5\pi}\cos(12\omega_1 t - \theta_7 - 120) \\ &- \frac{3\hat{I}_5}{7\pi}\cos(12\omega_1 t - \theta_5) - \frac{3\hat{I}_5}{7\pi}\cos(12\omega_1 t - \theta_5 - 240) - \frac{3\hat{I}_5}{7\pi}\cos(12\omega_1 t - \theta_5 - 120) \\ &= 0 \end{aligned}$$

Which means all harmonics are eliminated by using three modules sequentially displaced among them.

4.2: Pulse width modulation

We are going to follow the same methodology we have done in the square wave modulation with pulse width modulation. Thus, we perform a power balance across an ideal inverter and assuming the dc voltage to be constant V_d. However, the output voltage is pulse width modulated due to the PWM gating technique for the inverter.

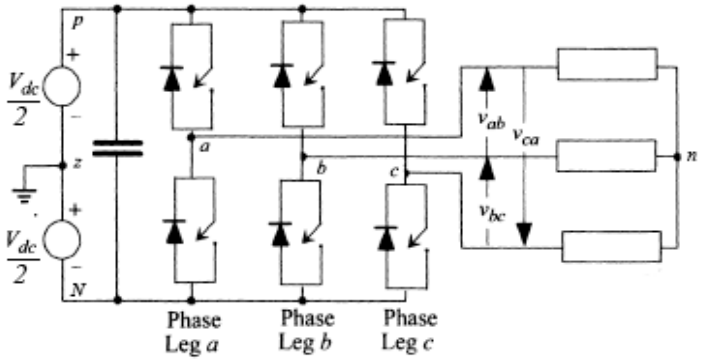

Figure 4-10 Topology of three phase voltage source inverter

We can find the analytical harmonic solution for the double-edge naturally sampled PWM of the three phase inverter in [9], which is presented in Figure 4-10, as follows:

$$v_{az} = \frac{V_d}{2} M \cos(\omega_o t) + \frac{2V_d}{\pi} \sum_{m=1}^{\infty} \sum_{n=-\infty}^{\infty} \frac{1}{m} J_n(m\frac{\pi}{2}M) \sin([m+n]\frac{\pi}{2}) \cos(m\omega_c t + n\omega_o t)$$

$$v_{bz} = \frac{V_d}{2} M \cos(\omega_o t - \frac{2\pi}{3}) + \frac{2V_d}{\pi} \sum_{m=1}^{\infty} \sum_{n=-\infty}^{\infty} \frac{1}{m} J_n(m\frac{\pi}{2}M) \sin([m+n]\frac{\pi}{2}) \cos(m\omega_c t + n[\omega_o t - \frac{2\pi}{3}])$$

$$v_{cz} = \frac{V_d}{2} M \cos(\omega_o t + \frac{2\pi}{3}) + \frac{2V_d}{\pi} \sum_{m=1}^{\infty} \sum_{n=-\infty}^{\infty} \frac{1}{m} J_n(m\frac{\pi}{2}M) \sin([m+n]\frac{\pi}{2}) \cos(m\omega_c t + n[\omega_o t + \frac{2\pi}{3}]) \qquad (4-10)$$

Where v_{az} is the voltage between phase A and the midpoint between the capacitor of the dc side, M is the modulation index, $J_n(x)$ is the Bessel function of order n and argument x, ω_o is the fundamental angular frequency ω_c is the carrier angular frequency which is equal to $\omega_c = m_f * \omega_o$, m is the carrier index and n is the base band index which can be defined in the following;

Harmonic component can be identified $h = m * m_f + n$ which is the expression for the harmonic component if m_f is a multiple of 3 [9].

Breaking down the equations in (4-10) we can find that it consists of a double summation of three separate parts: Bessel function $J_n(m\frac{\pi}{2}M)$, a trigonometric function $\sin([m+n]\frac{\pi}{2})$ and the actual harmonic waveform $\cos(m\omega_c t + n\omega_o t)$.

4.2.1 Trigonometric function $sin([m+n]\frac{\pi}{2})$

This term eliminates the even combinations of $m+n$ of the side band harmonics using that trigonometric function: the results are shown in table 4-3. We will limit our analysis to values of $m = 1,2\ and\ n = 0, \pm1, \pm2, \pm3$.

Table 4-3 *the results of the function* $sin([m+n]\frac{\pi}{2})$ *for m=1, 2 and n=0,*$\pm1, \pm2, \pm3$

$$\sin([m+n]\frac{\pi}{2})$$

m = 1	*n = 0*	1		
	n = 1	0	*n = -1*	0
	n = 2	-1	*n = -2*	-1
	n = 3	0	*n = -3*	0
m = 2	*n = 0*	0		
	n = 1	-1	*n = -1*	1
	n = 2	0	*n = -2*	0
	n = 3	1	*n = -3*	-1

4.2.2 Harmonic order given by $cos(m\omega_c t + n\omega_o\ t)$.

Due to the fact the carrier angular frequency is equal to $\omega_c = m_f * \omega_o$, It can also be written in that way $\cos((m * m_f + n)\omega_o\ t)$. Thus, the harmonic order is given by m and n.

It should be noted that when we need to shift the control voltages of different phases or different inverters, we should return to the original formulation such that $\cos(m\omega_c t + n[\omega_o\ t \pm \theta + \xi])$ where θ is the shift between the phases $\theta = 0, 120, -120$ and ξ is the shift angle between the various modules. The same applies for the carrier signal: when shifting it by an angle ψ_c , it will take the following form $\cos(m[\omega_c t + \psi_c] + n\omega_o\ t)$; where, ψ_c is the phase shift between carrier signals of different inverters.

This leads to the generic formulation of our model for any harmonic

$$\cos(m[\omega_c t + \psi_c] + n[\omega_o\ t \pm \theta + \xi]) \qquad (4-11)$$

4.2.3 Bessel function

The general expression of Bessel function is given by

$$J_n(x) = \sum_{k=0}^{\infty} \frac{(-1)^k (x/2)^{n+2k}}{k!\,(n+k)!} = \frac{(1)(x/2)^n}{(1)(n)!} + \frac{(-1)(x/2)^{n+2}}{(1)(n+1)} + \frac{(1)(x/2)^{n+4}}{2(n+1)(n+2)} + \cdots$$

It can be simplified to the first three terms, taking the argument $x = m\frac{\pi}{2}M$:

$$J_n\left(m\frac{\pi}{2}M\right) = \frac{(m\frac{\pi}{2})^n M^n}{2^n n!} \cdot \left[1 - \frac{(m\frac{\pi}{2})^2 M^2}{2^2(n+1)} + \frac{(m\frac{\pi}{2})^4 M^4}{2^5(n+1)(n+2)}\right]$$

It should be noted that simplified Bessel function is accurate for $M < 1$ Figure 4-11. If the amplitude index is more than 1 we should use the exact expression.

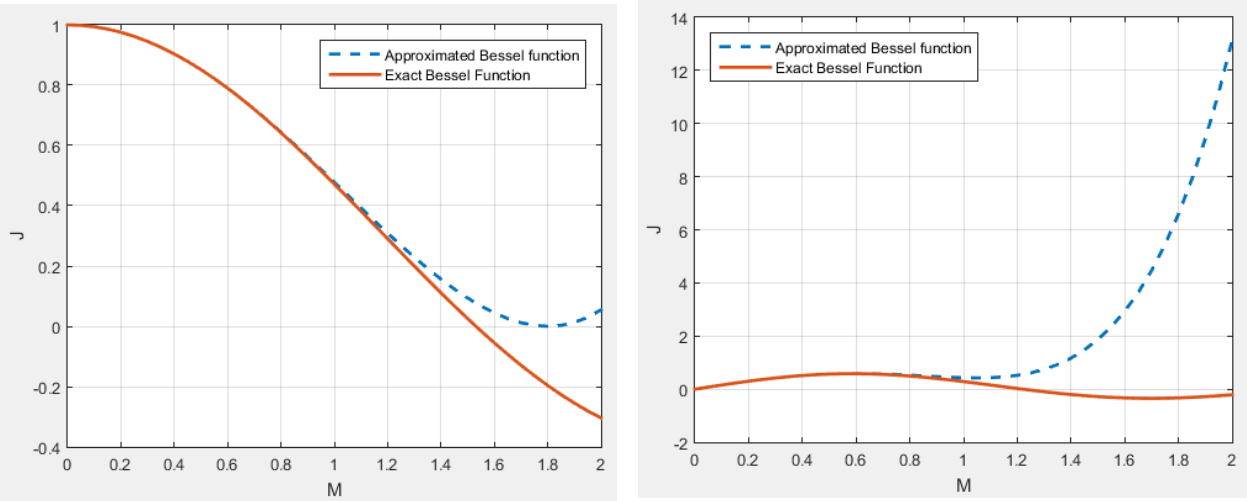

Figure 4-11 Comparison between the exact and approximated Bessel functions as a function of amplitude modulation ratio M a) shows the variation for harmonic order mf b) shows the variation for harmonic order 2mf-1

4.2.4 Pulse width modulated harmonic voltage and current amplitudes

The amplitude of a harmonic voltage component is given by multiplying the $J_n\left(m\frac{\pi}{2}M\right)$ with the coefficients $\frac{1}{m} * \frac{2V_d}{\pi}$ and with trigonometric function $\sin\left([m+n]\frac{\pi}{2}\right)$.The steps of calculating and combining all of these coefficients can be found in the Appendix A1. The results of the voltage amplitudes are presented in Table 4-4.

Table 4-4 Harmonic voltage amplitudes calculated for m=1, 2 and n=0,±1, ±2, ±3

$\hat{V}_1 = \frac{V_d * M}{2}$	$\hat{V}_{mf} = \frac{2\,V_d}{\pi}\left(\frac{512-32\pi^2M^2+\pi^4M^4}{512}\right)$	$m = 1$
$\hat{V}_{mf+2} = \frac{-2\,V_d}{\pi}\left(\frac{(\pi M)^2}{32}.\frac{3072-64\pi^2M^2+\pi^4M^4}{3072}\right)$	$\hat{V}_{mf-2} = \frac{-2\,V_d}{\pi}\left(\frac{(\pi M)^2}{32}.\frac{3072-64\pi^2M^2+\pi^4M^4}{3072}\right)$	
$\hat{V}_{2mf+1} = \frac{-V_d}{\pi}\left(\frac{\pi M}{2}.\frac{96-12\pi^2M^2+\pi^4M^4}{96}\right)$	$\hat{V}_{2mf-1} = \frac{V_d}{\pi}\left(\frac{\pi M}{2}.\frac{96-12\pi^2M^2+\pi^4M^4}{96}\right)$	$m = 2$
$\hat{V}_{2mf+3} = \frac{V_d}{\pi}\left(\frac{(\pi M)^3}{48}.\frac{320-20\pi^2M^2+\pi^4M^4}{320}\right)$	$\hat{V}_{2mf-3} = \frac{V_d}{\pi}\left(\frac{(\pi M)^3}{48}.\frac{320-20\pi^2M^2+\pi^4M^4}{320}\right)$	

The current amplitudes can be easily calculated by dividing the voltage amplitude by its impedance and as for the waveforms the currents will be shifted from the voltage by the impedance angle. These are shown in Table 4-5.

Current Amplitudes:

Table 4-5 Harmonic current amplitudes and the angle between the current and voltages for m=1, 2 and n=0,±1, ±2, ±3

$\hat{I}_1 = \frac{\sqrt{(VAn - E\cos\delta)^2 + (E\sin\delta)^2}}{\sqrt{R^2 + (\omega L)^2}}$ (see table 4.1)	$\phi = \tan^{-1}\left(\frac{\omega_o L}{R}\right) - \tan^{-1}\left(\frac{E\sin\delta}{vAn - E\cos\delta}\right)$
$\hat{I}_{mf} = \frac{\hat{V}mf}{\sqrt{R^2 + (mf\,\omega_o L)^2}}$	$\theta_{mf} = \tan^{-1}\left(mf\,\frac{\omega_o L}{R}\right)$
$\hat{I}_{mf-2} = \frac{Vmf-2}{\sqrt{R^2 + ((mf-2)\,\omega_o L)^2}}$	$\theta_{mf-2} = \tan^{-1}\left(\frac{(mf-2)\,\omega_o L}{R}\right)$
$\hat{I}_{mf+2} = \frac{\hat{V}mf+2}{\sqrt{R^2 + ((mf-2)\,\omega_o L)^2}}$	$\theta_{mf+2} = \tan^{-1}\left(\frac{(mf+2)\,\omega_o L}{R}\right)$
$\hat{I}_{2mf+1} = \frac{\hat{V}2mf+1}{\sqrt{R^2 + ((2mf+1)\,\omega_o L)^2}}$	$\theta_{2mf+1} = \tan^{-1}\left(\frac{(2mf+1)\,\omega_o L}{R}\right)$
$\hat{I}_{2mf-1} = \frac{\hat{V}2mf-1}{\sqrt{R^2 + ((2mf-1)\,\omega_o L)^2}}$	$\theta_{2mf-1} = \tan^{-1}\left(\frac{(2mf-1)\,\omega_o L}{R}\right)$
$\hat{I}_{2mf+3} = \frac{\hat{V}2mf+3}{\sqrt{R^2 + ((2mf+3)\,\omega_o L)^2}}$	$\theta_{2mf+3} = \tan^{-1}\left(\frac{(2mf+3)\,\omega_o L}{R}\right)$
$\hat{I}_{2mf-3} = \frac{\hat{V}2mf-3}{\sqrt{R^2 + ((2mf-3)\,\omega_o L)^2}}$	$\theta_{2mf-3} = \tan^{-1}\left(\frac{(2mf-3)\,\omega_o L}{R}\right)$

4.2.5 Generic expression for the currents and voltages on the ac side of the inverter:

After calculating the amplitudes of both currents and voltages we can write the general expression of both of them as function of time and the generic shift angles we want to introduce according to equation [4-7]. These are represented in the following:

$$\boldsymbol{v_{az}}(t) = \hat{V}_1 \cos\ (\omega_o t + \xi)$$
$$+\hat{V}_{mf-2} \cos(\omega_c t + \psi_c - 2\,\omega_o t - 2\xi)$$
$$+\hat{V}_{mf} \cos(\omega_c t + \psi_c)$$
$$+\hat{V}_{mf+2} \cos(\omega_c t + \psi_c + 2\,\omega_o t + 2\xi)$$
$$+\hat{V}_{2mf-3} \cos(2\omega_c t + 2\,\psi_c - 3\,\omega_o t - 3\xi)$$
$$+\hat{V}_{2mf-1} \cos(2\omega_c t + 2\,\psi_c - \omega_o t - \xi)$$
$$+\hat{V}_{2mf+1} \cos(2\omega_c t + 2\,\psi_c + \omega_o t + \xi)$$
$$+\hat{V}_{2mf+3} \cos(2\omega_c t + 2\,\psi_c + 3\omega_o t + 3\xi)$$

$n = -2$, $n = 0$, $n = +2$ → $m = 1$

$n = -3$, $n = -1$, $n = +1$, $n = +3$ → $m = 2$

$$\boldsymbol{v_{bz}}(t) = \hat{V}_1 \cos\left(\omega_o t + \xi - \frac{2\pi}{3}\right) + \hat{V}_{mf-2} \cos\left(\omega_c t + \psi_c - 2\omega_o t - 2\xi + \frac{4\pi}{3}\right) + \hat{V}_{mf} \cos(\omega_c t + \psi_c) +$$
$$\hat{V}_{mf+2} \cos\left(\omega_c t + \psi_c + 2\omega_o\, t + 2\xi - \frac{4\pi}{3}\right) + \hat{V}_{2mf-3} \cos(2\omega_c t + 2\psi_c - 3\omega_o\, t - 3\xi) +$$
$$\hat{V}_{2mf-1} \cos\left(2\omega_c t + 2\psi_c - \omega_o\, t - \xi + \frac{2\pi}{3}\right) + \hat{V}_{2mf+1} \cos\left(2\omega_c t + 2\psi_c + \omega_o\, t + \xi - \frac{2\pi}{3}\right) +$$
$$\hat{V}_{2mf+3} \cos(2\omega_c t + 2\psi_c + 3\omega_o\, t + 3\xi)$$

$$\boldsymbol{v_{cz}}(t) = \hat{V}_1 \cos\left(\omega_o\, t + \xi + \frac{2\pi}{3}\right) + \hat{V}_{mf-2} \cos\left(\omega_c t + \psi_c - 2\,\omega_o\, t - 2\xi - \frac{4\pi}{3}\right) + \hat{V}_{mf} \cos(\omega_c t + \psi_c) +$$
$$\hat{V}_{mf+2} \cos\left(\omega_c t + \psi_c + 2\,\omega_o t + 2\xi + \frac{4\pi}{3}\right) + \hat{V}_{2mf-3} \cos(2\omega_c t + 2\psi_c - 3\omega_o\, t - 3\xi) +$$
$$\hat{V}_{2mf-1} \cos\left(2\omega_c t + 2\psi_c - \omega_o\, t - \xi - \frac{2\pi}{3}\right) + \hat{V}_{2mf+1} \cos\left(2\omega_c t + 2\psi_c + \omega_o\, t + \xi + \frac{2\pi}{3}\right) +$$
$$\hat{V}_{2mf+3} \cos\ (2\omega_c t + 2\psi_c + 3\omega_o\, t + 3\xi)$$

In order to understand the current flowing in the load, we have to calculate voltages to the neutral point of the load.

$$\boldsymbol{v_{an}}(t) = \frac{2}{3} v_{az} - \frac{v_{bz}}{3} - \frac{v_{cz}}{3} = v_{az} - \frac{v_{az} + v_{bz} + v_{cz}}{3}$$

$$\boldsymbol{v_{bn}}(t) = \frac{2}{3} v_{bz} - \frac{v_{az}}{3} - \frac{v_{cz}}{3} = v_{bz} - \frac{v_{az} + v_{bz} + v_{cz}}{3}$$

$$\boldsymbol{v_{cn}}(t) = \frac{2}{3} v_{cz} - \frac{v_{az}}{3} - \frac{v_{bz}}{3} = v_{cz} - \frac{v_{az} + v_{bz} + v_{cz}}{3}$$

Where “n” is the neutral point of the load shown in figure 4-10.

$$
\begin{aligned}
\boldsymbol{v_{an}}(t) = \frac{2}{3}v_{az} - \frac{v_{bz}}{3} - \frac{v_{cz}}{3} = v_{az} - \frac{v_{az}+v_{bz}+v_{cz}}{3} \\
&= V_1\cos(\omega_o t+\xi) + V_{mf-2}\cos(\omega_c t+\psi_c-2\omega_o t-2\xi) + V_{mf}\cos(\omega_c t+\psi_c) \\
&+ V_{mf+2}\cos(\omega_c t+\psi_c+2\omega_o t+2\xi) + V_{2mf-3}\cos(2\omega_c t+2\psi_c-3\omega_o t-3\xi) \\
&+ V_{2mf-1}\cos(2\omega_c t+2\psi_c-\omega_o t-\xi) + V_{2mf+1}\cos(2\omega_c t+2\psi_c+\omega_o t+\xi) \\
&+ V_{2mf+3}\cos(2\omega_c t+2\psi_c+3\omega_o t+3\xi) \\
&- \left[\frac{V_1}{3}\left(\cos(\omega_o t+\xi)+\cos\left(\omega_o t+\xi-\frac{2\pi}{3}\right)+\cos\left(\omega_o t+\xi+\frac{2\pi}{3}\right)\right)\right. \\
&+ \frac{V_{mf-2}}{3}\left(\cos(\omega_c t+\psi_c-2\omega_o t-2\xi)+\cos\left(\omega_c t+\psi_c-2\omega_o t-2\xi+\frac{4\pi}{3}\right)\right. \\
&\left.+\cos\left(\omega_c t+\psi_c-2\omega_o t-2\xi-\frac{4\pi}{3}\right)\right) \\
&+ \frac{V_{mf}}{3}(\cos(\omega_c t+\psi_c)+\cos(\omega_c t+\psi_c)+\cos(\omega_c t+\psi_c)) \\
&+ \frac{V_{mf+2}}{3}\left(\cos(\omega_c t+\psi_c+2\omega_o t+2\xi)+\cos\left(\omega_c t+\psi_c+2\omega_o t+2\xi-\frac{4\pi}{3}\right)\right. \\
&\left.+\cos\left(\omega_c t+\psi_c+2\omega_o t+2\xi+\frac{4\pi}{3}\right)\right) \\
&+ \frac{V_{2mf-3}}{3}(\cos(2\omega_c t+2\psi_c-3\omega_o t-3\xi)+\cos(2\omega_c t+2\psi_c-3\omega_o t-3\xi) \\
&+\cos(2\omega_c t+2\psi_c-3\omega_o t-3\xi)) \\
&+ \frac{V_{2mf-1}}{3}\left(\cos(2\omega_c t+2\psi_c-\omega_o t-\xi)+\cos\left(2\omega_c t+2\psi_c-\omega_o t-\xi+\frac{2\pi}{3}\right)\right. \\
&\left.+\cos\left(2\omega_c t+2\psi_c-\omega_o t-\xi-\frac{2\pi}{3}\right)\right) \\
&+ \frac{V_{2mf+1}}{3}\left(\cos(2\omega_c t+2\psi_c+\omega_o t+\xi)+\cos\left(2\omega_c t+2\psi_c+\omega_o t+\xi-\frac{2\pi}{3}\right)\right. \\
&\left.+\cos\left(2\omega_c t+2\psi_c+\omega_o t+\xi+\frac{2\pi}{3}\right)\right) \\
&+ \frac{V_{2mf+3}}{3}(\cos(2\omega_c t+2\psi_c+3\omega_o t+3\xi)+\cos(2\omega_c t+2\psi_c+3\omega_o t+3\xi) \\
&\left.+\cos(2\omega_c t+2\psi_c+3\omega_o t+3\xi))\right]
\end{aligned}
\qquad (4-12)
$$

Voltages $\boldsymbol{v_{bn}}(t)$ and $\boldsymbol{v_{cn}}(t)$ will have similar expressions derived in the same manner as (4-12).

It can be noticed from (4-12) that voltages $V_{mf}, V_{2mf-3}, V_{2mf+3}$ will cancel out due to the neutral point "n". That means the corresponding currents for these harmonics $I_{mf}, I_{2mf-3}, I_{2mf+3}$ will not flow and will not be present in the harmonic equation of the current.

The current harmonic equation will have the same formulation of the voltages but with an angle delay due to the impedance.

$$
\begin{aligned}
\boldsymbol{i_a}(t) = \hat{I_1}\cos(\omega_o t+\xi-\phi) + \hat{I}_{mf-2}\cos(\omega_c t+\psi_c-2\omega_o t-2\xi-\theta_{mf-2}) \\
&+ \hat{I}_{mf+2}\cos(\omega_c t+\psi_c+2\omega_o t+2\xi-\theta_{mf+2}) \\
&+ \hat{I}_{2mf-1}\cos(2\omega_c t+2\psi_c-\omega_o t-\xi-\theta_{2mf-1}) \\
&+ \hat{I}_{2mf+1}\cos(2\omega_c t+2\psi_c+\omega_o t+\xi-\theta_{2mf+1})
\end{aligned}
$$

For the other phases will have the same formulation but with a shift of $120\ and\ -120$ respectively.

It should be pointed out that the phase shift between phases, ± 120, is multiplied by n as mentioned before in (4-7) that's why we can see that the shift changes from $+120\ to\ +240$

$$\begin{aligned}
\boldsymbol{i_b}(t) = {} & \hat{I_1}\cos\left(\omega_o t + \xi - \phi - \frac{2\pi}{3}\right) + \hat{I}_{mf-2}\cos\left(\omega_c t + \psi_c - 2\,\omega_o t - 2\xi - \theta_{mf-2} + \frac{4\pi}{3}\right) \\
& + \hat{I}_{mf+2}\cos\left(\omega_c t + \psi_c + 2\,\omega_o t + 2\xi - \theta_{mf+2} - \frac{4\pi}{3}\right) \\
& + \hat{I}_{2mf-1}\cos\left(2\omega_c t + 2\psi_c - \omega_o t - \xi - \theta_{2mf-1} + \frac{2\pi}{3}\right) \\
& + \hat{I}_{2mf+1}\cos\left(2\omega_c t + 2\psi_c + \omega_o t + \xi - \theta_{2mf+1} - \frac{2\pi}{3}\right) \\
\boldsymbol{i_c}(t) = {} & \hat{I_1}\cos\left(\omega_o t + \xi - \phi + \frac{2\pi}{3}\right) \\
& + \hat{I}_{mf-2}\cos\left(\omega_c t + \psi_c - 2\,\omega_o t - 2\xi - \theta_{mf-2} - \frac{4\pi}{3}\right) \\
& + \hat{I}_{mf+2}\cos\left(\omega_c t + \psi_c + 2\,\omega_o t + 2\xi - \theta_{mf+2} + \frac{4\pi}{3}\right) \\
& + \hat{I}_{2mf-1}\cos\left(2\omega_c t + 2\psi_c - \omega_o t - \xi - \theta_{2mf-1} - \frac{2\pi}{3}\right) \\
& + \hat{I}_{2mf+1}\cos\left(2\omega_c t + 2\psi_c + \omega_o t + \xi - \theta_{2mf+1} + \frac{2\pi}{3}\right)
\end{aligned} \qquad (4-13)$$

4.2.6 Instantaneous dc current ripple expression development:

The same methodology presented earlier in square wave modulation in section 4.1.4 will be followed; If two components of voltages and currents of the same harmonic order are multiplied, they will add to the constant dc component of $i_{dc}(t)$, while the interaction between different harmonic orders will result in the ripple component of the dc current.

$$V_d.\,i_{dc}(t) = V_d[\,I_{dc} + i_r(t)] = i_A(t).\,v_{An}(t) + i_B(t).\,v_{Bn}(t) + i_c(t).\,v_{cn}(t)$$

Dc component of the expression of the dc side current I_{dc} :

$$\begin{aligned}
I_{dc} = {} & \frac{3\,\hat{V}_1\hat{I}_1}{V_d}\cos\phi + \frac{3\hat{V}_{mf-2}\hat{I}_{mf-2}}{V_d}\cos\left(\theta_{mf-2}\right) + \frac{3\hat{V}_{mf+2}\hat{I}_{mf+2}}{V_d}\cos\left(\theta_{mf+2}\right) \\
& + \frac{3\hat{V}_{2mf-1}\hat{I}_{2mf-1}}{V_d}\cos\left(\theta_{2mf-1}\right) + \frac{3\hat{V}_{2mf+1}\hat{I}_{2mf+1}}{V_d}\cos\left(\theta_{2mf+1}\right)
\end{aligned}$$

Ripple component of the expression of the dc side current $i_r(t)$ **:**

As it is mentioned earlier, it's due to the interaction between voltages and currents of different harmonic orders.

As an example let's see the interaction between the fundamental voltage and the current of harmonic order $mf - 2$

$$\frac{v_{An_1} i_{A_{mf-2}}}{V_d} = [\frac{1}{V_d}][\hat{V}_1 \cos\ (\omega_o t + \xi)] * [\hat{I}_{mf-2} \cos(\omega_c t + \psi_c - 2\,\omega_o t - 2\xi - \theta_{mf-2})]$$

And from the trigonometric function $\cos a \cos b = \frac{1}{2}(\cos(a+b) + \cos(a-b))$ we can expand the expression as follows

$$\frac{v_{An_1} i_{A_{mf-2}}}{V_d} = \frac{\hat{V}_1 \hat{I}_{mf-2}}{2V_d}\left(cos\ (\omega_c t + \psi_c - \omega_o\, t - \xi - \theta_{mf-2}) + cos(\omega_c t + \psi_c - 3\,\omega_o\, t - 3\xi - \theta_{mf-2})\right)$$

Similarly we can find the expressions for the rest of the phases

$$\frac{v_{Bn_1} i_{B_{mf-2}}}{V_d} = \frac{\hat{V}_1 \hat{I}_{mf-2}}{2V_d}\left(cos\ (\omega_c t + \psi_c - \omega_o\, t - \xi - \theta_{mf-2} + \frac{2\pi}{3}) + cos(\omega_c t + \psi_c - 3\,\omega_o\, t - 3\xi - \theta_{mf-2})\right)$$

$$\frac{v_{Cn_1} i_{C_{mf-2}}}{V_d} = \frac{\hat{V}_1 \hat{I}_{mf-2}}{2V_d}\left(cos\ (\omega_c t + \psi_c - \omega_o\, t - \xi - \theta_{mf-2} - \frac{2\pi}{3}) + cos(\omega_c t + \psi_c - 3\,\omega_o\, t - 3\xi - \theta_{mf-2})\right)$$

Looking closely at the equations by the addition of the components of the three phases, we will find one of the harmonics will disappear due to the shift of ± 120 while the other will add up to three times the component of one phase

$$\frac{\hat{V}_1 \hat{I}_{mf-2}}{2V_d}[(cos\ (\omega_c t + \psi_c - \omega_o\, t - \xi - \theta_{mf-2}) + (\ cos\ (\omega_c t + \psi_c - \omega_o\, t - \xi - \theta_{mf-2} + \frac{2\pi}{3}) + (\ cos\ (\omega_c t + \psi_c - \omega_o\, t - \xi - \theta_{mf-2} - \frac{2\pi}{3}))] = 0$$

$$\frac{\hat{V}_1 \hat{I}_{mf-2}}{2V_d}[\ cos(\omega_c t + \psi_c - 3\,\omega_o\, t - 3\xi - \theta_{mf-2}) + cos(\omega_c t + \psi_c - 3\,\omega_o\, t - 3\xi - \theta_{mf-2}) + cos(\omega_c t + \psi_c - 3\,\omega_o\, t - 3\xi - \theta_{mf-2}) = \frac{3\hat{V}_1 \hat{I}_{mf-2}}{2V_d} cos(\omega_c t + \psi_c - 3\,\omega_o\, t - 3\xi - \theta_{mf-2})$$

The interaction between the rest of the voltages and currents can be found in appendix A1.

By summing up all the harmonic components of all interactions of all phases we end up by the generic expression of the ripple content of the dc current.

$$
\begin{aligned}
i_r(t) = {} & \frac{3\hat{V}_1\hat{I}_{mf-2}}{2V_d}\cos\left((m_f-3)\omega_o\,t+\psi_c-3\xi-\theta_{mf-2}\right)\\
& +\frac{3\hat{V}_1\hat{I}_{mf+2}}{2V_d}\cos\left((m_f+3)\omega_o\,t+\psi_c+3\xi-\theta_{mf+2}\right)\\
& +\frac{3\hat{V}_1\hat{I}_{2mf-1}}{2V_d}\cos\left((2m_f)\omega_o\,t+2\psi_c-\theta_{2mf-1}\right)\\
& +\frac{3\hat{V}_1\hat{I}_{2mf+1}}{2V_d}\cos\left((2m_f)\omega_o\,t+2\psi_c-\theta_{2mf+1}\right)\\
& +\frac{3\hat{V}_{mf-2}\hat{I}_1}{2V_d}\cos\left((m_f-3)\omega_o\,t+\psi_c-3\xi+\phi\right)\\
& +\frac{3\hat{V}_{mf-2}\hat{I}_{mf+2}}{2V_d}\cos\left((2m_f)\omega_o\,t+2\psi_c-\theta_{mf+2}\right)\\
& +\frac{3\hat{V}_{mf-2}\hat{I}_{2mf-1}}{2V_d}\cos\left((3m_f-3)\omega_o\,t+3\psi_c-3\xi-\theta_{2mf-1}\right)\\
& +\frac{3\hat{V}_{mf-2}\hat{I}_{2mf+1}}{2V_d}\cos\left((m_f+3)\omega_o\,t+\psi_c+3\xi-\theta_{2mf+1}\right)\\
& +\frac{3\hat{V}_{mf+2}\hat{I}_1}{2V_d}\cos\left((m_f+3)\omega_o\,t+\psi_c+3\xi-\phi\right)\\
& +\frac{3\hat{V}_{mf+2}\hat{I}_{mf-2}}{2V_d}\cos\left((2m_f)\omega_o\,t+2\psi_c-\theta_{mf-2}\right)\\
& +\frac{3\hat{V}_{mf+2}\hat{I}_{2mf-1}}{2V_d}\cos\left((m_f-3)\omega_o\,t+\psi_c-3\xi-\theta_{2mf-1}\right)\\
& +\frac{3\hat{V}_{mf+2}\hat{I}_{2mf+1}}{2V_d}\cos\left((3m_f+3)\omega_o\,t+3\psi_c+3\xi-\theta_{2mf+1}\right)\\
& +\frac{3\hat{V}_{2mf-1}\hat{I}_1}{2V_d}\cos\left((2m_f)\omega_o\,t+2\psi_c-\phi\right)\\
& +\frac{3\hat{V}_{2mf-1}\hat{I}_{mf-2}}{2V_d}\cos\left((3m_f-3)\omega_o\,t+3\psi_c-3\xi-\theta_{mf-2}\right)\\
& +\frac{3\hat{V}_{2mf-1}\hat{I}_{mf+2}}{2V_d}\cos\left((m_f-3)\omega_o\,t+\psi_c-3\xi+\theta_{mf+2}\right)\\
& +\frac{3\hat{V}_{2mf-1}\hat{I}_{2mf+1}}{2V_d}\cos\left((4m_f)\omega_o\,t+4\psi_c-\theta_{2mf+1}\right)\\
& +\frac{3\hat{V}_{2mf+1}\hat{I}_1}{2V_d}\cos\left((2m_f)\omega_o\,t+2\psi_c+\phi\right)\\
& +\frac{3\hat{V}_{2mf+1}\hat{I}_{mf-2}}{2V_d}\cos\left((m_f+3)\omega_o\,t+\psi_c+3\xi+\theta_{mf-2}\right)\\
& +\frac{3\hat{V}_{2mf+1}\hat{I}_{mf+2}}{2V_d}\cos\left((3m_f+3)\omega_o\,t+3\psi_c+3\xi-\theta_{mf+2}\right)\\
& +\frac{3\hat{V}_{2mf+1}\hat{I}_{2mf-1}}{2V_d}\cos\left((4m_f)\omega_o\,t+4\psi_c-\theta_{2mf-1}\right) \qquad (4-14)
\end{aligned}
$$

Equation (4-14) can be summarized in the Table 4-6:

Table 4-6 Summary of the equation [4-14] which is the generic expression for the ripples in the dc side current

h	Amplitude*(3/(2V_d))	Shift in the carrier signal of angular frequency ω_c	Shift in the control signal of angular frequency ω_o
$m_f - 3$	$V_1 I_{mf-2}$ $V_{mf-2} I_1$ $V_{mf+2} I_{2mf-1}$ $V_{2mf-1} I_{mf+2}$	ψ_c	-3ξ
$m_f + 3$	$V_1 I_{mf+2}$ $V_{mf+2} I_1$ $V_{mf-2} I_{2mf+1}$ $V_{2mf+1} I_{mf-2}$	ψ_c	3ξ
$3m_f - 3$	$V_{mf-2} I_{2mf-1}$ $V_{2mf-1} I_{mf-2}$	$3\psi_c$	-3ξ
$2m_f$	$V_1 I_{2mf-1}$ $V_{2mf-1} I_1$ $V_1 I_{2mf+1}$ $V_{2mf+1} I_1$ $V_{mf-2} I_{mf+2}$ $V_{mf+2} I_{mf-2}$	$2\psi_c$	-
$3m_f + 3$	$V_{mf+2} I_{2mf+1}$ $V_{2mf+1} I_{mf+2}$	$3\psi_c$	3ξ
$4m_f$	$V_{2mf-1} I_{2mf+1}$ $V_{2mf+1} I_{2mf-1}$	$4\psi_c$	-

From the table 4-6 we can deduce that certain harmonics can be eliminated by shifting the triangular signals of different pwm signals to different inverters using the same methodology mentioned in section 4.1.4, Adding two sinusoidal waveforms shifted in time by half of its cycle will result in the elimination of such harmonic content (Figure 4-9). Also adding three sinusoidal waveforms shifted from each other by 120 degrees will have a null summation.

Using two inverter modules (or its multiples)

If we choose to eliminate the harmonic component $(m_f - 3)$ because it's the lowest order harmonic, we will use a displacement angle $\psi_c = 0$ for the first inverter and $\psi_c = 180$ for the second inverter. Using these displacement angles between the two modules triangular waveforms will also eliminate the harmonic components of $m_f + 3\ and\ 3m_f \pm 3$. Thus the expression of the dc current ripple have only $2m_f\ and\ 4m_f$ components shown in (4-15).

$$
\begin{aligned}
i_r(t)_{two-mod} = & \frac{6\hat{V}_1\hat{I}_{2mf-1}}{2V_d}\cos\left((2m_f)\omega_o\,t + 2\psi_c - \theta_{2mf-1}\right) \\
& + \frac{6\hat{V}_1\hat{I}_{2mf+1}}{2V_d}\cos\left((2m_f)\omega_o\,t + 2\psi_c - \theta_{2mf+1}\right) \\
& + \frac{6\hat{V}_{mf-2}\hat{I}_{mf+2}}{2V_d}\cos\left((2m_f)\omega_o\,t + 2\psi_c - 3\xi - \theta_{mf+2}\right) \\
& + \frac{6\hat{V}_{mf+2}\hat{I}_{mf-2}}{2V_d}\cos\left((2m_f)\omega_o\,t + 2\psi_c - \theta_{mf-2}\right) \\
& + \frac{6\hat{V}_{2mf-1}\hat{I}_1}{2V_d}\cos\left((2m_f)\omega_o\,t + 2\psi_c - \phi\right) \\
& + \frac{6\hat{V}_{2mf-1}\hat{I}_{2mf+1}}{2V_d}\cos\left((4m_f)\omega_o\,t + 4\psi_c - \theta_{2mf+1}\right) \\
& + \frac{6\hat{V}_{2mf+1}\hat{I}_1}{2V_d}\cos\left((2m_f)\omega_o\,t + 2\psi_c + \phi\right) \\
& + \frac{6\hat{V}_{2mf+1}\hat{I}_{2mf-1}}{2V_d}\cos\left((4m_f)\omega_o\,t + 4\psi_c - \theta_{2mf-1}\right) \qquad (4-15)
\end{aligned}
$$

Using three inverter modules (or its multiples)

We will follow the same procedure to have ±120 degrees shift between the harmonic components of order $(m_f - 3)$ because it's the lowest order harmonic component, We will use displacement angles for the inverters such that $\psi_c = 0$ for the first inverter, $\psi_c = 120$ for the second inverter and $\psi_c = 240$ for the third inverter. Using these displacement angles between the three modules triangular waveforms will also eliminate the harmonic components of $m_f + 3$, $2m_f$, $4m_f$. Thus the expression of the dc current ripple have only $3m_f \pm 3$ and is shown in (4-16).

$$
\begin{aligned}
i_r(t)_{three-mod} = & \frac{9\hat{V}_{mf-2}\hat{I}_{2mf-1}}{2V_d}\cos\left((3m_f - 3)\omega_o\,t + 3\psi_c - 3\xi - \theta_{2mf-1}\right) \\
& + \frac{9\hat{V}_{mf-2}\hat{I}_{2mf+1}}{2V_d}\cos\left((3m_f + 3)\omega_o\,t + \psi_c + 3\xi - \theta_{2mf+1}\right) \\
& + \frac{9\hat{V}_{mf+2}\hat{I}_{2mf-1}}{2V_d}\cos\left((3m_f - 3)\omega_o\,t + \psi_c - 3\xi - \theta_{2mf-1}\right) \\
& + \frac{9\hat{V}_{mf+2}\hat{I}_{2mf+1}}{2V_d}\cos\left((3m_f + 3)\omega_o\,t + 3\psi_c + 3\xi - \theta_{2mf+1}\right) \\
& + \frac{9\hat{V}_{2mf-1}\hat{I}_{mf-2}}{2V_d}\cos\left((3m_f - 3)\omega_o\,t + 3\psi_c - 3\xi - \theta_{mf-2}\right) \\
& + \frac{9\hat{V}_{2mf+1}\hat{I}_{mf+2}}{2V_d}\cos\left((3m_f + 3)\omega_o\,t + 3\psi_c + 3\xi - \theta_{mf+2}\right) \qquad (4-16)
\end{aligned}
$$

4.3: Expression validation using Matlab/Simulink for PWM:

4.3.1: PWM model

It is done by the comparison of a triangular waveform with the sinusoidal waveform of 3 phase shifted by 120 degrees (Figure 4.11, 4.12) in order to generate the gating pulses for the 6 IGBT switches of the 3 legs of the 3 phase inverters. (Figure 4.13)

For each leg, the pulses of the “upper switch” is complement to the “lower switch” in order not to short circuit the branch. (Figure 4.14)

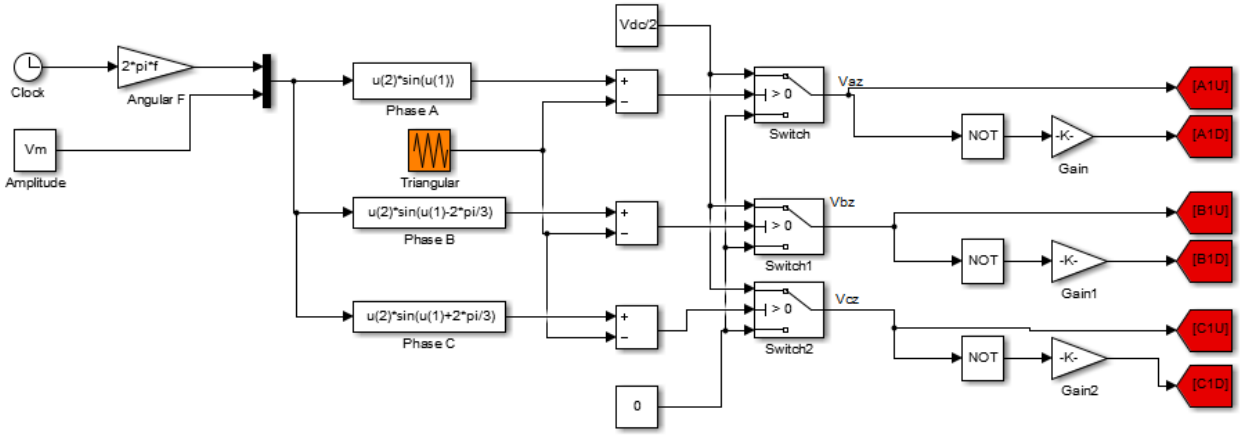

Figure 4-12 PWM generation of 3 phase inverter

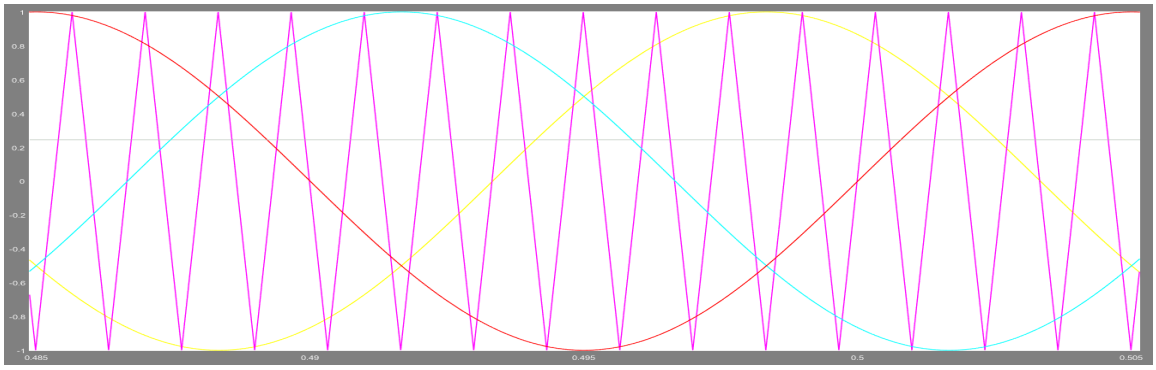

Figure 4-13 a three phase signal with a triangular of m_f=15 and m_a=1

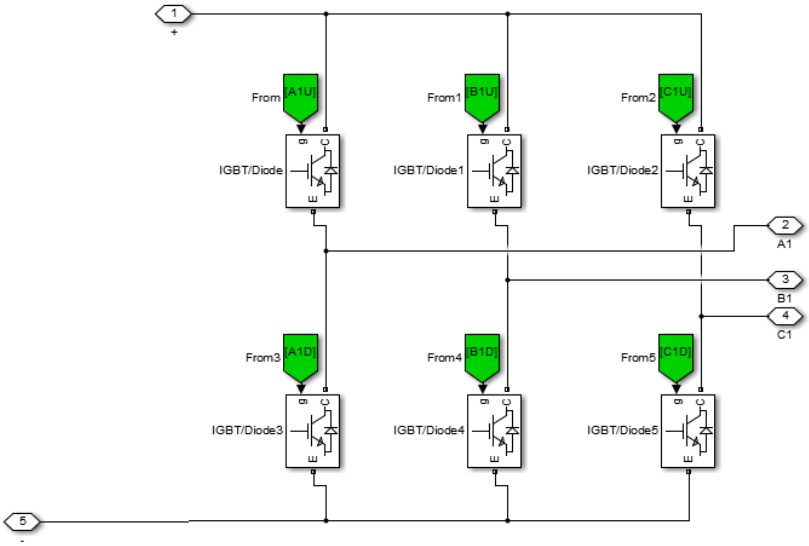

Figure 4-14 model for 3 phase inverter

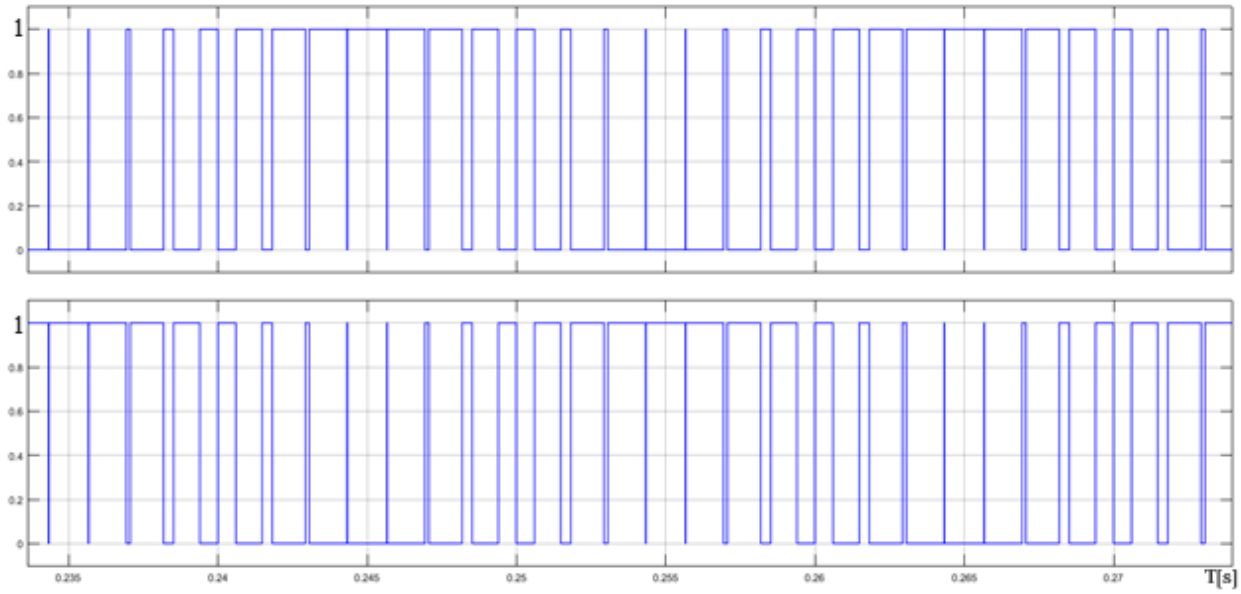

Figure 4-15 Complement gating signals for leg A (A1U&A1D) generated by the PWM model

4.3.2: Single Inverter model

The model is supplied in the practical life from a capacitor that stabilizes the voltage of the dc bus, Assuming its voltage is kept constant, it can be modelled as a DC source. A first test is carried out by supplying a 3 phase resistive load: we can see the current harmonics produced on the dc side due to the switching of the IGBTs in the inverter (Figure 4.15). All the harmonic components will be repeated in per unit values referred to the dc component.

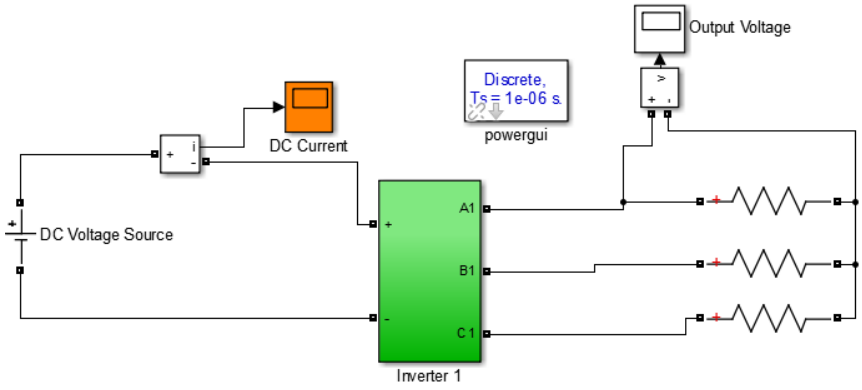

Figure 4-16 Model for a single inverter

According to the equation derived in section 4.2.6 we can deduce the harmonic content of the dc side ripple which is presented in table 4-6. As the m_f chosen for this preliminary analysis is 15, thus the harmonics will be of the order $h = 12, 18, 30, 42, 48, 60$ as shown in Table 4-7.

Table 4-7 harmonic components of the dc side current as well as the torque for mf=15

$\boldsymbol{mf-3}$	**12**
$\boldsymbol{mf+3}$	18
$\boldsymbol{2mf}$	30
$\boldsymbol{3mf-3}$	42
$\boldsymbol{3mf+3}$	48
$\boldsymbol{4mf}$	60

From the FFT analysis we can obtain the harmonics of the dc side current. (Figure 4.16)

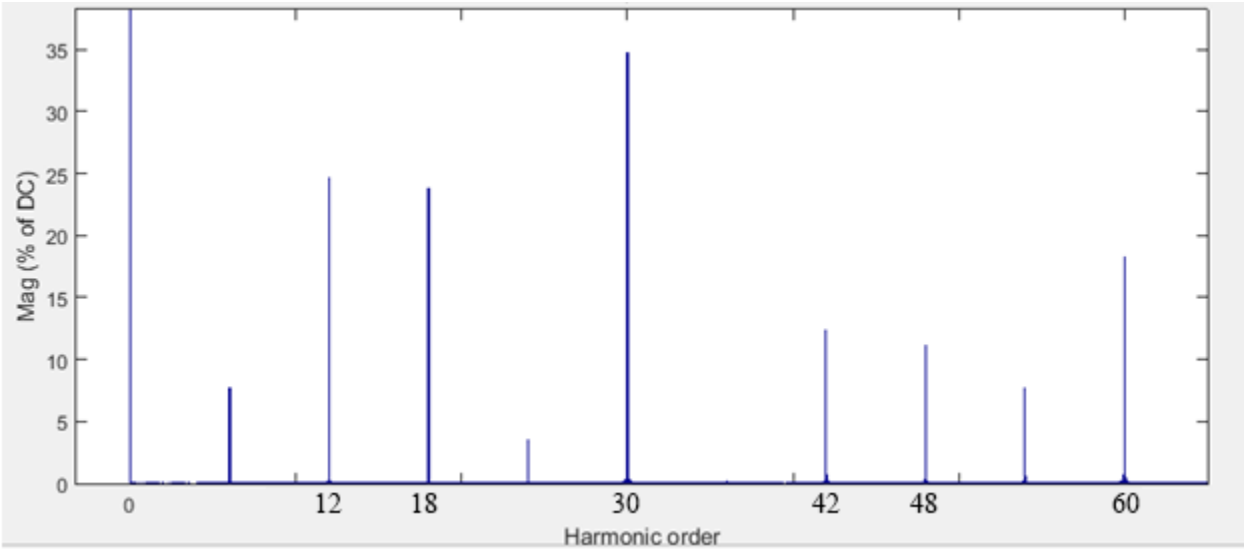

Figure 4-17 FFT analysis of the dc side current of the single module inverter controlled using PWM modulation with mf=15

As it can be noticed there are further harmonic components appearing in the fft analysis and that's because in the expression of the Bessel function (Appendix A1) we only considered $n = 0, \pm1, \pm2, \pm3$ and if the same derivation is done for more values of n we will obtain all the harmonic components in the harmonic Spectrum.

4.3.3: Two Inverter model whose triangular waveform is displaced by 180°

Shifting the triangular signal from one module to the other with a Transport delay block (Figure 4-17) in Simulink by an angle equal to 180 degrees or half the period of the triangular waveform ($T_c/2$) will result to different gating signals of the inverter 1.

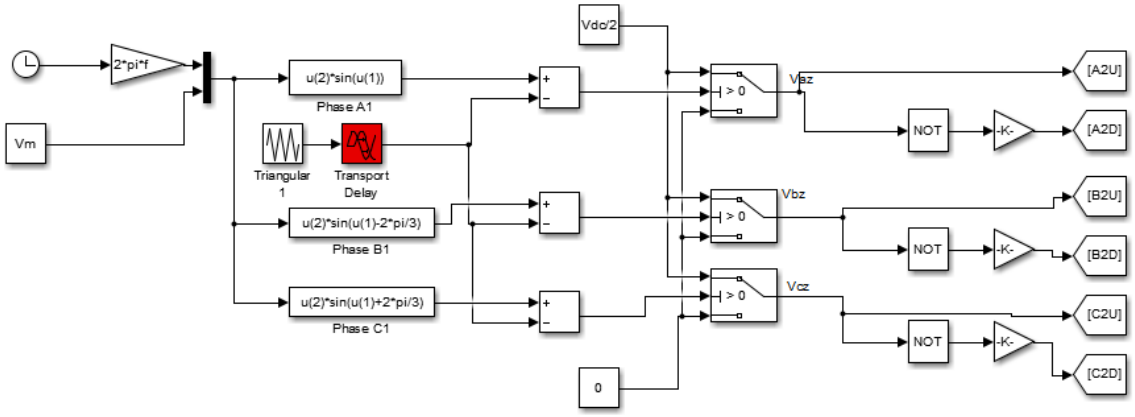

Figure 4-18 the PWM pulse generator for the second module shifted by $T_c/2$

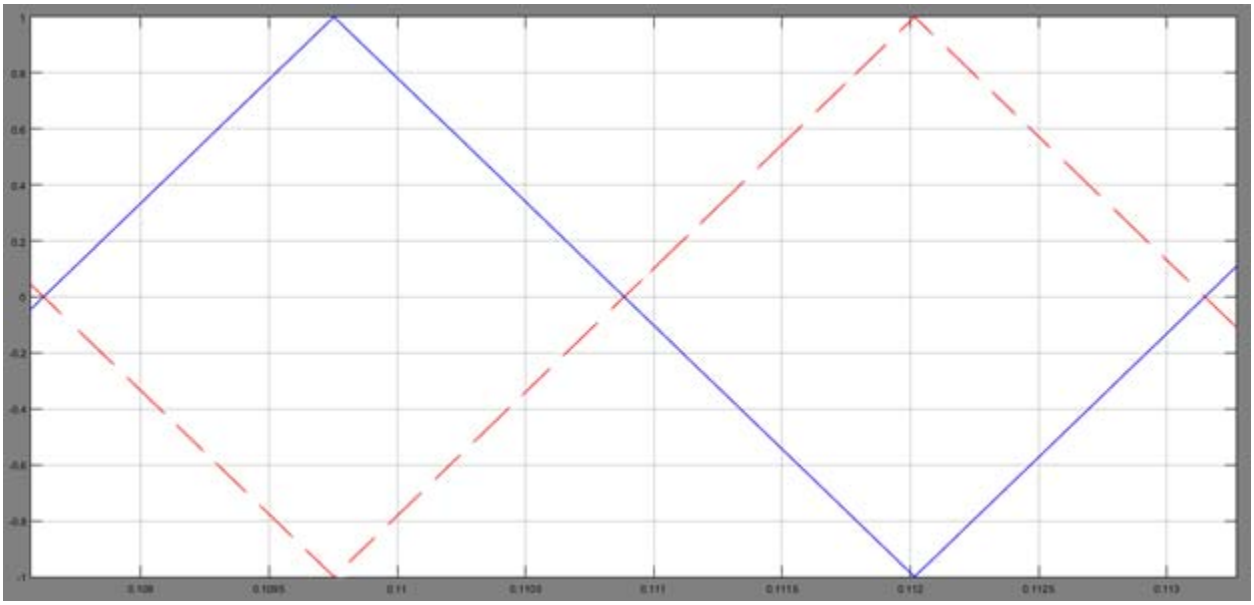

Figure 4-19 Triangular waveforms shifted by 180 degrees

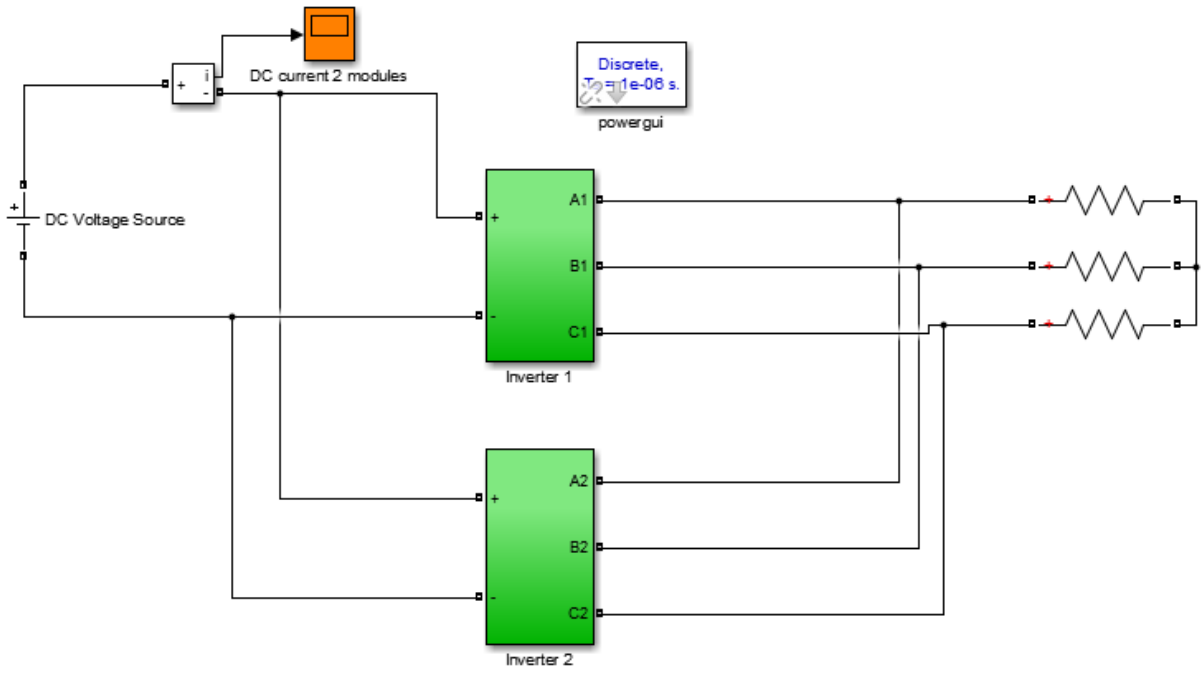

Figure 4-20 model for 2 inverters connection

According to our equation and results in table 4-6, we will eliminate all harmonic contents except the $2m_f$ and $4m_f$ harmonics (30th, 60th), which can be shown from the FFT tool of the model for the dc side current. (Figure 4-20)

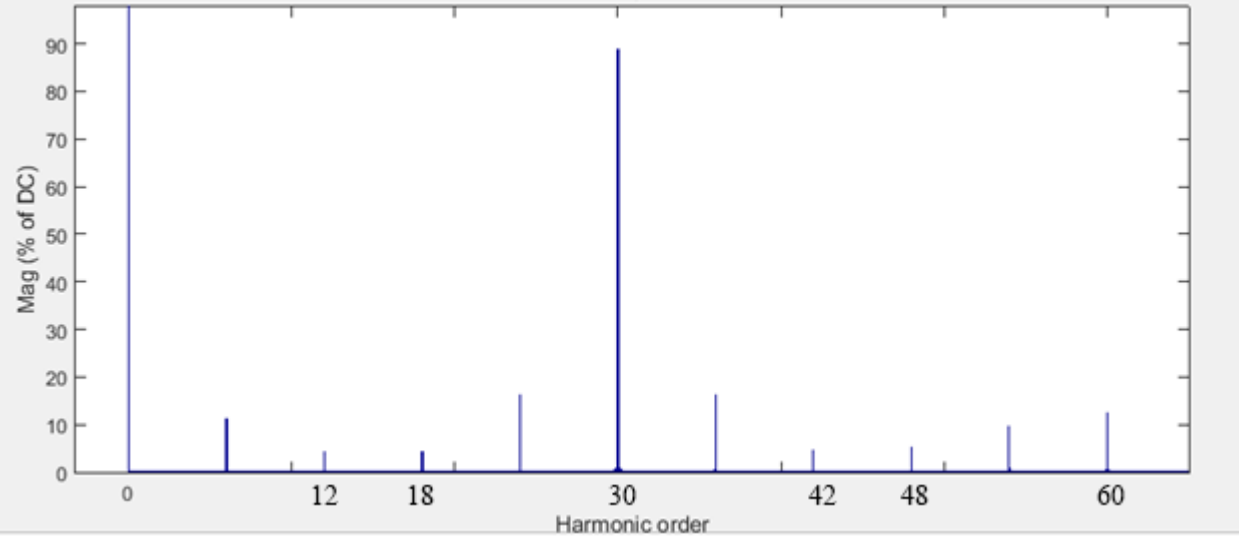

Figure 4-21 FFT analysis of the dc side current of the two module inverters displaced by $T_c/2$ with SPWM and mf=15

It can be clearly noticed from figure 4-20 that all the harmonics of the order $m_f - 3 = 12$, $m_f + 3 = 18$, $3m_f - 3 = 42$ and $3m_f + 3 = 48$ are dramatically reduced due to the shift by half of a cycle of the second carrier signal for the second inverter.

4.3.4: Three Inverter model whose triangular waveform displaced by 120° & -120°

Using the same transport delay block explained in the previous section we will generate 3 sets of gating pulses for three different inverters whose triangular waveforms are displaced by $T_c/3$ and $2T_c/3$ respectively. (Figure 4-21, Figure 4-22)

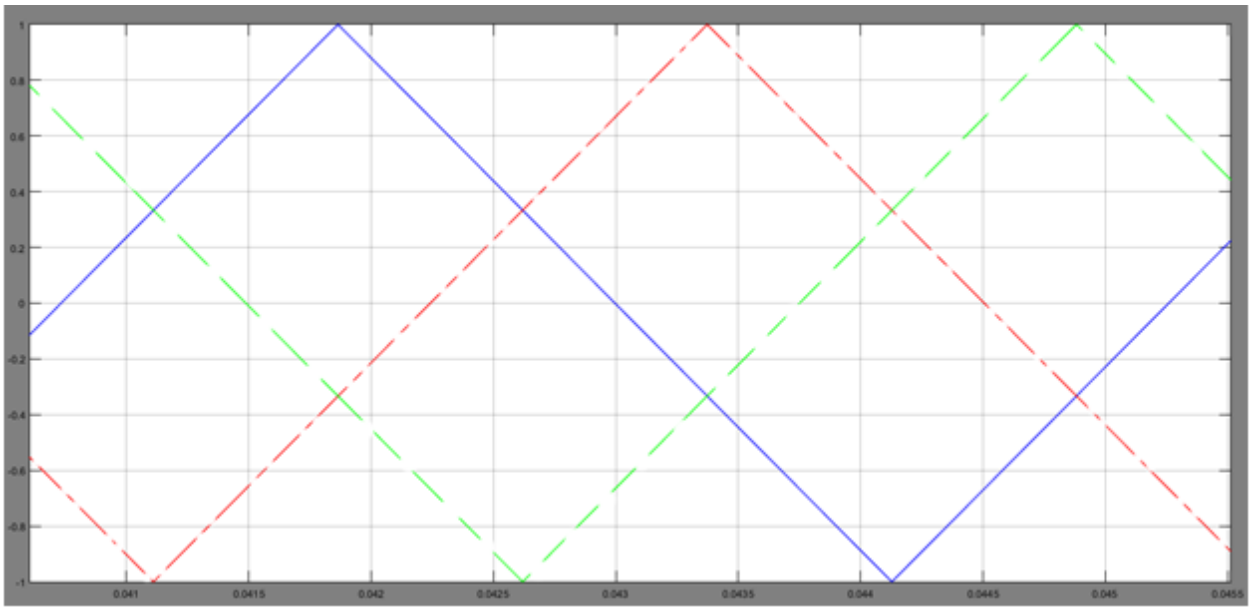

Figure 4-22 Triangular waveforms shifted by 120 and -120 degrees

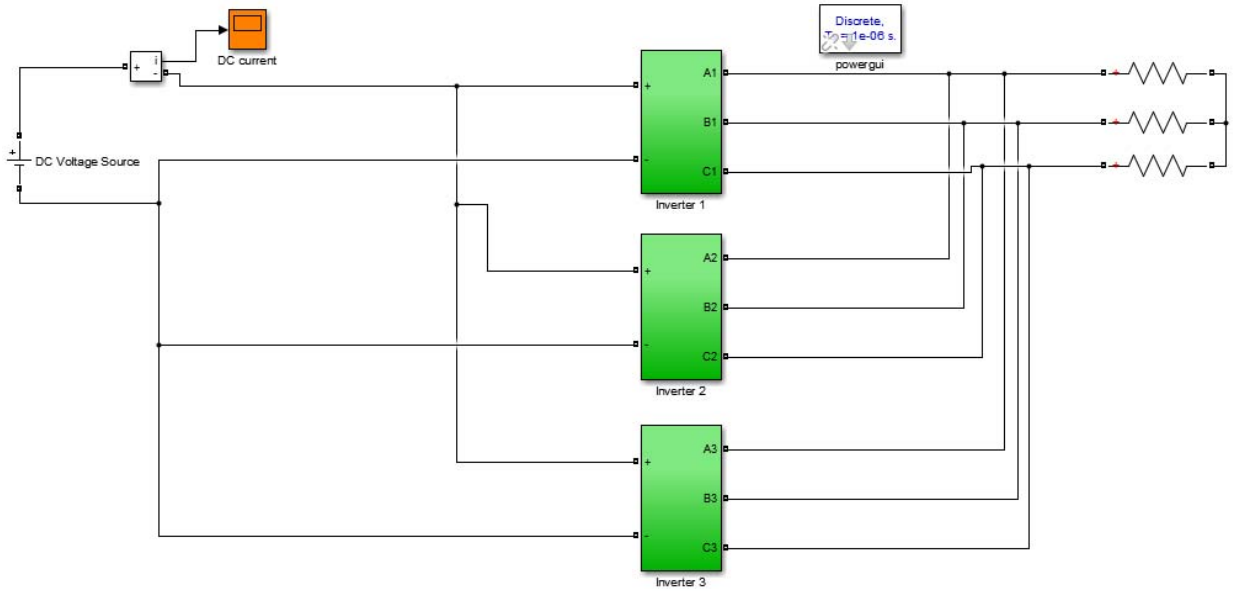

Figure 4-23 model for 3 inverters connection

According to our equation and results in table 4-6, we will eliminate all harmonic contents except the $3m_f$*-3* and $3m_f$ *+3* harmonics with m_f=15 which means the (42nd and 48th), which can be shown from the FFT tool of the model for the dc side current. (Figure 4.23)

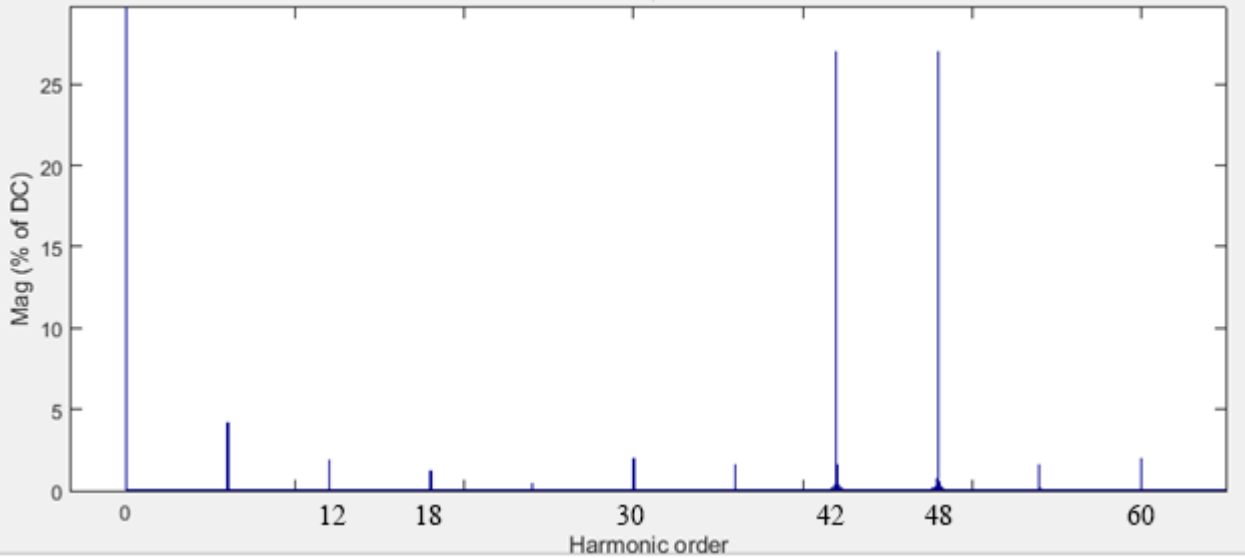

Figure 4-24 FFT analysis of the dc side current of the three module inverters displaced by $T_c/3$ and $2T_c/3$

It can be clearly noticed from Figure 4-23 that all the other harmonics except for the 42nd and 48th harmonics are clearly reduced and we have a much better harmonic profile than single inverter system.

If we would like to add more inverters we should follow the formula:

$$\psi_c^{(k)} = \frac{360}{n} \qquad (4-17)$$

Where, n is the number of modules and $\psi_c^{(k)}$ is the value of the shift angles. For example if we will implement six modules we will need to shift the modules from each other by 60^0 meaning the angles will be 0, 60, 120, 180, 240, 300 degrees. Using 6 modules enhances the THD from 65.3% to 35.32%.

Chapter 5: Permanent magnet Synchronous machine model

A synchronous motor with permanent magnets: the excitation magnetic field, in such machines, is provided by permanent magnets. The limitations imposed by the magnetic materials currently available to the construction of machines: the size and cost of the magnets are very high. However, this is an important field of application and in significant growth, including numerically controlled machine tools, industrial automation, robotics, light traction, heavy traction, and wind generation. Furthermore, due to the virtual absence of rotor losses these machines do not require forced ventilation and are therefore suitable for applications like aerospace or contaminated environments.

5.1 Synchronous machine model

In the following, the mathematical model of the synchronous machine is briefly recalled. This model has implied some simplifications regarding the constructive nature of the machine, but it appears to be sufficiently adequate to its control.

Consider the machine shown in figure 5-1.

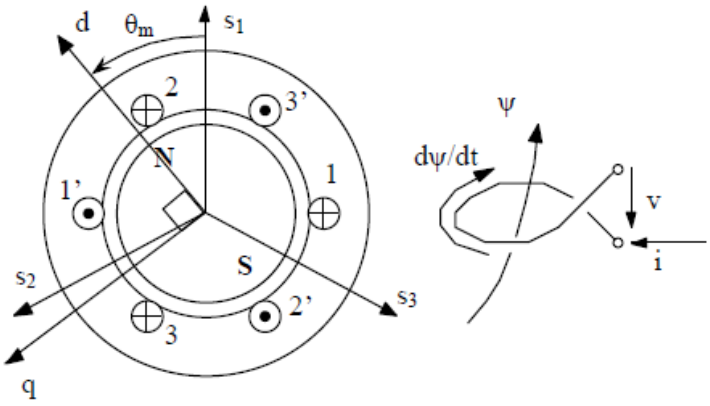

Figure 5-1 Schematic Diagram of the Permanent magnet motor

It consists of a cylindrical stator with a symmetrical three-phase winding so as to generate a distribution of sinusoidal magnetomotive force in the air-gap, and a rotor flux created by permanent magnets (for the windings apply the conventions of Figure 5-1) and without damper cages. The stator and the rotor are made of laminated material with infinite permeability. Saturation, hysteresis of iron and anisotropy of the machine due to the slots are neglected.[10]

5.1.1: Vector control of PMSM

According to [10] , The vector control of synchronous machine is based on a suitable choice of reference axes *d* and *q*, used by the controller of the power converter so that a component of the space phasor of the stator current acts only on the flux while the other on the electromagnetic torque (in the air-gap). In this way, the synchronous motor is controlled like a DC machine where the regulator acts separately on the excitation current (flux) and the armature current (torque).

$$v_{sd} = R_s i_{sd} + L_d p i_{sd} - \dot{\theta}_m L_q i_{sq}$$

$$v_{sq} = R_s i_{sq} + L_q p i_{sq} + \dot{\theta}_m \psi_{pm} + \dot{\theta}_m L_d i_{sd}$$

$$\psi_{sd} = L_d i_{sd} + \psi_{pm}$$

$$\psi_{sq} = L_q i_{sq}$$

$$p\dot{\theta}_m = \frac{n_p}{J}(T_e - T_r)$$

$$T_e = n_p \,\mathrm{Im}(\overline{i_s}\underline{\psi_s}) = n_p((L_d - L_q) i_{sd} i_{sq} + \psi_{pm} i_{sq})$$

However we will consider only the isotropic case of synchronous machine, so it results $L_d = L_q = L_s$ and the torque expression becomes:

$$T_e = n_p(\psi_{pm} i_{sq})$$

Since the last expression, it is evident therefore that, for the torque birth, only the quadrature component of stator current is effective, while direct component has no effect on the torque. So in order to minimize the magnitude of the current space phasor (and consequently the losses), vector control should operate on the power converter in such a way that is, at any time:

$i_{sd} = 0$, Therefore the equations of the voltages become,

$$v_{sq} = R_s i_{sq} + L_s p i_{sq} + \dot{\theta}_m \psi_{pm}$$

$$v_{sd} = -\dot{\theta}_m L_s i_{sq}$$

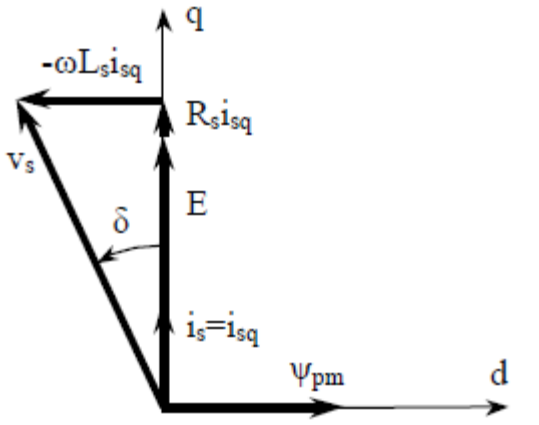

Figure 5-2 Steady state vector diagram of PMSM

Thus the machine in our model is working in steady state with the vector diagram shown in figure 5-2. The rated data of the machine is listed in Table 5-1

Table 5-1 data of one module of an axial flux modular PM machine

Rated Power	1000 KW
Rated speed	17 rpm
Number of poles	104
Rated frequency	14.73 Hz
Rated current	925 A_{rms}
Line-to-neutral EMF, at rated speed	495 V_{rms}
Synchronous inductance	3.276 mH
Phase resistance	14.3 mΩ
Rotor Inertia (1 module)	J = $3.7 \cdot 10^4$ kg·m^2

5.1.2: Machine model in Simulink:

Because we are working with a multi-modular PMSM and in order to model such modules in simulink and to fully control the machine we had to model the machine in form of equations and hence it would be easy to insert another module of the equations. See Figures 5-3

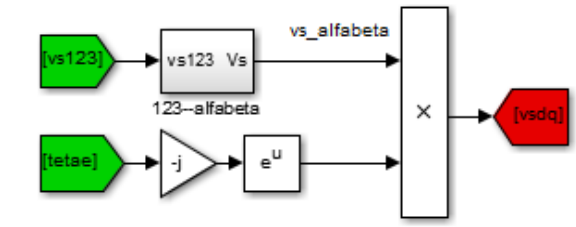

(a) Converting the voltages of the inverter from phase voltages into the dq reference frame

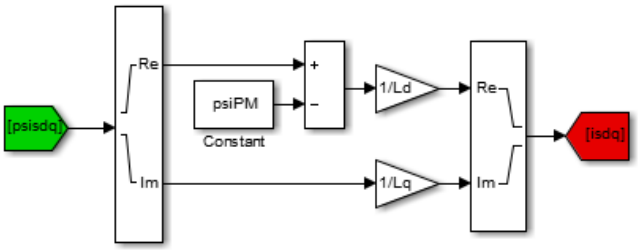

(b) Computation of the current in the dq reference frame

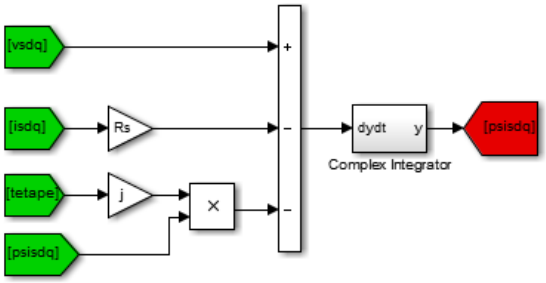

(c) Computation of the flux in the dq ref frame

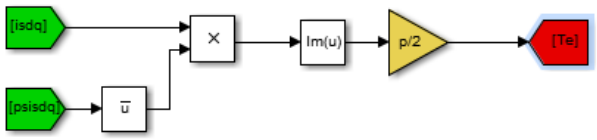

(d) Computation of the electromagnetic torque, where p/2 is the number of pole pairs

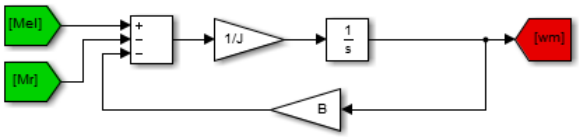

(e) The mechanical equation of the machine

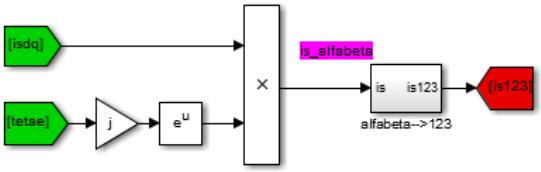

(f) Converting the dq currents into phase currents as an output of the machine

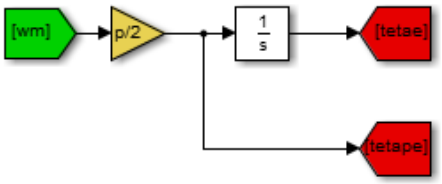

(g) Relation between the speed and the electric position and mechanical one

Figure 5-3 Mathematical machine model for 1 module of the PMSM on Simulink

It's apparent now that in order to add another module it's quite easy because we know that the modules of the machine are mounted on the same shaft; hence the same mechanical speed ω_m and the mechanical equation will be the same but in the case of the multi-modular machine the coefficients of the inertia and damping (*J, B*) they will be multiplied with the number of modules (n) and the equation of the electromagnetic equation the current *isdq* and the flux *psidq* will be the summation of the currents of the modules and the summation of the flux of the modules which is quite reasonable because as we increase the number of modules we will increase the torque produced as well and it will be n times the electromagnetic torque of one module.

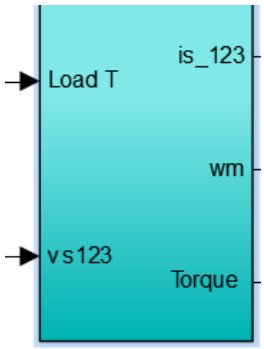

Figure 5-4 Grouped model of PMSM

5.2: Controllers design

The controller has to drive the power converter so that it always results $i_{sd} = i_{sd\ ref}$ (which we will assume to be zero because we are working in the steady state region using the full flux from the permanent magnets), while the component i_{sq} must be such that the produced torque is able to maintain the required speed of the machine.
The overall scheme of the drive with speed control loop is the following:
In the Figure 5-5[10], the block $T(\theta_m)^{-1}$ performs the transformation from space phasor variables to phase quantities through park transformation [10].

Taking into account the stator dynamics, the control scheme changes, as shown in Figure 5-5. In this case the power converter has to establish a voltage reference, while the current regulation is now performed by the controller

The structure of the current controller is based on the differential equations of the machine:

$$v_{sd} = R_s i_{sd} + L_s p i_{sd} - \omega_m L_s i_{sq}$$

$$v_{sq} = R_s i_{sq} + L_s p i_{sq} + \omega_m \psi_{pm} + \omega_m L_s i_{sd}$$

You notice immediately that, in terms of voltages on the two axes, there are different terms: $R_s i_{sd} + L_s p i_{sd}$ (indicated as u_{sd}) and $R_s i_{sq} + L_s p i_{sq}$ (indicated as u_{sq}) are the voltages that actually act on their own current; the terms $-\omega_m L_s i_{sq}$ and $\omega_m L_s i_{sd}$ show the existence of a coupling between the two loops; the term $\omega_m \psi_{pm}$ represents an electromotive force, proportional to the mechanical speed.

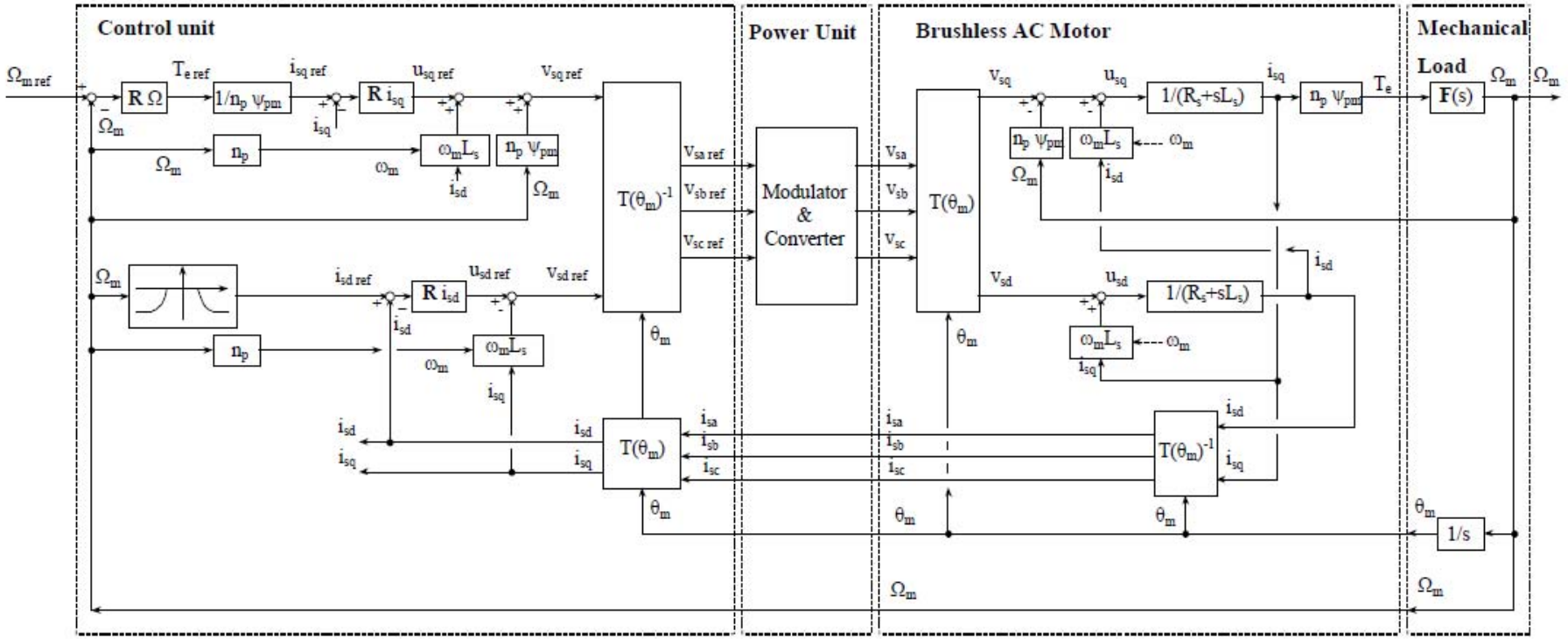

Figure 5-5 Full control scheme (Voltage controlled power converter)

5.2.1: Current regulators design

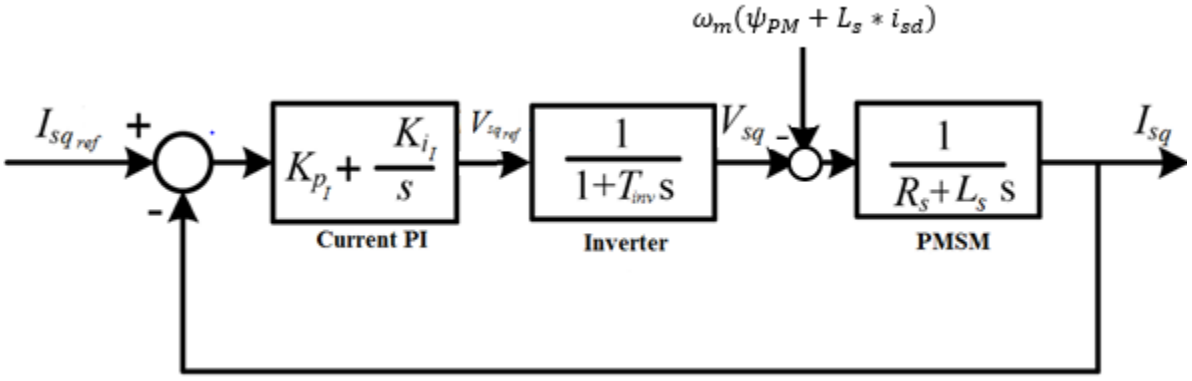

Figure 5-6 Current control scheme for the q axis current

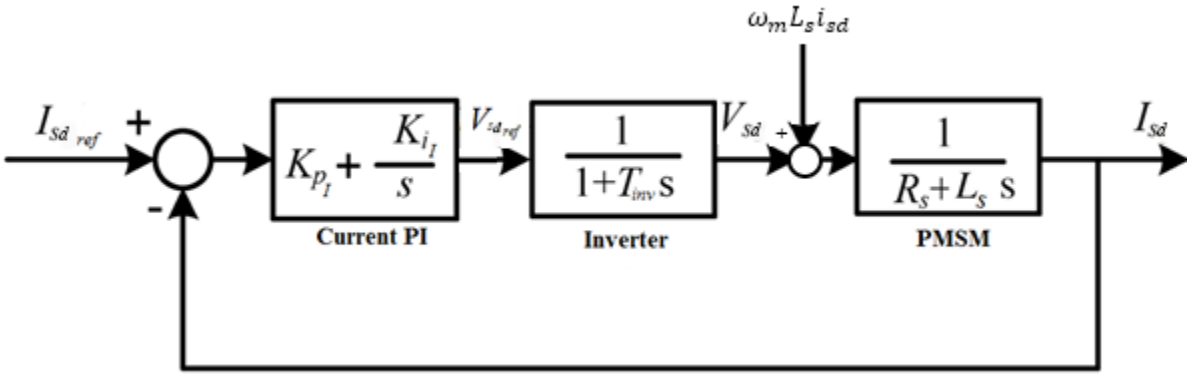

Figure 5-7 Current control scheme for the d axis current

We have to note that if you do not compensate the coupling terms, the loop controller should "work" even when the reference of the other loop varies. The motional term, however, would require full compensation through the integral action of the regulator itself; in the case of a machine starting from a speed different from zero, it would lead to some undesirable effects, such as, for example, a sudden stop of the machine in the first instant of the operation.[10]

The inverter is represented as a delay block, where T_{inv} is the inverse of the switching frequency f_c that we are using to drive the machine.

We assumed that the machine is isotropic: thus $L_d=L_q=L_s$. Therefore, the current regulators of both d and q axes will be the same.

5.2.1.1: Calculation of the PI constants in Matlab

The controller in Simulink is represented in figure 5-8 in which Ccurr.Kp and Ccurr.Ki are the constants of Kp and Ki for the regulator.

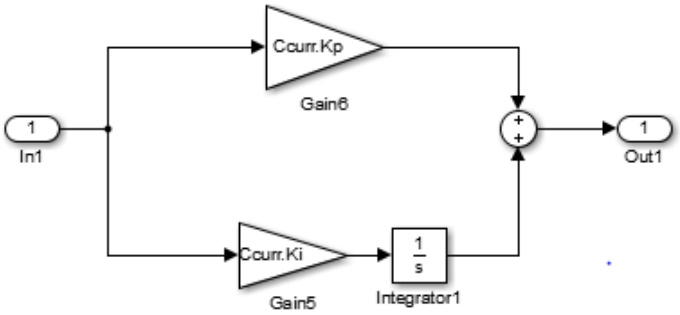

Figure 5-8 Current controller in Simulink

Positive phase margin is the requirement for the stable system. Moreover, increasing the phase margin results in the system more accurate regulation and better dynamic response with less overshot and ringing

The open-loop transfer function GI(s) of the system under control in the current control loop is:

$$GI(s)_i = \frac{1}{(1 + sT_{inv})(R_s + sL_s)}$$

Using the matlab code in Appendix (A3) we can identify the correct values of the constants of the controller to achieve a stable system, and we can find that as we increase the switching frequency we will have a more stable system for any phase margin value from 0 to 90 degrees because the constants will have a positive value in such range using high switching frequencies.

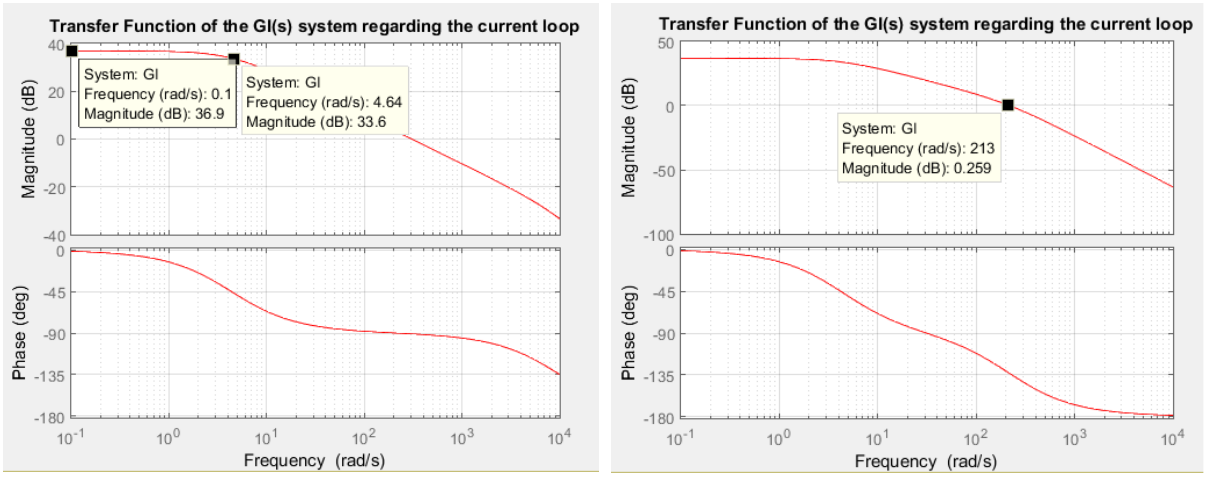

Figure 5-9 transfer function showing the effect of switching frequency on the system under control current controller bandwidth a) switching frequency is set to mf=678 b) switching frequency is set to mf=15

Fig 5-9 shows that the chosen switching frequency affects the determination of the cut off frequency of the current controller. If we choose the frequency modulation ratio m_f to be 678 the cutoff frequency is around 301 rad/s. While choosing m_f equal to 15 the cutoff frequency is around 210 rad/sec.

We choose m_f to be 678 (the carrier frequency is around 10 KHz) in order to see that the model is working well at high frequencies.

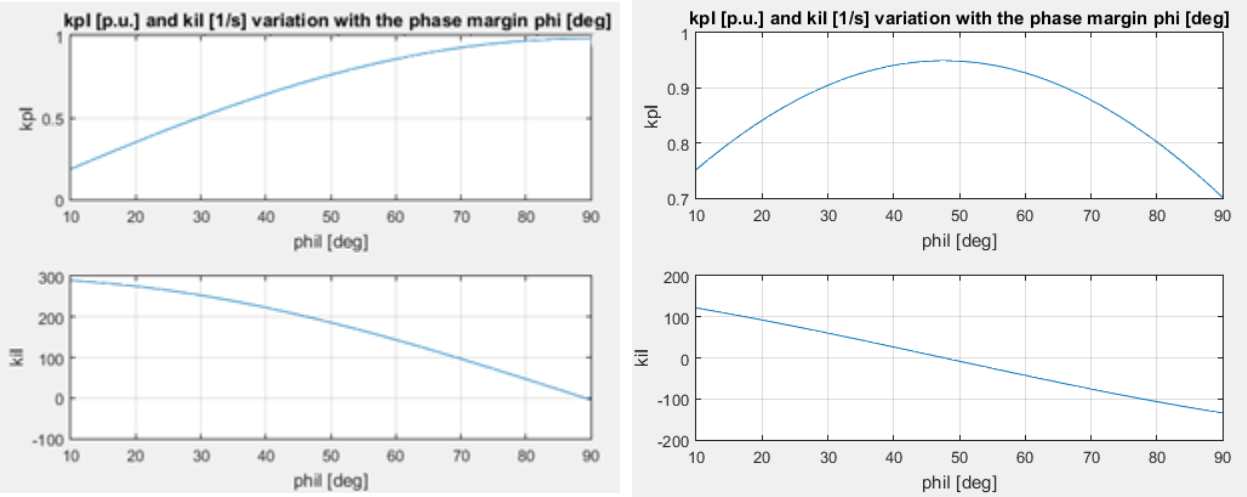

Figure 5-10 Phase margin for both KpI and KiI for our machine parameters a) mf=678 and cutoff frequency 300 rad/s b) mf=15 and cutoff frequency 210 rad/s

Fig 5-10 shows the relation of the values of the constants of the PI controller (K_{pl} and K_{il}) with the phase margin "φ_I". Fig 5-10a shows m_f equal 678 we will find that this switching frequency the machine will always be stable as it is positive till 90 degrees and we can choose an appropriate value of the phase margin to be 70°. While looking at Fig 5-10b which shows m_f equal to 15 shows negative values for the phase margin more than 45°. Having a negative values means instability so we are left with two options: Either to choose phase margin less than 45°, or further decrease the cutoff frequency to a value less than 210 rad/s.

Fig 5-11 shows the values of PI constants at lower cutoff frequency 100 rad/sec. Lowering the cutoff frequency results in the increase of the phase margin region with positive K_{il}. Hence we can choose higher value of phase margin for example 60°.

We obtain the values of Kp_i=0.9291 [p.u.] and Ki_l=96.5939 [s^{-1}] for m_f=678 and cutoff frequency "ω_{cI}" 300 rad/s. the values of Kp_i=0.3563 [p.u.] and Ki_l=5.1016 [s^{-1}] for m_f=15 and cut off frequency 100 rad/s. Table 5-2.

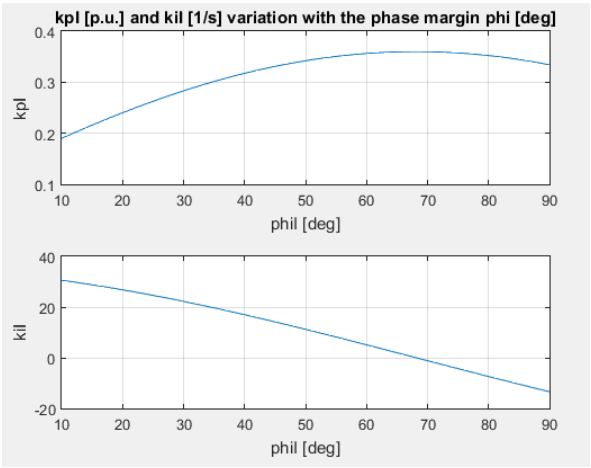

Figure 5-11 Variation of the PI constants of the current controller with phase margin at mf=15 and cut off frequency 100 rad/sec

As previously discussed for multimodular machine, what changes is the mechanical equation parameters, thus in order to implement the control for multimodular machine, each module will be controlled with a separate controller in which all the controllers of the current will be identical.
The whole Transfer function for the Current Regulator

$$L(s)_i = \frac{Kp_I + \frac{Ki_I}{s}}{(1 + sT_{inv})(R_s + sL_s)}$$

The closed loop transfer function will be

$$F(s)_i = \frac{L(s)_i}{1 + L(s)_i}$$

Table 5-2 Current controllers constant at mf=678 ($f_c \approx 10$ KHz) and mf=15

$\boldsymbol{m_f = 678}$, cut off frequency 300 rad/s, phase margin 70		$\boldsymbol{m_f = 15}$ cut off frequency 100 rad/s, phase margin 60	
$\boldsymbol{K_{pI} = 0.9291}$ [p.u.]	$K_{iI} = 96.5939\ [s^{-1}]$	$K_{pI} = 0.3563$ [p.u.]	$K_{iI} = 5.1016\ [s^{-1}]$

The effect of selecting a proper phase margin will be explained in details in 5.2.1.3.

5.2.2: Speed regulator design:

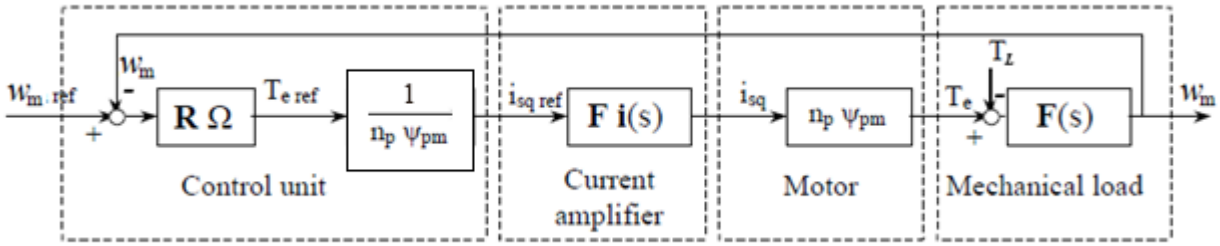

Figure 5-12 Scheme for the design of the speed regulator

In order to design the speed regulator it is necessary to know the transfer function of the overall system, described before. The output of the speed controller is the desired value of the electromagnetic torque which is proportional to the quadrature component of the stator current. The scheme is shown in Figure 5-12.

Fi(s) is the closed loop transfer function of the current controller, while the mechanical load transfer function is:

$$F(s) = \frac{1}{(Js + B)}$$

Where J is the mechanical inertia of the machine while B is the damping factor of the machine

The system under control has the following transfer function:

$$T(s)_w = \frac{Fi(s)}{(Js + B)}$$

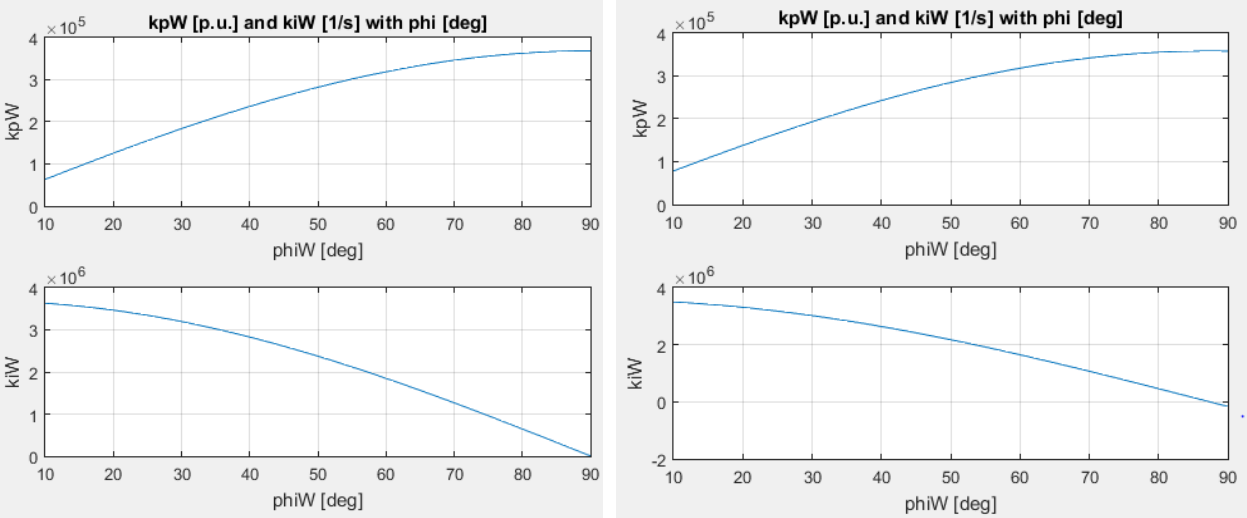

Figure 5-13 Variation of the PI constants of the speed controller with phase margin a) mf=678 and cutoff frequency 300 rad/s b) mf=15 and cut off frequency 100 rad/sec

Using the code of appendix (A3) we can find the values of the constants of the speed controller with the same manner of the current regulator. Using phase margin "φ_W" of 70° and a critical frequency "ω_{cW}" much less than the current controller for example 10 rad/s (Figure 5-13), we can find the values of the Kp_w to be $3.464*10^5$ [p.u.] and Ki_w to be $1.27*10^6$ [s^{-1}] at mf equals 678. At m_f equals 15, Kp_w is $3.1836*10^5$ [p.u.] and Ki_w to be $1.6486*10^6$ [s^{-1}].

Note that for designing the speed controller for multimodular machine the constants will change because the transfer function of the mechanical load becomes

$$F(s) = \frac{1}{n_m(Js + B)}$$

Where n_m is the number of the modules, so for each system we have to calculate the Kp_w and Ki_w according to the number of modules of our machine shown in table 5-3.

Table 5-3 Speed controller constant at mf=678 and mf=15 for one module, two modules and three modules systems

	$\boldsymbol{m_f = 678\ (f_s \approx 10\ KHz)}$		$\boldsymbol{m_f = 15}$	
	$\omega_{cI} = 300\frac{rad}{s}$ $\quad \varphi_I = 70^o$ $\omega_{cW} = 10\frac{rad}{s}$ $\quad \varphi_W = 70^o$		$\omega_{cI} = 100\frac{rad}{s}$ $\quad \varphi_I = 60^o$ $\omega_{cW} = 10\frac{rad}{s}$ $\quad \varphi_W = 70^o$	
$\boldsymbol{n_m = 1}$	$K_{pW} = 3.1911 * 10^5$	$K_{iW} = 1.8491 * 10^6$	$K_{pW} = 3.1836 * 10^5$	$K_{iW} = 1.6486 * 10^6$
$\boldsymbol{n_m = 2}$	$K_{pW} = 6.3821 * 10^5$	$K_{iW} = 3.6982 * 10^6$	$K_{pW} = 6.3673 * 10^5$	$K_{iW} = 3.2971 * 10^6$
$\boldsymbol{n_m = 3}$	$K_{pW} = 9.5732 * 10^5$	$K_{iW} = 5.5474 * 10^6$	$K_{pW} = 9.5509 * 10^5$	$K_{iW} = 4.9457 * 10^6$

5.3: Simulink model

5.3.1: Single module machine:

As the control scheme and the inverter model can be shown in Fig 5-14 (shown in Simulink schematic in appendix (A5)), we can point out some notes. First the output of the inverter is not directly fed to the machine block Fig 5-15 because the machine model accepts only signals so that's why we feed the machine from the signal coming from the voltmeter connected to a highly value resistor 1E5 ohms.

Second, in order to exploit the inverter coherence with the machine model, we supply the inverter with the current source whose value is the current of the machine. This current source is connected in parallel to the high value resistor, and because of its high value the current doesn't flow through the resistor but flows through the inverter itself.

Third, the control sinusoidal waveforms of the PWM modulator are the same phase voltages which are the output of the controllers. Notice these values are to be divided by $\frac{Vdc}{2}$ in order to deal with per unit values to compare it with the triangular waveform of unity amplitude.

Fourth, as for the machine we use the "associated reference directions" which means that the machine is considered operating as a motor. In order to make it work as a generator the load torque is negative.

Fifth, our analysis about the effect of the sequential controlled two level inverters will be carried out at low frequency ($\boldsymbol{m_f} = 15$). For the single module machine, we will carry out the simulation also for ($\boldsymbol{m_f} = 678$).

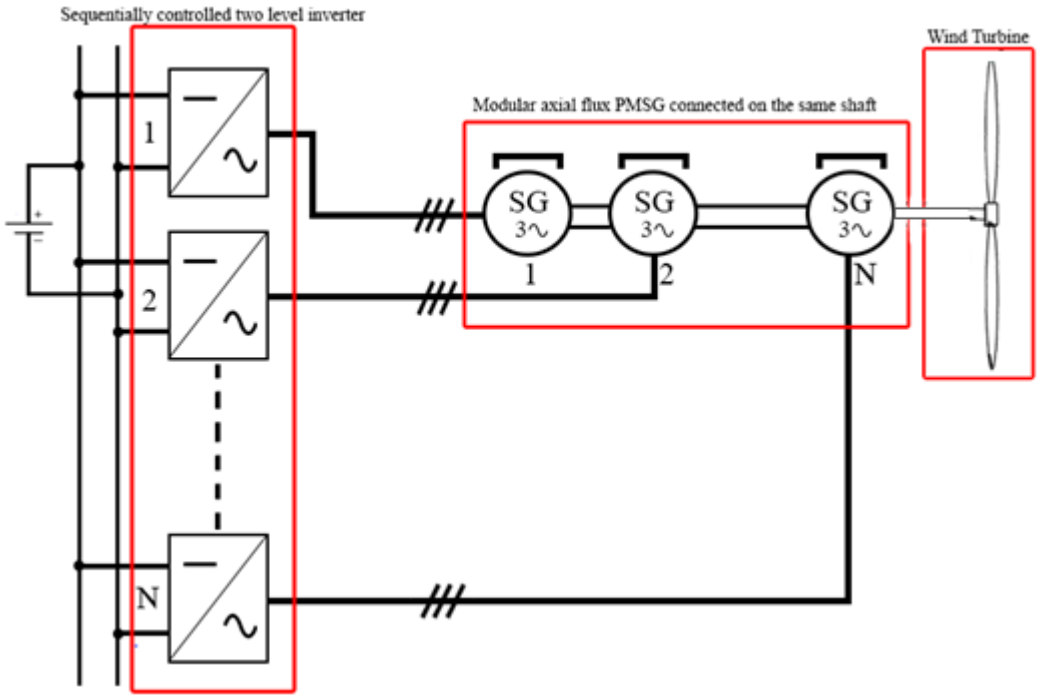

Figure 5-14 overall schematic of the connection between the "N" two level inverters and the "N" modules of AF PMSG

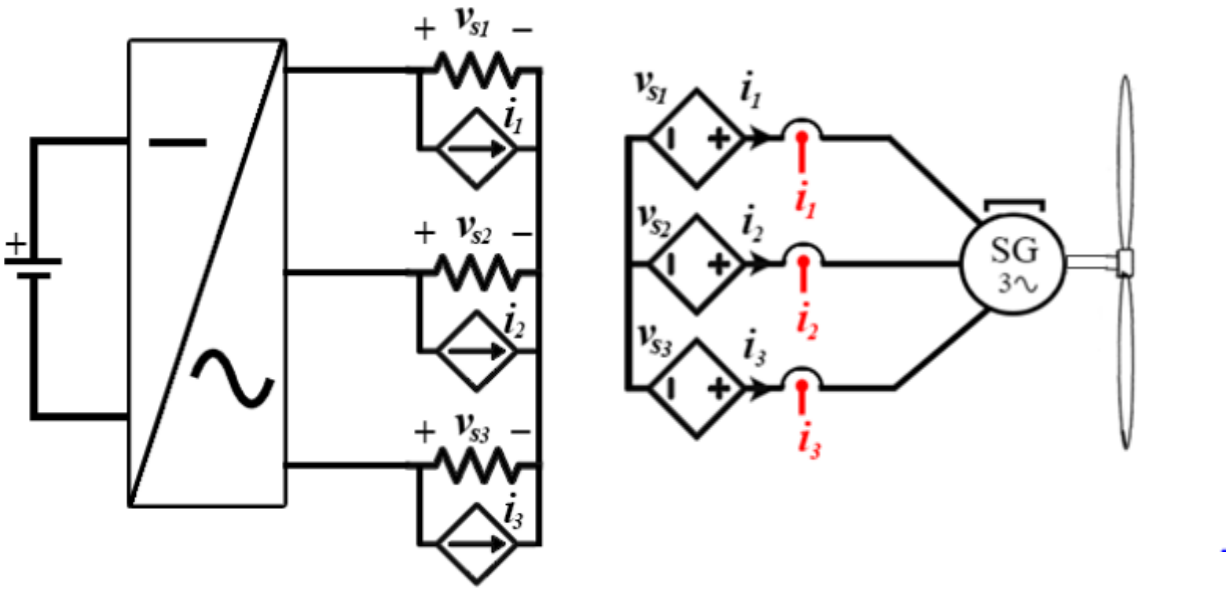

Figure 5-15 the equivalent connection between the inverter and the machine done on matlab Simulink

5.3.1.1: High frequency simulations $m_f = 678$ ($f_c \cong 10\ KHz$, $f_s = 14.73\ Hz$):

Both speed and driving torque are increasing gradually using a ramp (Figure 5-14a), the electromagnetic torque is less than the driving torque and that's due to the acceleration of the machine. When the machine reaches a constant speed the driving torque and electromagnetic torque produced by the machine are equal (Figure 5-14b).

Hence we performed Fast Fourier Transform (FFT) on both current and torque at steady state and these are the harmonics obtained. (Figure 15-17, 15-18). As derived before in the mathematical model in chapter 4 (4-14) and table 4-6, the harmonics existing are Table 5-4 (and the same can be noted for torque)

Table 5-4 harmonic components of the dc side current as well as the torque for mf=678

$mf - 3$	**675**
$mf + 3$	681
$2mf$	1356
$3mf - 3$	2031
$3mf + 3$	2037
$4mf$	2712

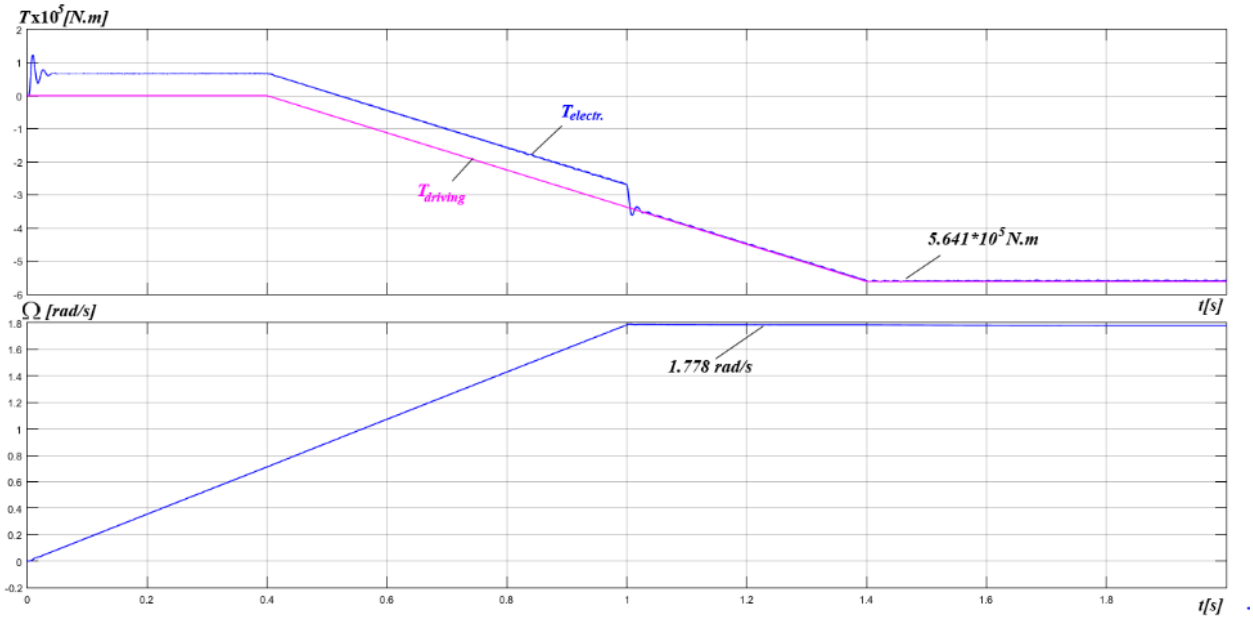

Figure 5-16 Torque and speed of one module machine at mf=678: Actual torque in blue and reference torque (load Torque) is delayed by 1.2 seconds and the machine speed reaches steady state of the rated speed 1.778 rad/s after 2 seconds

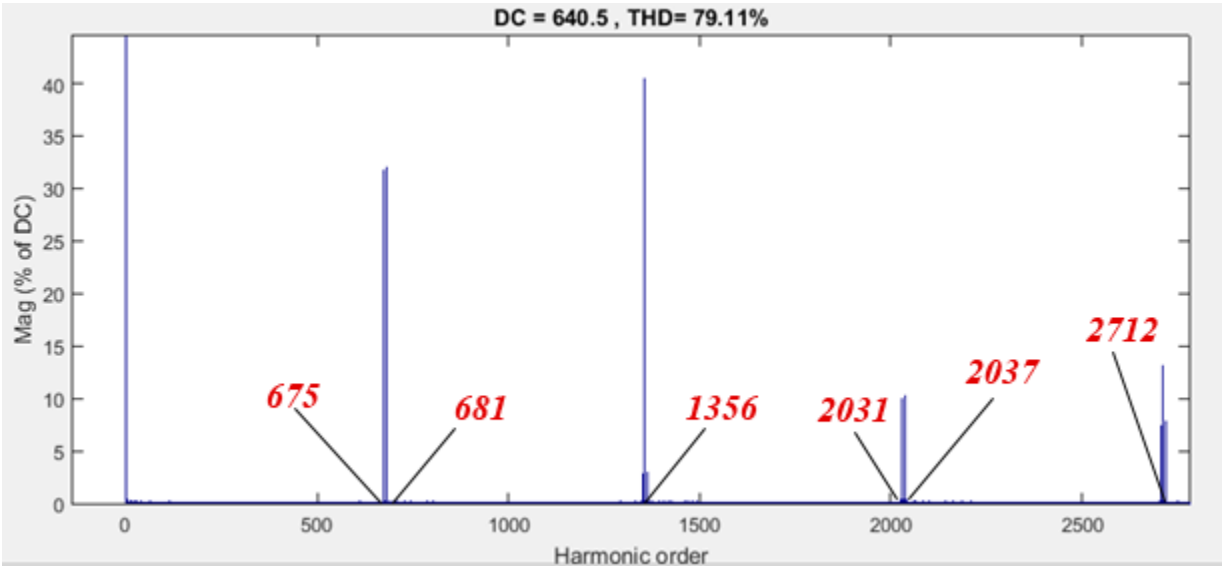

Figure 5-17 FFT Analysis for the steady state DC side current of one module machine at mf=678 where the amplitude of dc current is 640.5 A

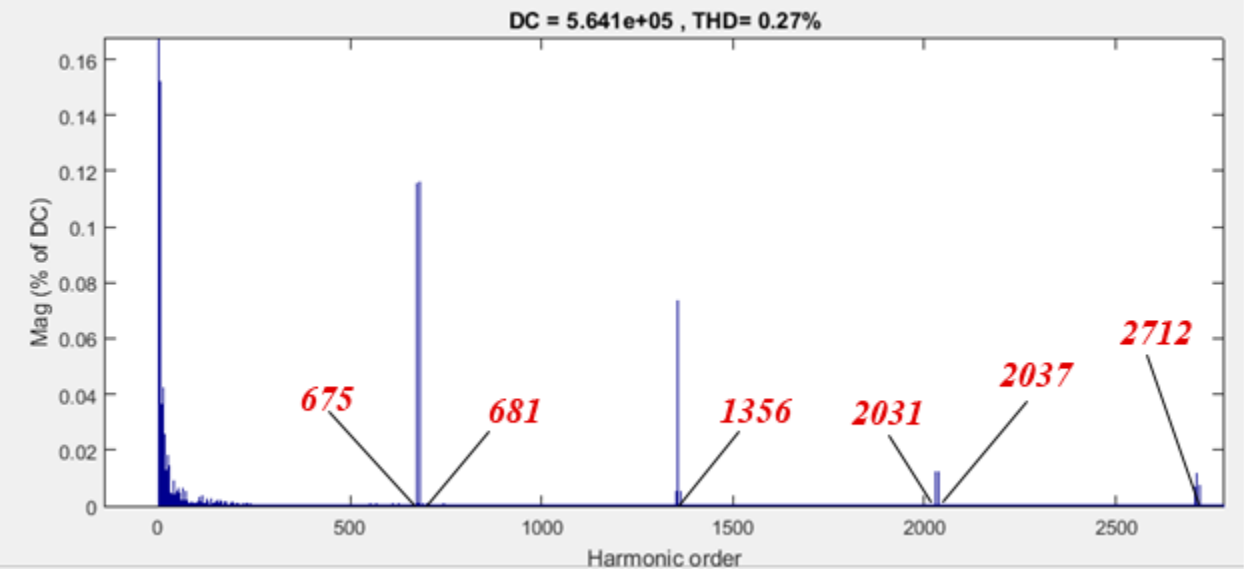

*Figure 5-18 FFT analysis for the steady state Torque of one module machine at mf=678 where the amplitude of the steady state torque is 5.641*10^5 N.m*

5.3.1.2: Low frequency simulations $m_f = 15$: ($f_c \cong 221\ Hz$, $f_s = 14.73\ Hz$)

Low frequency is chosen in order to decrease the switching losses.

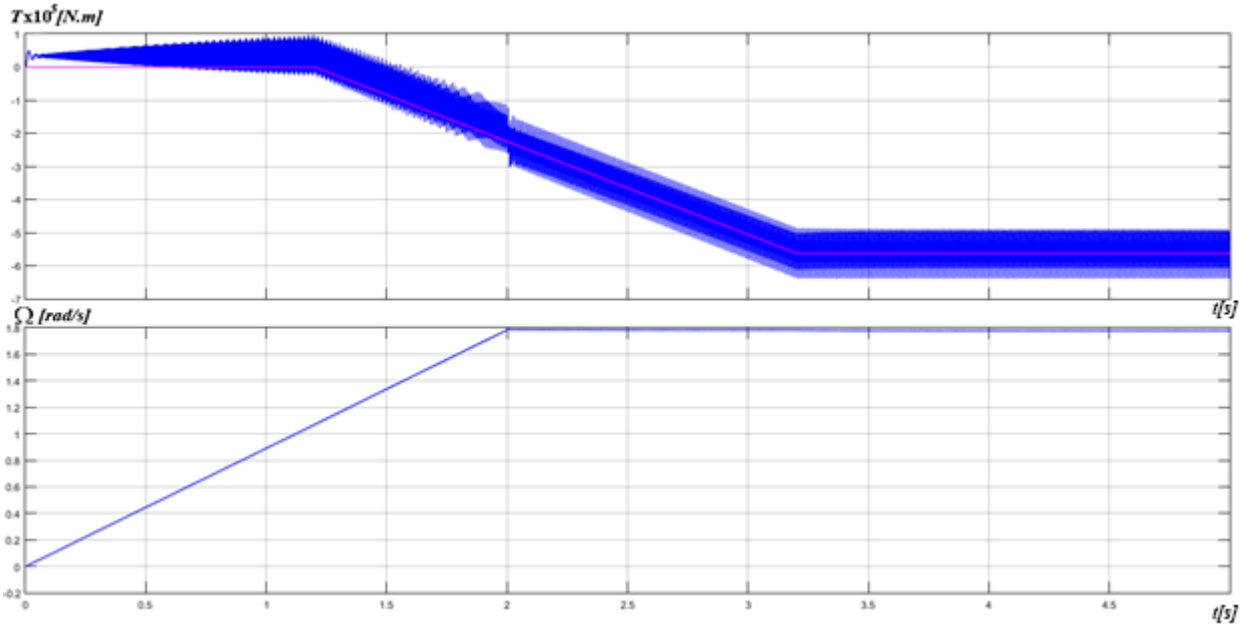

Figure 5-19 Torque and speed of one module machine at mf=15

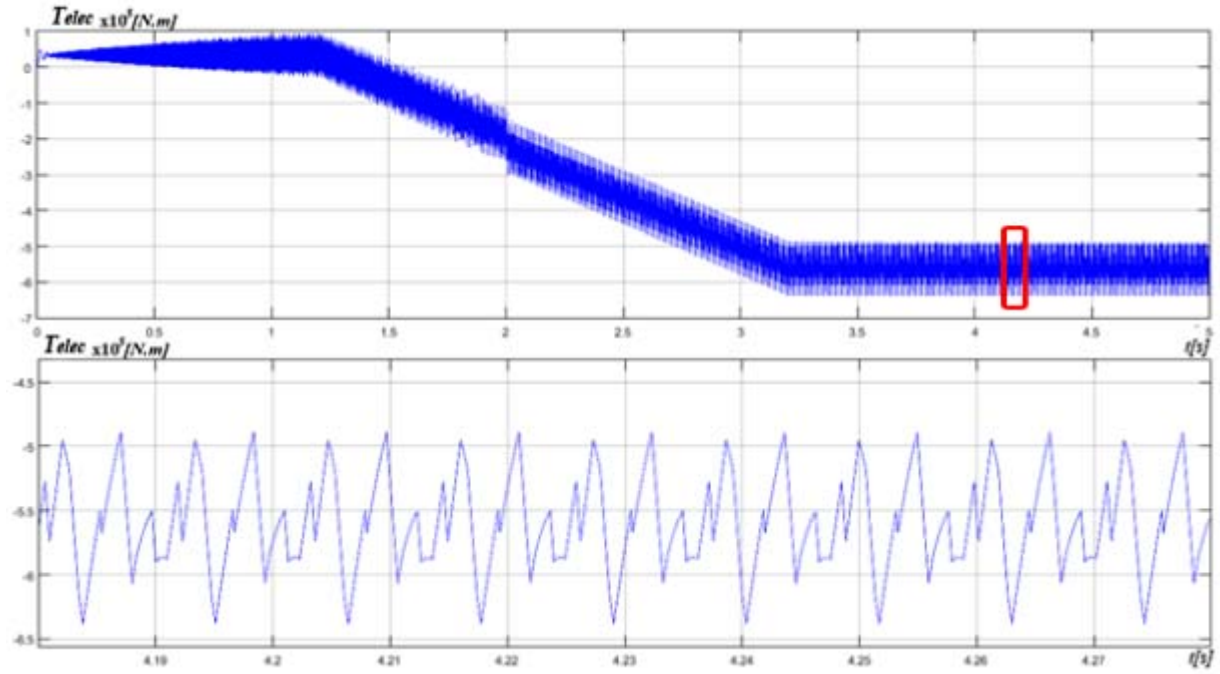

Figure 5-20 the steady state torque ripple of 1 module machine at mf=15

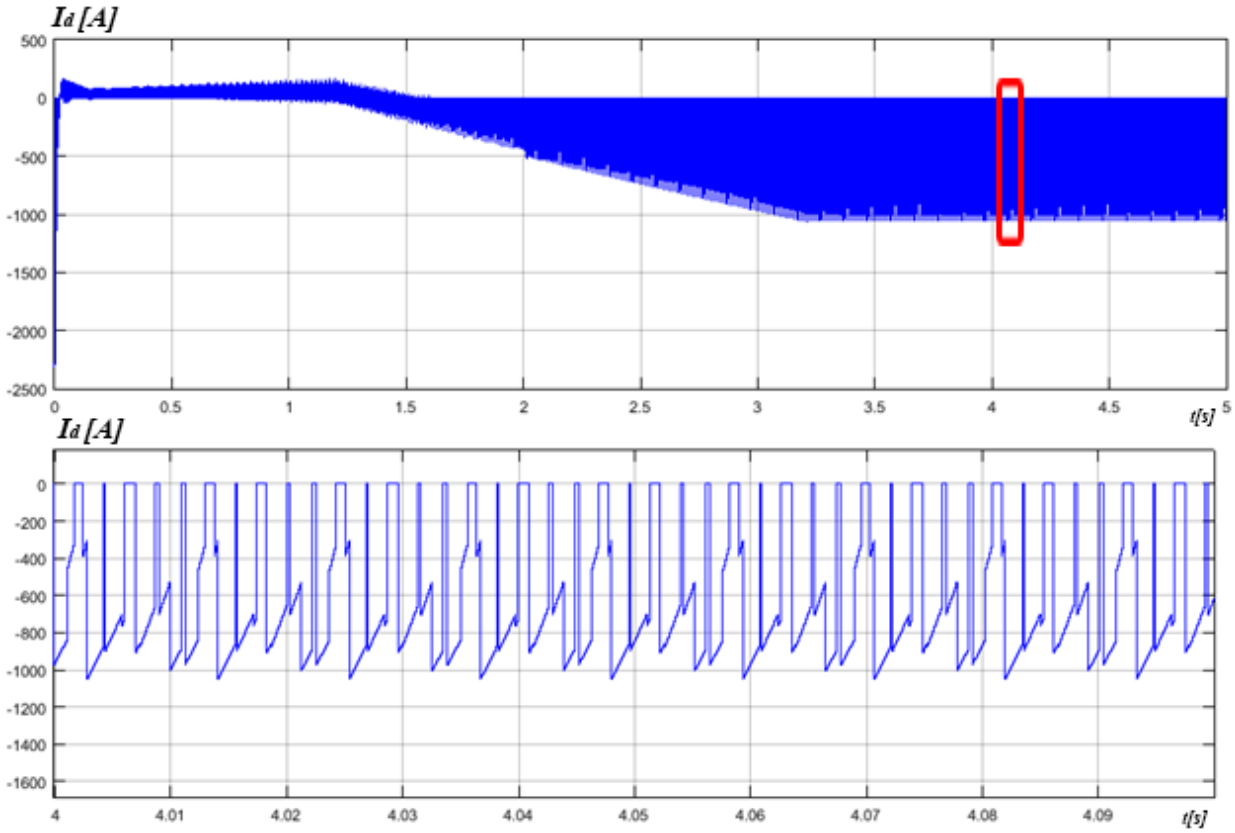

Figure 5-21 the steady state DC side current ripple of 1 module at mf=15

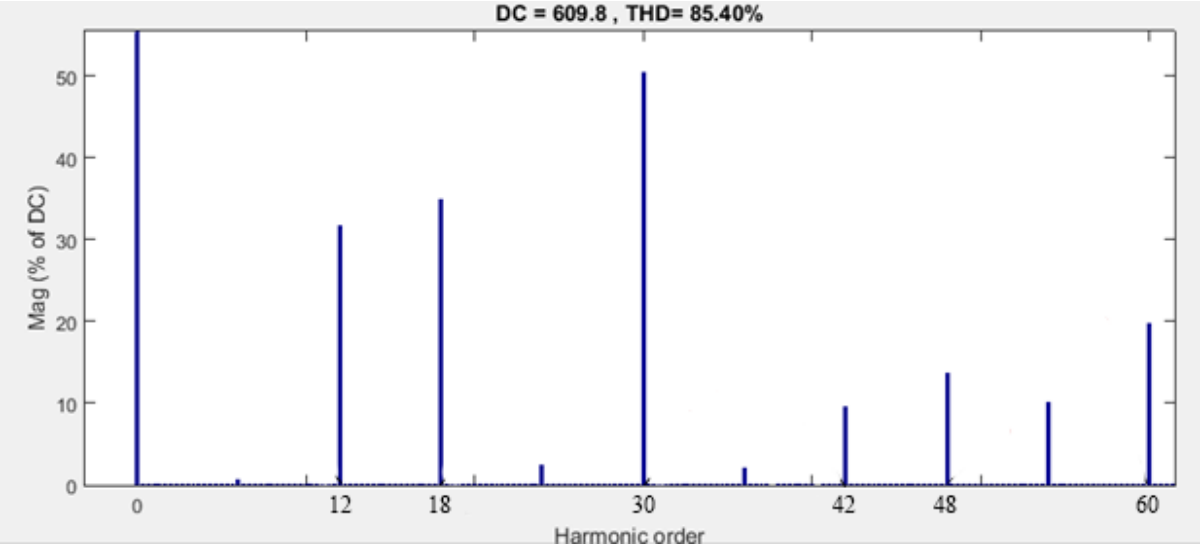

Figure 5-22 FFT Analysis for the steady state DC side current of one module machine at mf=15

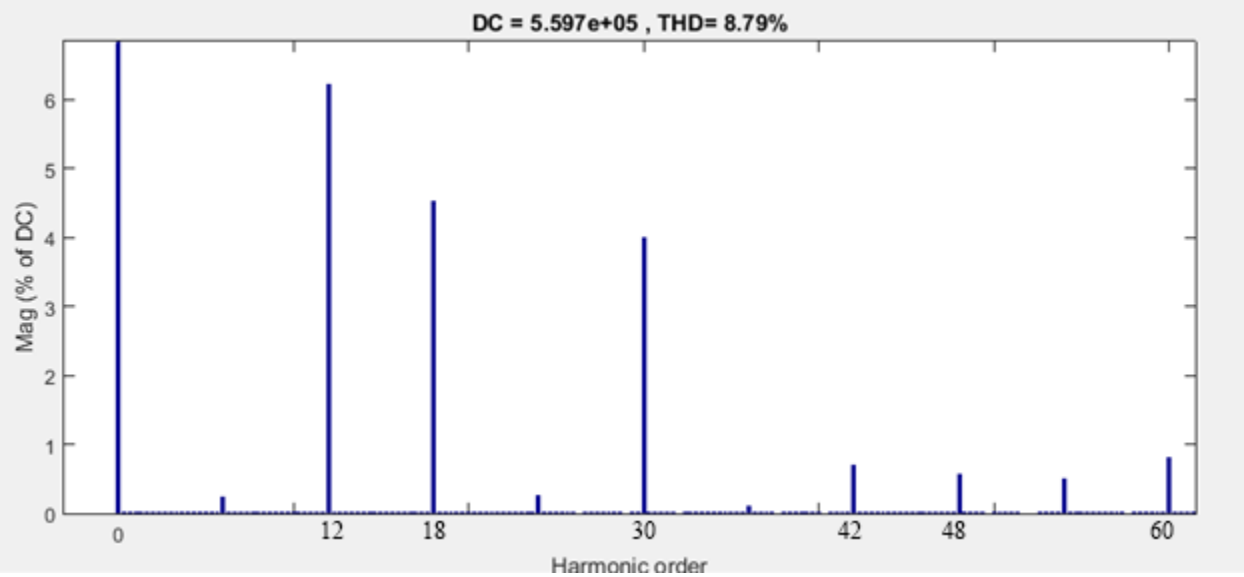

Figure 5-23 FFT Analysis for the steady state torque of one module machine at mf=15

Comparing the total harmonic distortions for current and torque at $\boldsymbol{m_f} = 678$ and $\boldsymbol{m_f} = 15$ Figures (5-17 5-18 5-22 5-23) we can see the THD decrease with increasing the switching frequency. Because we shift the harmonic components to a higher order harmonics so they have lower effect on the main components of the current and torque.

THD in the dc current side is high 85.4% (Fig. 5-22), which, if reduced, will help to reduce the size of the capacitor that is present in the actual circuit in order to keep the voltage constant, hence we may reduce size and cost of the system.

THD of the torque (Fig 5-23) is relatively small compared to the THD of the current and that would be explained in details in section 5.2.4

The harmonics existing in both the torque and current, Fig 5-23 and 5-24 as derived above in the mathematical model in chapter 4 (4-14) and table 4-6 are presented in Table 5-5

Table 5-5 harmonic components of the dc side current as well as the torque for mf=15

$\boldsymbol{mf-3}$	**12**
$\boldsymbol{mf+3}$	18
$\boldsymbol{2mf}$	30
$\boldsymbol{3mf-3}$	42
$\boldsymbol{3mf+3}$	48
$\boldsymbol{4mf}$	60

5.3.1.3: Effect of current controller bandwidth on the harmonics:

Decreasing the current loop bandwidth from $\omega_{cI} = 300\frac{rad}{s}$ to $\omega_{cI} = 20\frac{rad}{s}$ will cause its pole to interfere with the speed loop phase margin which will result in underdamped response which can be seen in the figure 5-24 and 5-25. That's why the total harmonic distortions of both torque and current increase when the current controller bandwidth decrease.

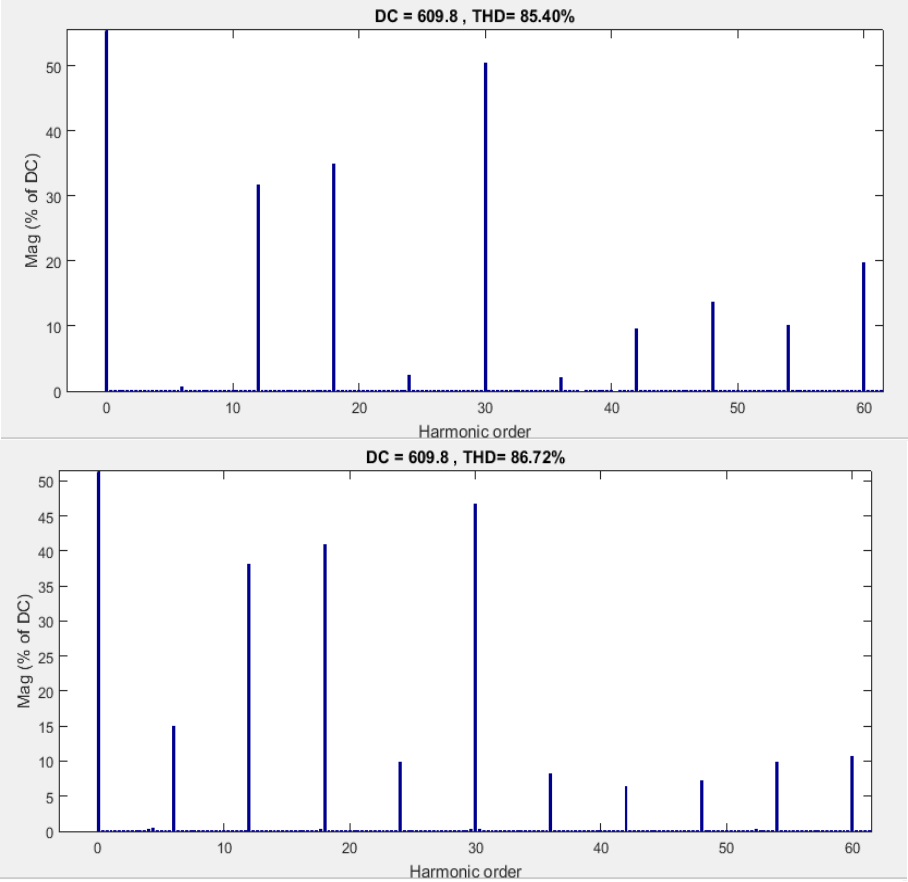

Figure 5-24 FFT Analysis for the steady state DC side current of one module machine at mf=15 and phase margin of phase controller is 60 degrees a) wc =300 rad/s b)) wc =20 rad/s

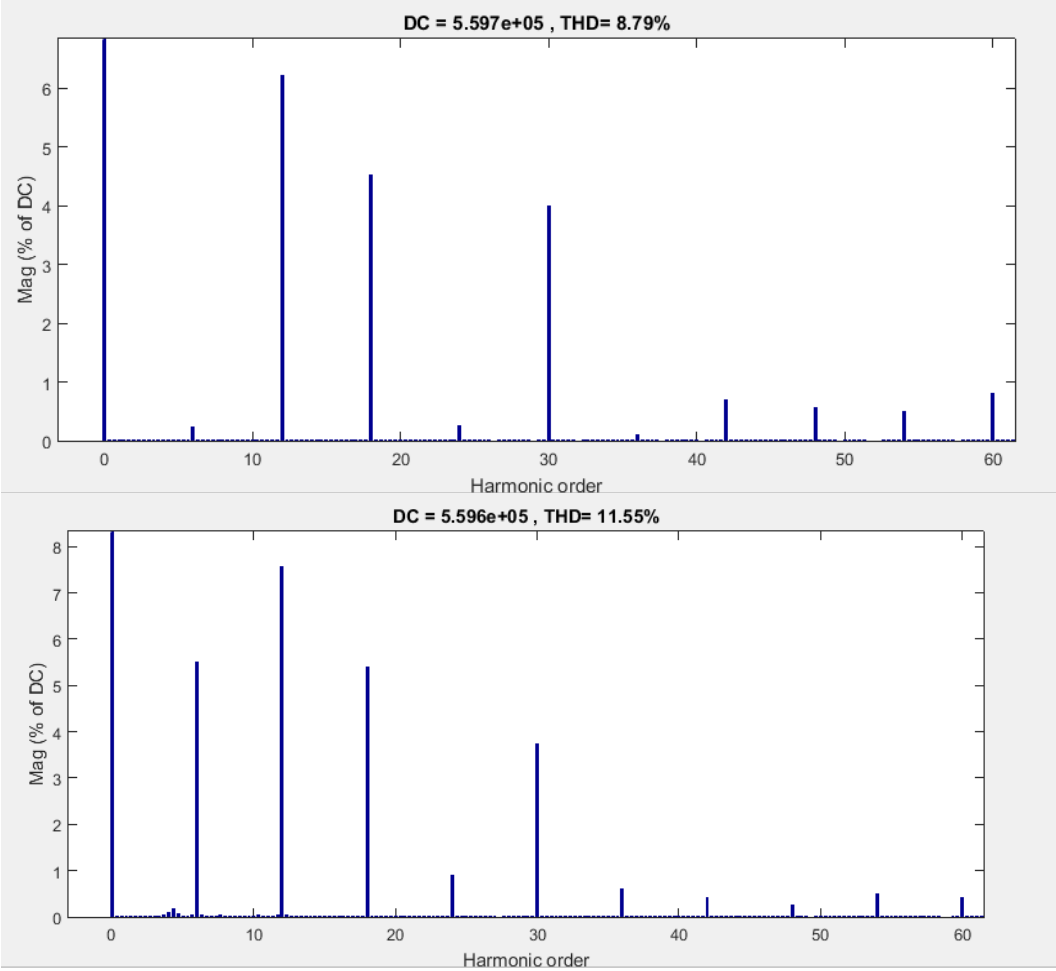

Figure 5-25 FFT Analysis for the steady state torque of one module machine at mf=15 showing the effect of lowering the bandwidth of the current controller on the torque harmonics a) w_c =300 rad/s b)) w_c =20 rad/s

That's why it is recommended to use the bandwidth of the inner loop (current loop) to be around 10 times the bandwidth of the outer loop (Speed Loop).

5.3.2: Two module machine:

The topology of the drive circuit is found in the Appendix (A5). In order to add another module all we have to do is to use the model of the machine of two modules explained above in section 5.1 and use separate current control loops to feed the machine. But we have only one speed controller because as it was previously mentioned in section 5.2.2 the two modules of the machine are mounted on the same shaft. The inverters triangular waveforms are shifted by 180 degrees from each other.

The new constants for the PI controller will be $K_{pW} = 6.3673 * 10^5\ [p.u.]$ and $K_{iW} = 3.2971 * 10^6\ [s^{-1}]$for the same machine data and $m_f = 15$.

Notice from (Figure 5-27) that using two modules of the machine will double the torque of the original machine because each module is rated as one megawatt of nominal power. Same can be said for the dc current in Figure 5-28.

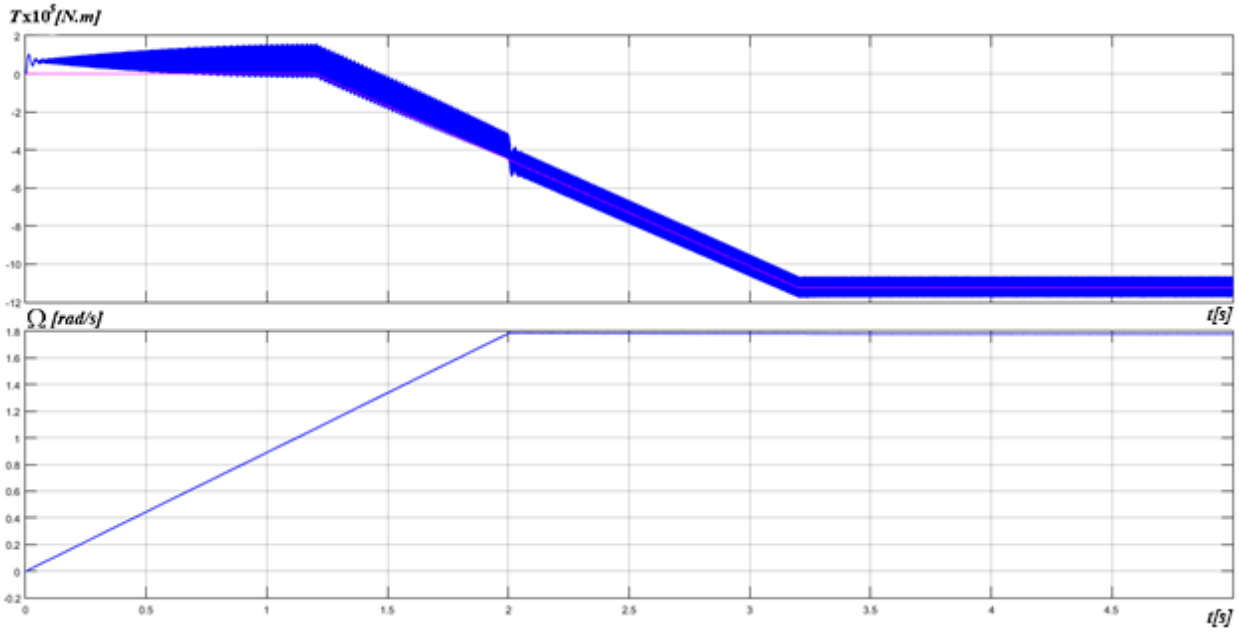

Figure 5-26 Actual torque vs the actual speed for two modules machine at mf=15

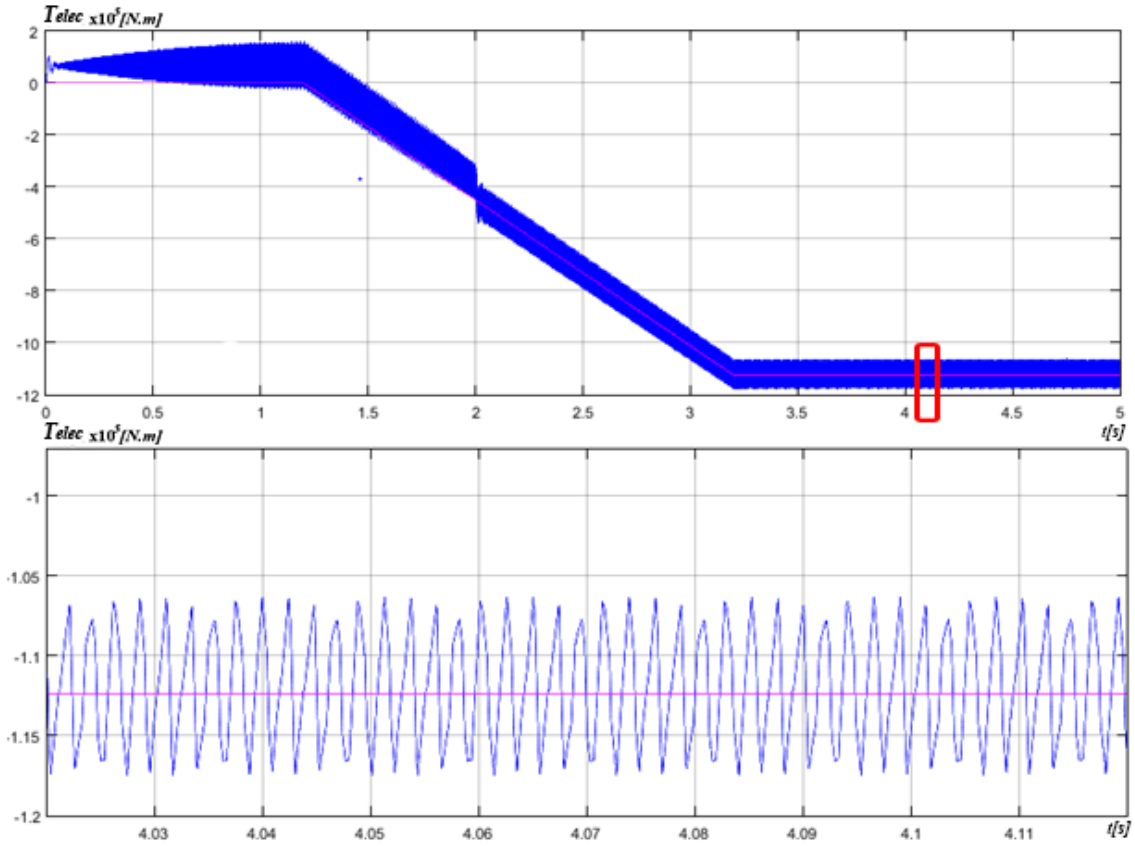

Figure 5-27 the steady state torque ripple of two module machine at mf=15

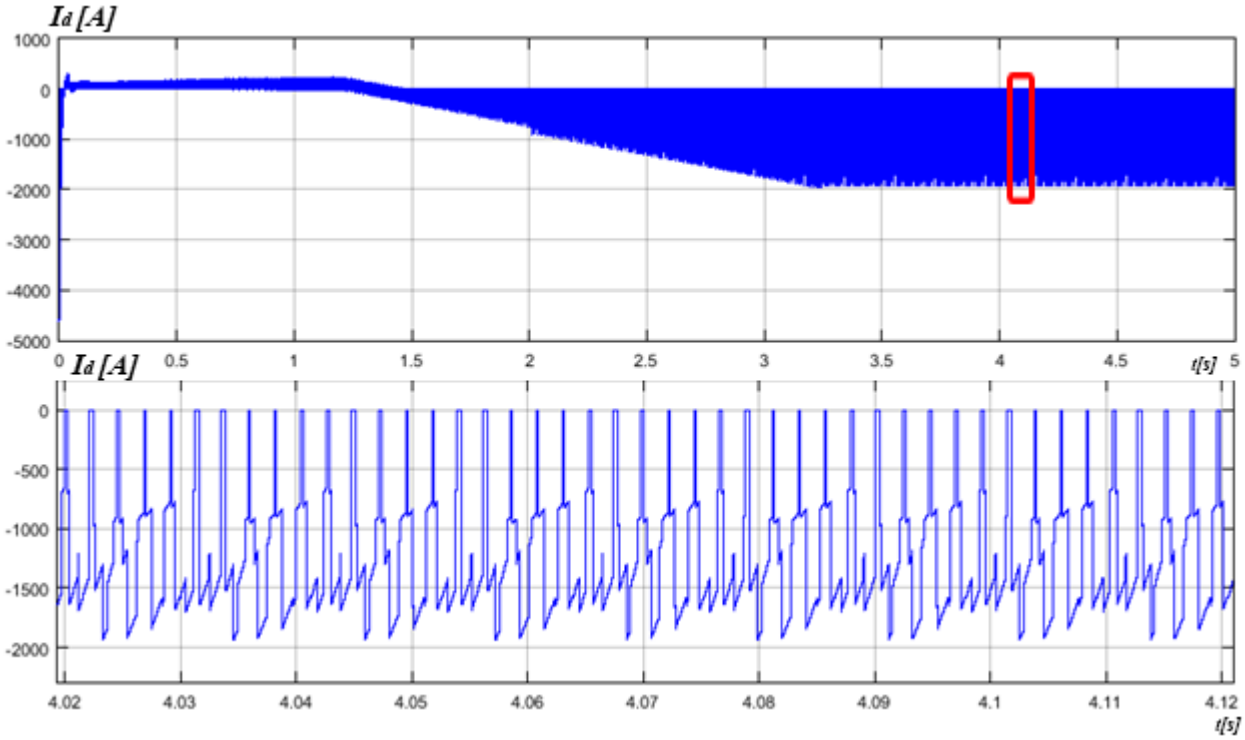

Figure 5-28 the steady state DC side current ripple of two module at mf=15

Hence we performed Fast Fourier Transform (FFT) on both current and torque at steady state and these are the harmonics obtained. From figure 5-29, 5-30) and the equation derived in chapter 4 $[4-15]$ is verified the disappearance of all harmonics except for 2mf, 4mf (30, 60)

Moreover, we can clearly notice the effect of the sequential control of the inverters using a displacement of 180 degrees between the two modules. It results in the reduction of THD% from 85.40% to 63.88% which is a reduction of $\frac{85.40-63.88}{85.40}$ =25.2% in the dc current ripples and also the harmonic distortion of the torque is reduced as well by $\frac{8.79-4.21}{8.79}$ = 52.1%.

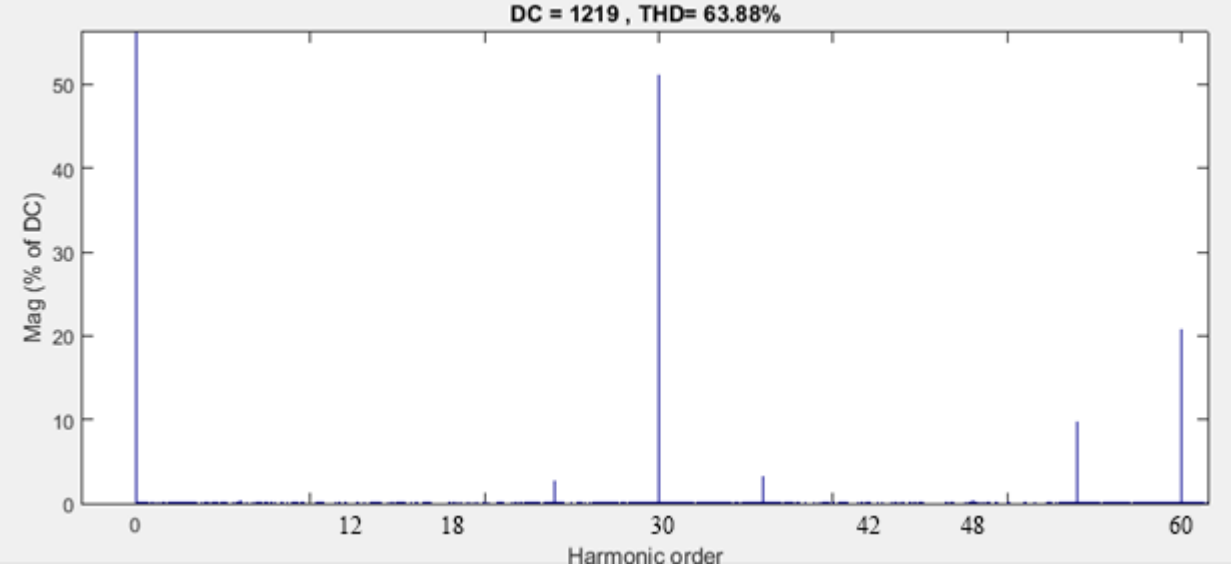

Figure 5-29 FFT Analysis for the steady state DC side current for two module machine at mf=15

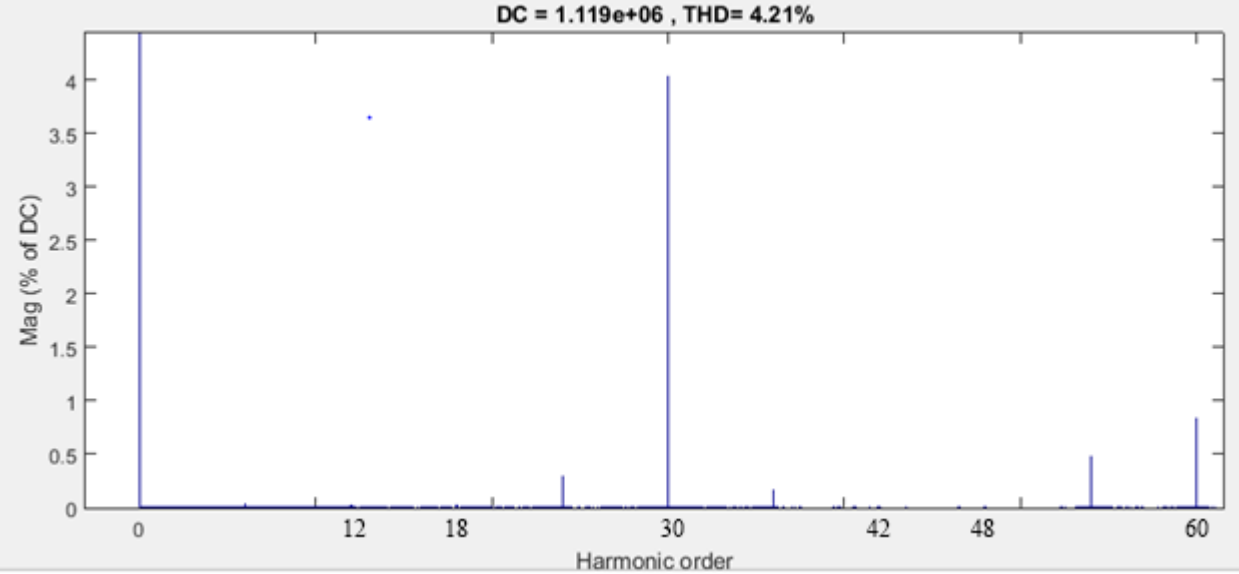

Figure 5-30 FFT analysis for the steady state Torque of the two module machine at mf=15

5.3.3: Three module machine:

As previously mentioned the methodology of adding an additional module is the same, and in this case the triangular waveform is shifted by 120,240 degrees respectively from the first inverter PWM.

The new constants for the PI controller will be $K_{pW} = 9.5509 * 10^5\ [p.u.]$and $K_{iW} = 4.9457 * 10^6\ [s^{-1}]$ for the same machine data and $m_f = 15$.

We can even notice the enhancement of the waveform of the dc side current and torque (Figure 5-32 and 5-33) from the effect of using three modules.

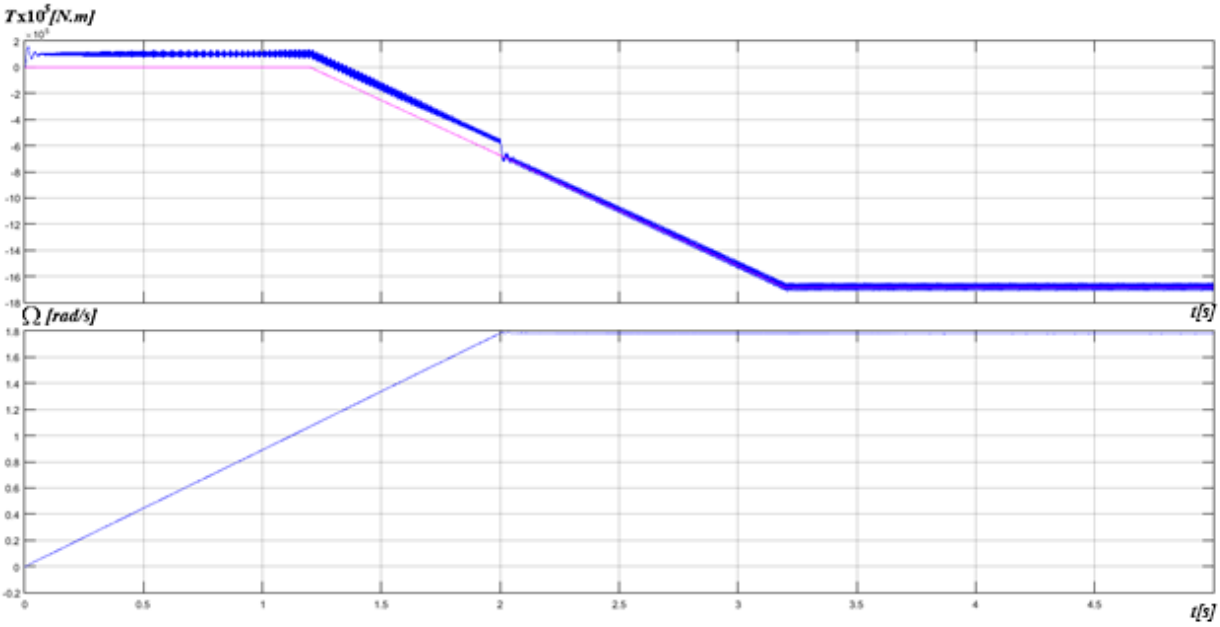

Figure 5-31 Actual torque vs the actual speed for three modules machine at mf=15

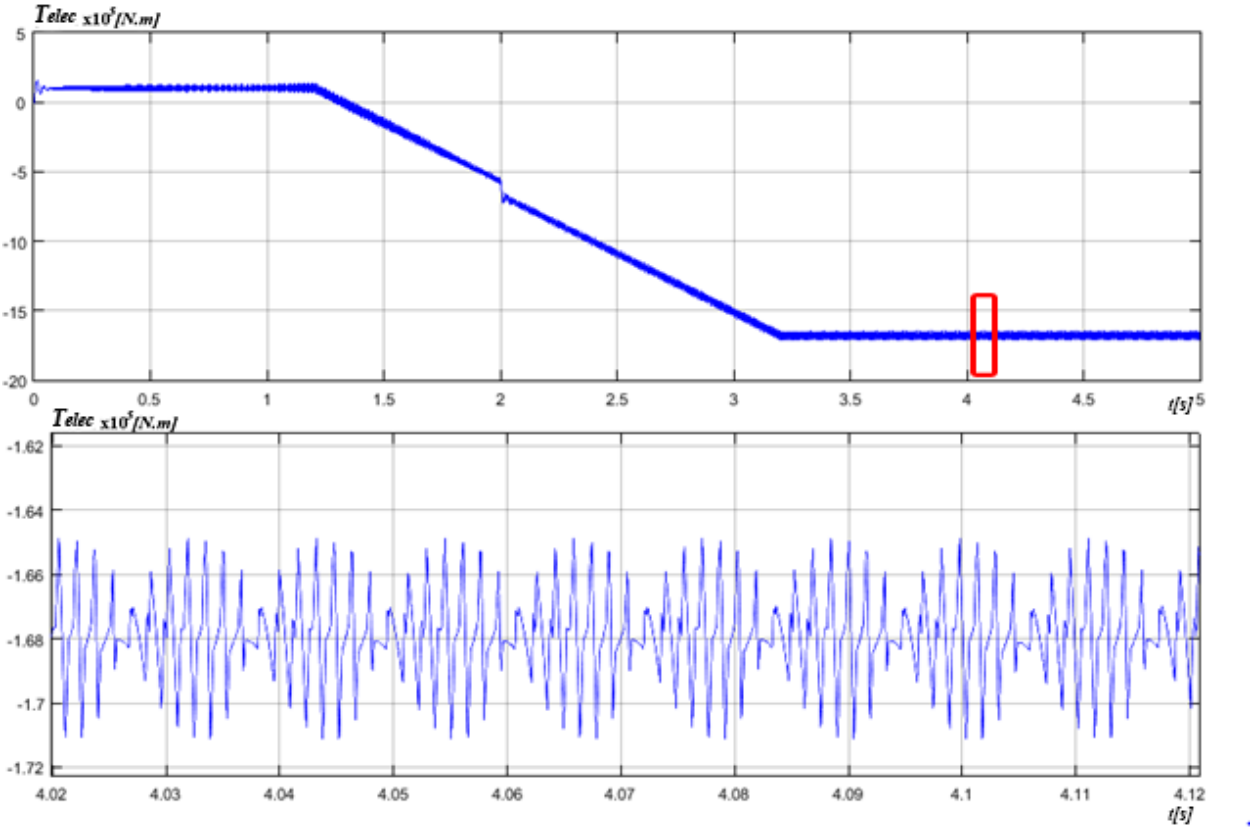

Figure 5-32 the steady state torque ripple of three module machine at mf=15

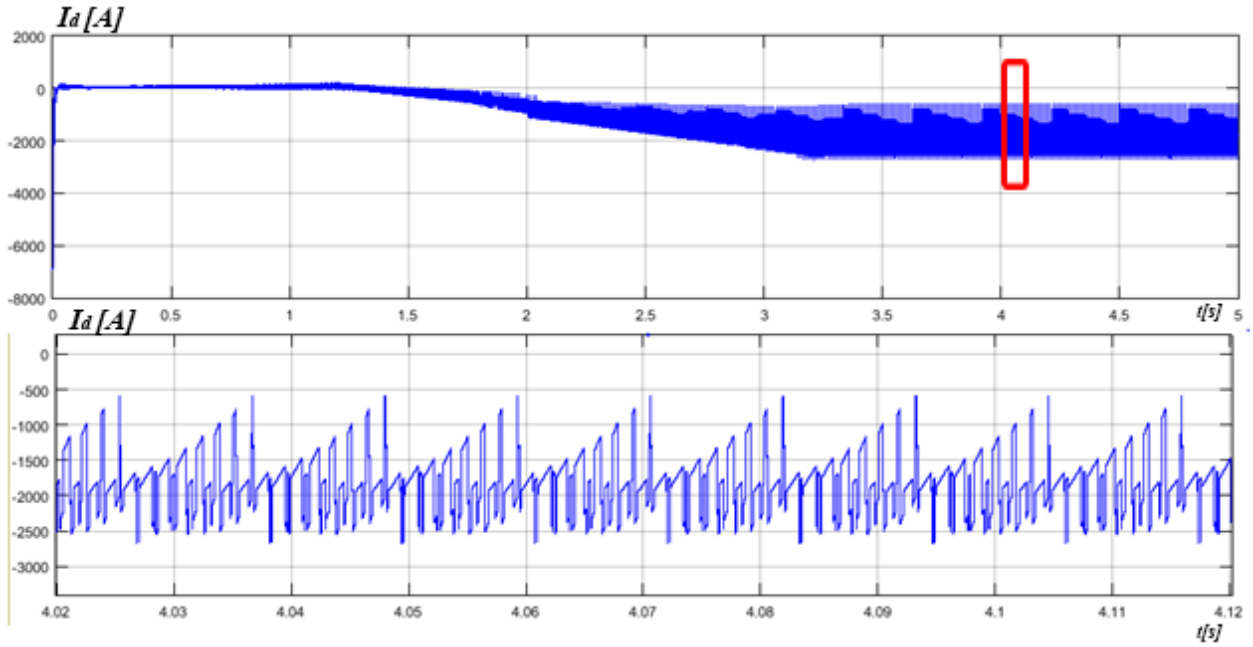

Figure 5-33 the steady state DC side current ripple of three module at mf=15

Hence we performed Fast Fourier Transform (FFT) on both current and torque at steady state and these are the harmonics obtained. (Figure 15-34, 15-35) and referring to equation $[4-11]$, all harmonics are eliminated except for 3mf-3 and 3mf+3 (42, 48)

The effectiveness can be noticed by the of THD% from 85.40% to 31.02% which is $\frac{85.40-31.02}{85.40}$ =63.7% reduction in the dc current ripples and also the harmonic distortion of the torque is reduced as well by $\frac{8.79-1.05}{8.79}$ = 88.1%.

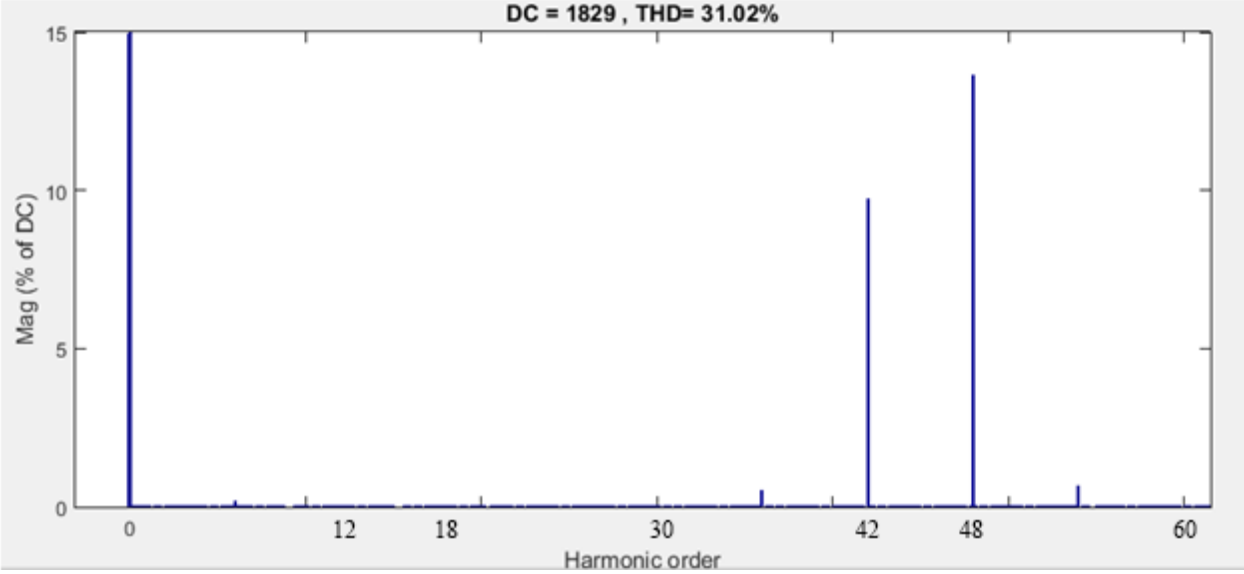

Figure 5-34 FFT Analysis for the steady state DC side current for three module machine at mf=15

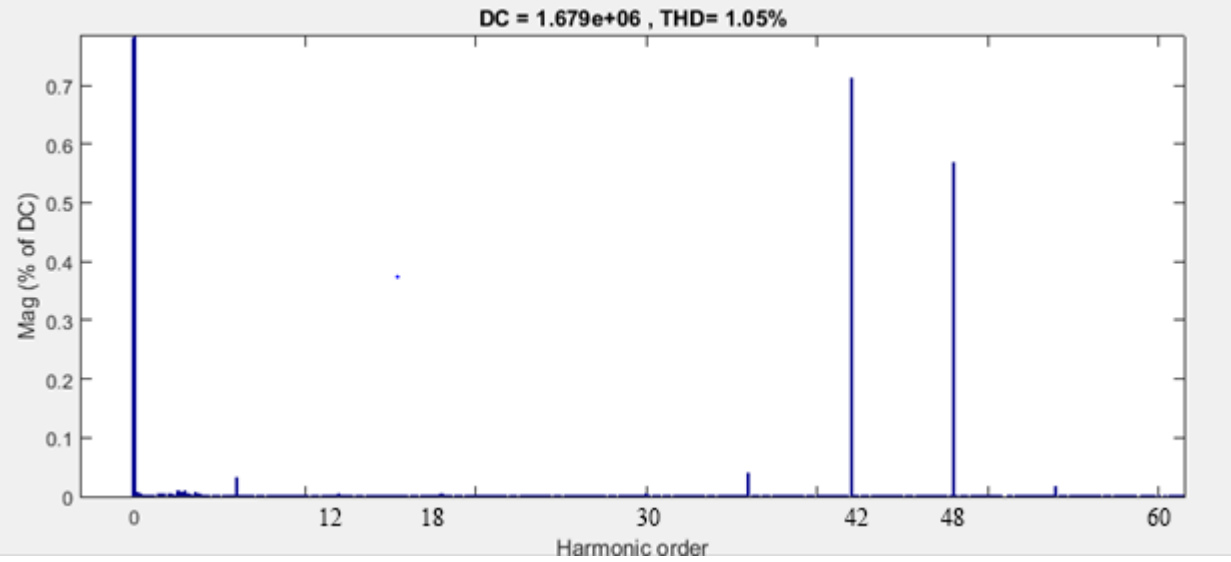

Figure 5-35 FFT analysis for the steady state Torque of the three module machine at mf=15

5.3.4: Torque THD versus Current THD

The input DC power, P_{DC}, is divided into switching losses in the inverter, P_{sw}, joule losses in the machine itself, P_{Joule}, power stored in the inductance of the machine, P_{induc}, and the mechanical power, P_{mech}.

$$P_{DC} = P_{sw} + P_{Joule} + P_{induc} + P_{mech}$$

$$V_{DC} * i_{DC} = P_{sw} + (i_d^2 + i_q^2)R_s + \frac{d}{dt}(\frac{1}{2} * L_d * i_d^2 + \frac{1}{2} * L_q * i_q^2) + T * \Omega$$

By simulating the power flow of our model (Figure 5-36 & 5-37), we can see that most of the ripple of the DC power is stored in the machine inductance, which is consistent with the theory, because we are using SPWM technique which shifts the harmonic to a higher order. The machine inductance was enough to filter out the harmonics from the current and not transferring it to the torque.

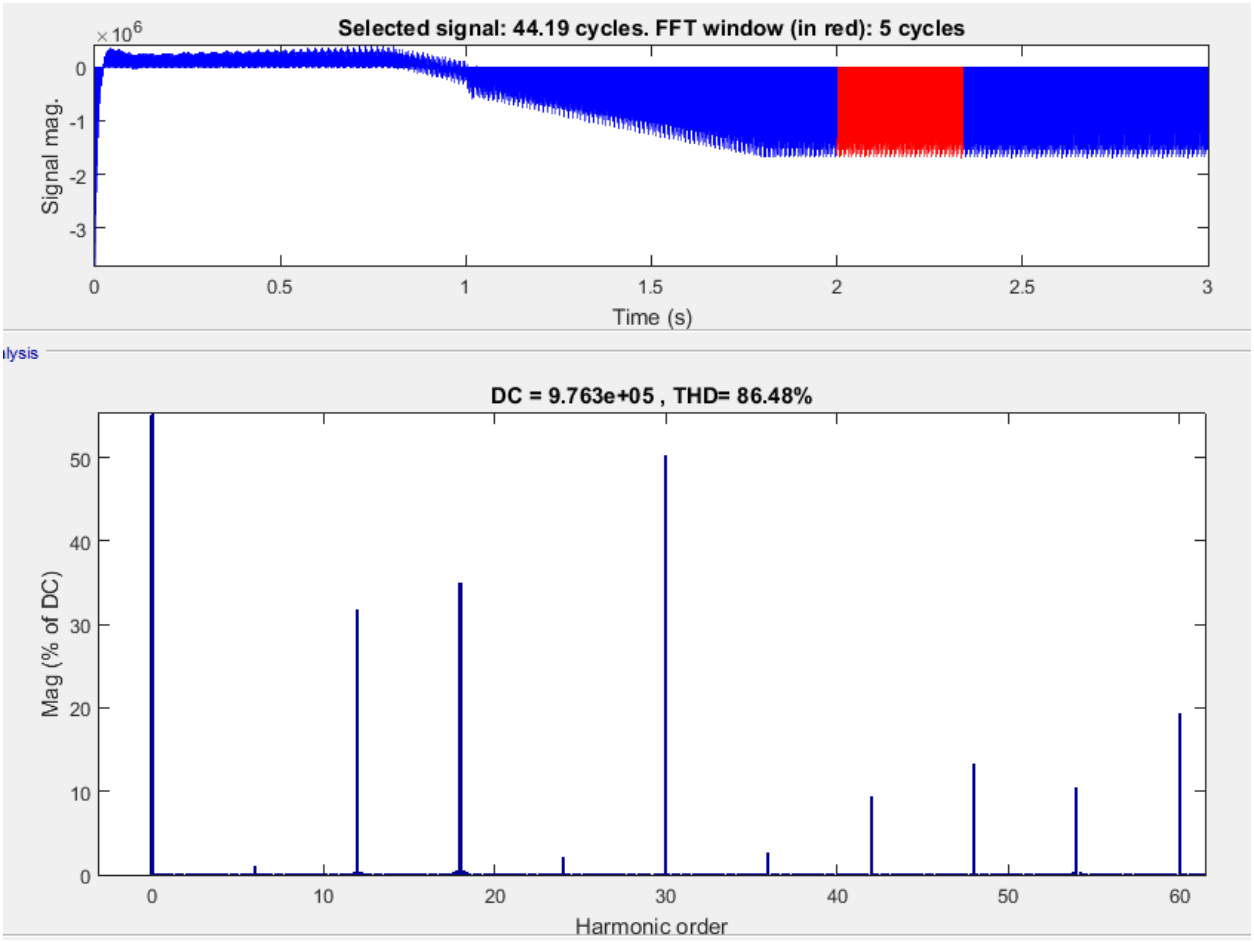

Figure 5-36 Instantaneous DC power of one module machine at mf=15

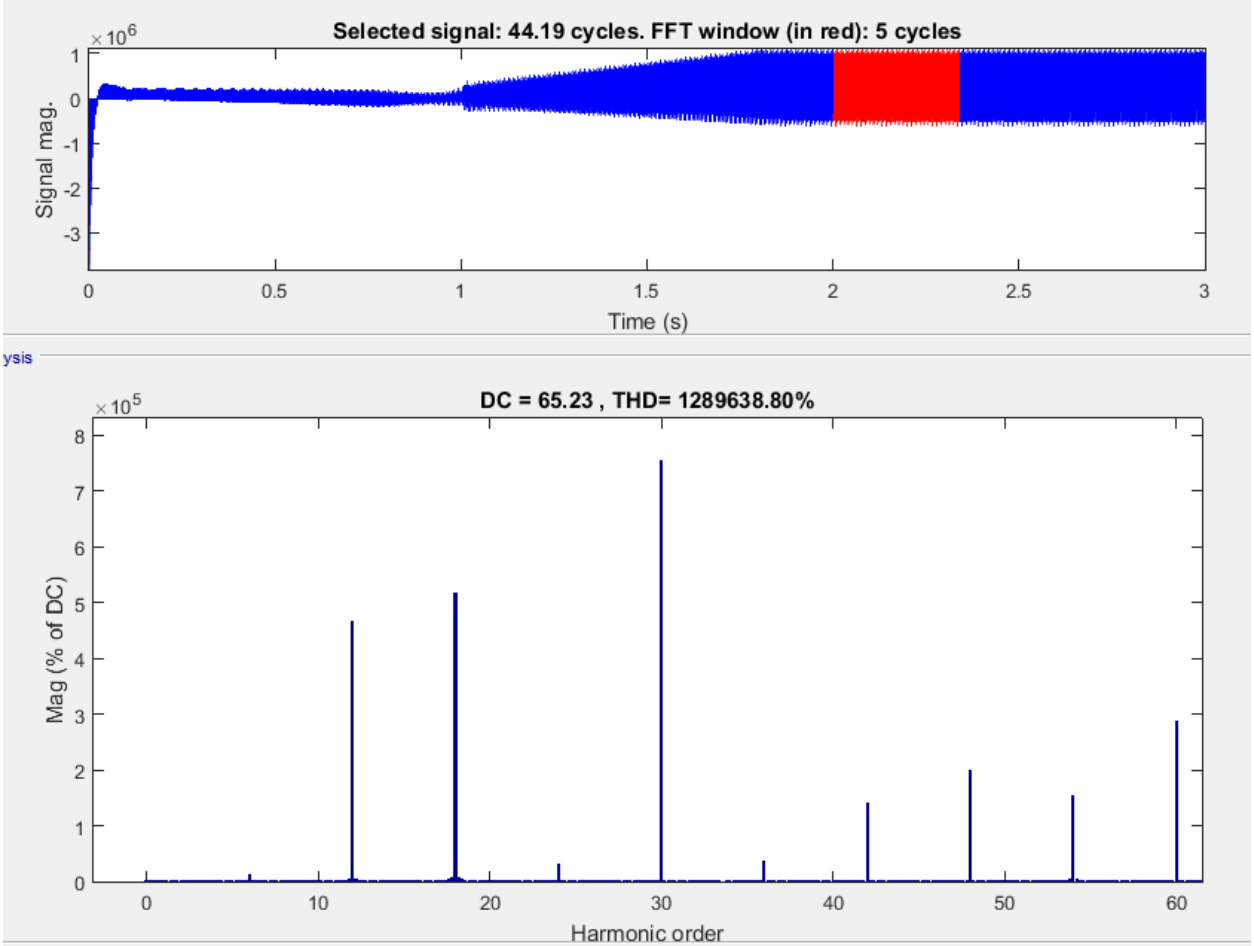

Figure 5-37 instantaneous power stored in the machine inductance of one module machine at mf=15

5.3.5: Comparison between Simulink results and our theoretical model

Let's use the associated reference directions for the voltage and the current
The phasor equation of the machine is

$$V_s = E + RI + j\omega L_s I$$

Because we are using a condition in which $i_d = 0$ and that results that stator current is equal only to the quadrature component of the current $i_s = ji_q$. The stator current is directed along the q-axis like the electromotive force E such E and I are 180 degrees out of phase. In this way the permanent magnet flux and the stator magneto-motive force are in quadrature and the torque is produced with the minimum stator current.
In a steady state condition, the driving torque is equal to the electromagnetic torque which is equal

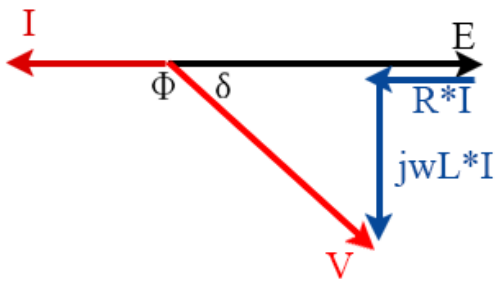

Figure 5-38 machine phasor diagram for the condition id=0

$$T_m = \frac{P_n}{\omega_{m-rated}} = \frac{P_n}{\frac{\omega_{m-rated}}{p} * 2} = \frac{10^6}{\frac{(2\pi * 14.73)2}{104}} = 561.850\ [kN.m]$$

$$T_e = \frac{p}{2} * \psi_{PM} * i_q$$

Where P_n is the rated power in table 5-1 which is one mega-watt, p is the number of poles , ψ_{PM} is the permanent magnet flux.

The permanent magnet flux ψ_{PM} can be calculated from the electromotive force of each phase which is given in the rated data of the machine (Table 5-1).

$$\psi_{PM} = \frac{\sqrt{3} * E_{phase}}{\omega_{rated}} = \frac{\sqrt{3} * 495}{14.73 * 2 * \pi} = 9.264\ [Wb]$$

since, $T_e = T_m$, therefore

$$i_{sq} = \frac{T_e}{\frac{p}{2} * \psi_{PM}} = 1166.36\ A$$

since the current component in the d-axis is zero, we can calculate directly the rms value of the phase current: $I_1 = \frac{i_{sq}}{\sqrt{3}}$. From the phasor diagram Figure 5-38 we can calculate the load angle δ and V_1

$$\delta = \tan^{-1}\left(\frac{X * I_1}{E_{phase} - R * I_1}\right) = 22.81^o$$

$$V_1 = \frac{E_{phase} - R * I_1}{\cos(\delta)} = 526.5656\ [V] \quad , \quad \hat{V}_1 = \sqrt{2} * V_1 = 744.66$$

It should be noted that the peak value of the fundamental doesn't agree with the value noted in table 4-4. In table 4-4, it was reported $\hat{V}_1 = \frac{V_d * M}{2}$ which in this case should be equal to 800 V (if M=1). But because we are now in a current controlled mode not a voltage controlled mode the amplitude modulation ratio M is no longer equal to 1.

Amplitude modulation ratio is calculated from the same relation $M = \frac{2 * \hat{V}_1}{V_d} = \frac{2 * 744.66}{1600} = 0.9308$. We use these values to calculate the amplitudes of currents and voltages.

At this point we can use equation $4 - 14$ that calculates the ripple current of the dc side (Appendix A-5).

It can be verified (Figures 5-38 and 5-39) that values obtained using the equation $4 - 14$ is in huge agreement with the Simulink model.

Also it should be noted that there is a disagreement for some of the harmonics: The harmonics of order $42\ (3m_f - 3), 48\ (3m_f + 3)\ and\ 60\ (4m_f)$. That's because during our development to the equation $4 - 14$, we considered values of $m = 1,2\ and\ n = 0, \pm 1, \pm 2, \pm 3$. Thus such difference between the two methods is due to the interaction of currents and voltages we didn't calculate. For example, the component $3m_f \pm 4$ (at $m = 3$, $n = \pm 4$) will interact with the fundamental voltages and currents that will add to the amplitude of $(3m_f - 3)$ and $(3m_f + 3)$.

$$\Delta i_{42} = \frac{v_1 * i_{41}}{V_d} + \frac{v_{41} * i_1}{V_d} \qquad and \qquad \Delta i_{48} = \frac{v_1 * i_{49}}{V_d} + \frac{v_{49} * i_1}{V_d}$$

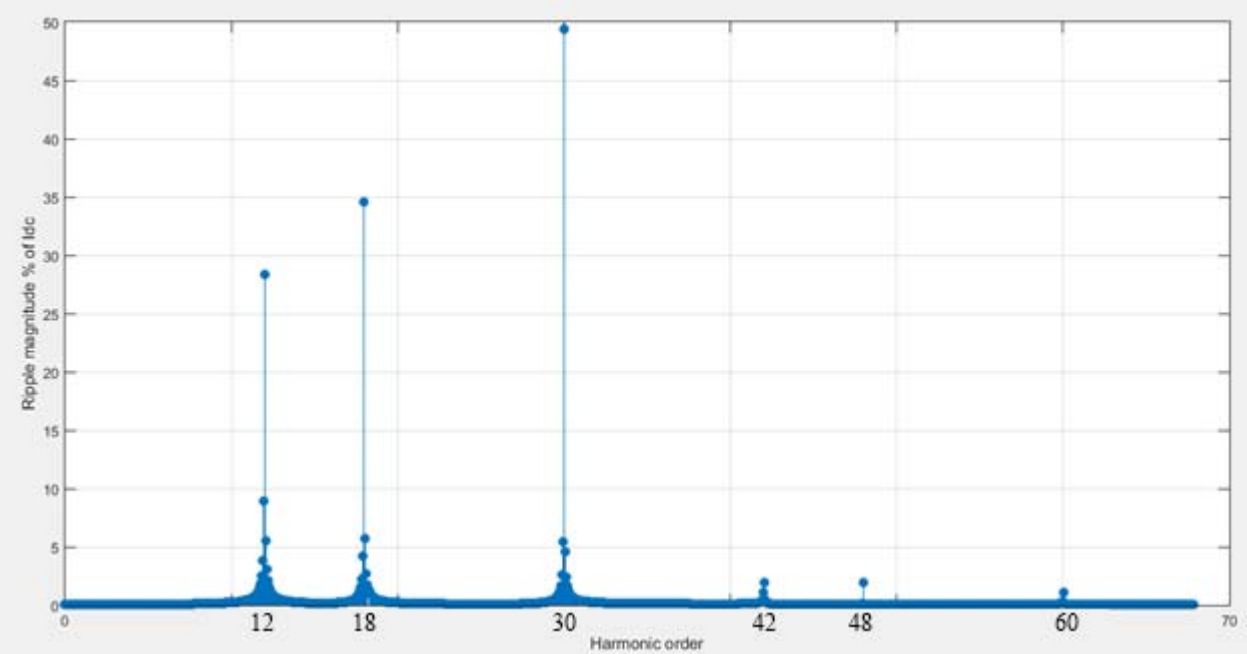

Figure 5-39 The FFT analysis of the dc side current using the developed equation 4-14 for mf=15

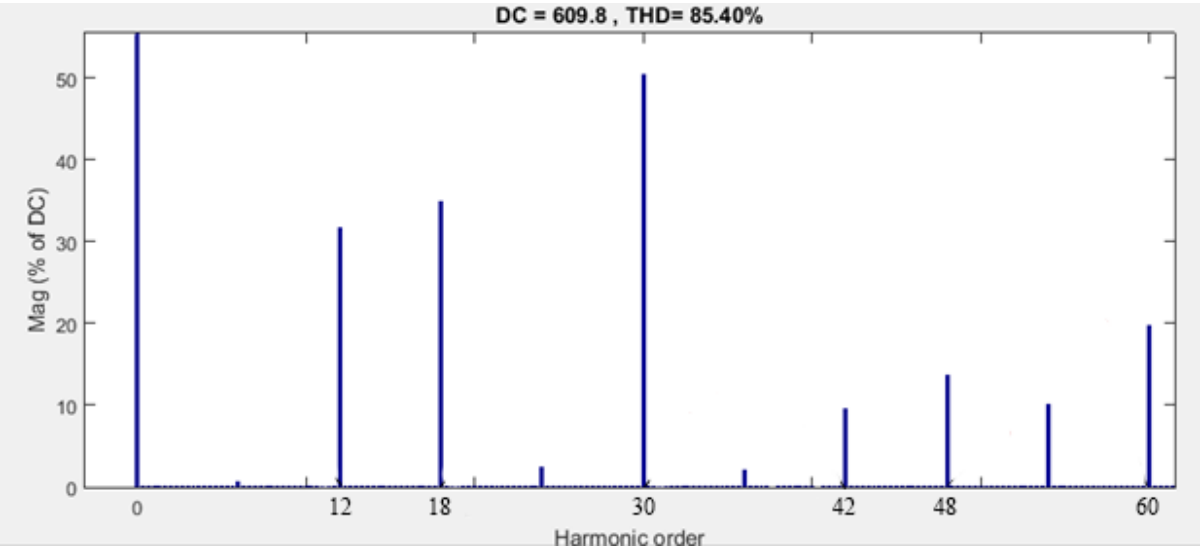

Figure 5-40 The FFT analysis of the dc side current using Matlab Simulink for mf=15

5.4: Effect of parameter change on the ripple components

5.4.1: Effect of changing controllers' parameters:

We are going to review the effect of changing the controllers bandwidth and phase margin on the total harmonic distortion.

5.4.1.1: Effect of changing controllers' bandwidth:

As we increase the bandwidth of both controllers (maintaining the current controller bandwidth is significantly higher than the speed controller bandwidth) the ripple contents of both current and torque increase Table 5-5.

Table 5-6 Effect of changing the bandwidth on the ripple components of the dc current and torque at mf=15: phase margins are 60° and 70° for the current and torque controllers respectively

Bandwidth of the controllers	Controllers constants	Dc current ripple	Steady State torque ripple
$\omega_{cI} = 30\frac{rad}{s}$ $\omega_{cW} = 4\frac{rad}{s}$	$K_{pI} = 0.0863$ $K_{iI} = 1.5282$ $K_{pW} = 1.3733 * 10^5$ $K_{iW} = 1.7833 * 10^5$	$THD_I = 84.10\%$	$THD_T = 8.57\%$
$\omega_{cI} = 50\frac{rad}{s}$ $\omega_{cW} = 8\frac{rad}{s}$	$K_{pI} = 0.1560$ $K_{iI} = 3.1901$ $K_{pW} = 2.7004 * 10^5$ $K_{iW} = 6.6595 * 10^5$	$THD_I = 85.07\%$	$THD_T = 8.64\%$
$\omega_{cI} = 100\frac{rad}{s}$ $\omega_{cW} = 10\frac{rad}{s}$	$K_{pI} = 0.3563$ $K_{iI} = 5.1016$ $K_{pW} = 3.4215 * 10^5$ $K_{iW} = 1.0707 * 10^6$	$THD_I = 86.24\%$	$THD_T = 8.84\%$
$\omega_{cI} = 130\frac{rad}{s}$ $\omega_{cW} = 13\frac{rad}{s}$	$K_{pI} = 0.4942$ $K_{iI} = 1.6285$ $K_{pW} = 4.6686 * 10^5$ $K_{iW} = 1.6391 * 10^6$	$THD_I = 86.37\%$	$THD_T = 9\%$

Increasing the bandwidth beyond 130 rad/s causes system instability (controllers constants are negative).

5.4.1.2: Effect of changing the current controller phase margin:

Decreasing the bandwidth of the current controller allow us to achieve higher cut off frequencies without showing instability. Table 5-5 and table 5-6 shows the results for current controller phase margin change from 60° to 45° respectively. Working with phase margin 45°, we are able to reach the cut off frequencies up to 220 rad/s.

It should be noted that working with a low phase margin (at a fixed cut off frequencies) will produce more ripples in the output. We can compare results at $\omega_{cI} = 30\frac{rad}{s}$,$\omega_{cW} = 4\frac{rad}{s}$ for phase margins 60° and 45° (Table 5-5 and Table 5-6) the THD% of the dc current and steady state torque increases.

Table 5-7 Effect of changing the phase margin of the dc current controller at mf=15: Phase margins are 45° and 70° for the current and torque controllers respectively

Bandwidth of the controllers	Controllers constants	Dc current ripple	Steady State torque ripple
$\omega_{cI} = 30\frac{rad}{s}$ $\omega_{cW} = 4\frac{rad}{s}$	$K_{pI} = 0.0702$ $K_{iI} = 2.1463$ $K_{pW} = 1.3722 * 10^5$ $K_{iW} = 1.8673 * 10^5$	$THD_I = 84.22\%$	$THD_T = 8.6\%$
$\omega_{cI} = 100\frac{rad}{s}$ $\omega_{cW} = 10\frac{rad}{s}$	$K_{pI} = 0.3310$ $K_{iI} = 14.1494$ $K_{pW} = 3.4195 * 10^5$ $K_{iW} = 1.2032 * 10^6$	$THD_I = 85.89\%$	$THD_T = 8.81\%$
$\omega_{cI} = 200\frac{rad}{s}$ $\omega_{cW} = 20\frac{rad}{s}$	$K_{pI} = 0.8817$ $K_{iI} = 12.6386$ $K_{pW} = 6.8824 * 10^5$ $K_{iW} = 4.1765 * 10^6$	$THD_I = 86.78\%$	$THD_T = 10.94\%$
$\omega_{cI} = 220\frac{rad}{s}$ $\omega_{cW} = 22\frac{rad}{s}$	$K_{pI} = 1.0170$ $K_{iI} = 4.9216$ $K_{pW} = 7.7768 * 10^5$ $K_{iW} = 4.9145 * 10^6$	$THD_I = 86.47\%$	$THD_T = 11.5\%$

5.4.2: Effect of changing PWM switching frequency:

As we increase the frequency modulation ratio (m_f), hence the switching frequency, the total harmonic distortion of the torque decreases as shown in Table 5-7. That's because the higher m_f the higher the order of the harmonic content which can be filtered out by the machine inductance.

It should be noted that the increase of m_f slightly affect the total harmonic distortion of the dc side current. That's because the electric line was modeled on Simulink with no inductance.

In Table 5-7, we can see the effect of the sequential control of two level inverters clearly. For example instead of using one module with $m_f = 675$ which has $THD_{T1} = 0.23\%$, we can use three modules at $m_f = 69$ and has the same THD. Also we can use two modules at $m_f = 15$ which has $THD_{T2} = 4.12\%$ instead of using one module at $m_f = 27$ which has $THD_{T1} = 4.72\%$.

Table 5-8 Effect of changing the frequency modulation ratio mf on the current and torque steady state ripple. The cutoff frequency of the current controller is 100 rad/s with phase margin 60 and the cutoff frequency of the speed controller is 10 rad/s with phase margin of 70

THD decrease with increasing number of modules →

m_f	$n_m = 1$	$n_m = 2$	$n_m = 3$
$m_f = 15$	$THD_{T1} = 8.79\%$	$THD_{T2} = 4.12\%$	$THD_{T3} = 1.05\%$
$m_f = 21$	$THD_{T1} = 6.13\%$	$THD_{T2} = 3.00\%$	$THD_{T3} = 0.74\%$
$m_f = 27$	$THD_{T1} = 4.72\%$	$THD_{T2} = 2.32\%$	$THD_{T3} = 0.58\%$
$m_f = 33$	$THD_{T1} = 3.84\%$	$THD_{T2} = 1.89\%$	$THD_{T3} = 0.47\%$
$m_f = 39$	$THD_{T1} = 3.24\%$	$THD_{T2} = 1.60\%$	$THD_{T3} = 0.40\%$
$m_f = 45$	$THD_{T1} = 2.81\%$	$THD_{T2} = 1.39\%$	$THD_{T3} = 0.35\%$
$m_f = 51$	$THD_{T1} = 2.47\%$	$THD_{T2} = 1.23\%$	$THD_{T3} = 0.31\%$
$m_f = 57$	$THD_{T1} = 2.21\%$	$THD_{T2} = 1.09\%$	$THD_{T3} = 0.28\%$
$m_f = 63$	$THD_{T1} = 2.00\%$	$THD_{T2} = 0.99\%$	$THD_{T3} = 0.25\%$
$m_f = 69$	$THD_{T1} = 1.83\%$	$THD_{T2} = 0.91\%$	$THD_{T3} = 0.23\%$
$m_f = 75$	$THD_{T1} = 1.68\%$	$THD_{T2} = 0.83\%$	$THD_{T3} = 0.21\%$
$m_f = 81$	$THD_{T1} = 1.56\%$	$THD_{T2} = 0.77\%$	$THD_{T3} = 0.20\%$
$m_f = 87$	$THD_{T1} = 1.45\%$	$THD_{T2} = 0.72\%$	$THD_{T3} = 0.19\%$
$m_f = 93$	$THD_{T1} = 1.36\%$	$THD_{T2} = 0.67\%$	$THD_{T3} = 0.17\%$
$m_f = 99$	$THD_{T1} = 1.28\%$	$THD_{T2} = 0.64\%$	$THD_{T3} = 0.17\%$
$m_f = 675$	$THD_{T1} = 0.23\%$	$THD_{T2} = 0.12\%$	$THD_{T3} = 0.13\%$

THD decrease with increasing the switching frequency ↓

Conclusion

We have developed an expression for the current ripple of the dc side and we have proven the validity of the expression using simulation on Matlab/Simulink. Also, we have proven both analytically and using simulation the effectiveness of sequential control of two level inverters connected in parallel on the dc side either driven by square wave modulation or pulse width modulation. Moreover, we showed that the decrease of the harmonic components increases by the increase of number of two level inverters connected in parallel.

We applied our method on the machine model of our case study; Axial flux Multi-modular permanent magnet synchronous generator. In which we designed the control system explaining the methodology behind designing both the current and speed controllers. Using simulation, we have shown that the torque ripples are much less than the dc current ripple and the role of the machine internal inductance in decreasing those harmonics.

Moreover, we have shown the consistency between the results from our mathematical model and the simulation results.

Finally, we have illustrated the effect of changing of some of the control parameters on the results using the simulation. And we have obtained the following results: by increasing the controllers' bandwidth, the ripple contents of both current and torque increases. Also, as we increase the frequency modulation ratio m_f, the total harmonic distortion of the torque decrease. We have shown the comparison of various switching frequencies using one, two and three modules. From such comparison we were able to emphasize the effect of using sequential control of the two level inverters. Instead of using a two level inverter with very high switching frequency to decrease the THD of the torque, we can use two or three inverters sequentially controlled at much lower switching frequency achieving the same torque THD.

References

1. [Alireza Khaligh and Omer C. Onar]- *Energy Harvesting: Solar, wind and ocean Energy conversion systems,* CRC press (2010).
2. [D. Bang, H. Polinder, G. Shrestha, J.A. Ferreira] - *Review of Generator Systems for Direct-Drive Wind Turbines,* Delft University of Technology Mekelweg 4, 2628 CD Delft the Netherlands.
3. [Zoran Ivanovski Msc.]- *Direct - Drive Wind Turbines* - International Journal of Scientific & Engineering Research Volume 2, Issue 10, Oct-2011, ISSN 2229-5518.
4. [Asko Parviainen] - *Design of Axial Flux permanent magnet low speed machines and performance comparison between radial flux and axial flux machines* – phd thesis at Lappeenranta University of Technology, Finland (2005).
5. [Fang lin luo , Hang Ye]- *Advanced DC/AC Inverter Applications in Renewable Energy* – CRC press (2013)
6. Power Electronics. 1. A.M. Gole, 2000. Sinusoidal Pulse width modulation
7. [Surin Khomfoi and Leon M. Tolbert] - *Chapter 31: Multilevel Power Converters* -The University of Tennessee
8. [G.I. Orfanoudakis, S. M. Sharkh, M.A. Yuratich and M.A. Abusara] – *Loss Comparison of two and three level inverter topolgies* – 5th IET Int. Conf. on Power Electronics, Machines and Drives (PEMD 2010) Brighton , UK.
9. [D. Grahame Holmes, Thomas A. Lipo] - *Pulse width modulation for power converters principles and practice*- IEEE Press , A John Wiley & Sons, inc., publication (2003).
10. [Francesco Castellidezza] – *Chapter 9: Electrical Drives course* – Politecnico di Milano, Italy

Appendix A-1

A-1.1: Square wave modulation:

$$v_{An}(t) = \hat{V}_{An(1)}\sin(\omega_1 t - \psi) + \hat{V}_{An(5)}\sin(5\omega_1 t - 5\psi) + \hat{V}_{An(7)}\sin(7\omega_1 t - 7\psi)$$

$$v_{Bn}(t) = \hat{V}_{An(1)}\sin(\omega_1 t - \psi - 120°) + \hat{V}_{An(5)}\sin(5\omega_1 t - 5\psi + 120°) + \hat{V}_{An(7)}\sin(7\omega_1 t - 7\psi - 120°)$$

$$v_{cn}(t) = \hat{V}_{An(1)}\sin(\omega_1 t - \psi - 240°) + \hat{V}_{An(5)}\sin(5\omega_1 t - 5\psi - 120°) + \hat{V}_{An(7)}\sin(7\omega_1 t - 7\psi - 240°)$$

Where the amplitudes are $\hat{V}_{An1} = \frac{2Vd}{\pi}$, $\hat{V}_{An(5)} = \frac{2Vd}{5\pi}$, $\hat{V}_{An(7)} = \frac{2Vd}{7\pi}$

$$i_A(t) = \hat{I}_1\sin(\omega_1 t - \psi - \phi) + \hat{I}_5\sin(5\omega_1 t - 5\psi - \theta_5) + \hat{I}_7\sin(7\omega_1 t - 7\psi - \theta_7)$$

$$i_B(t) = \hat{I}_1\sin(\omega_1 t - \psi - \phi - 120°) + \hat{I}_5\sin(5\omega_1 t - 5\psi - \theta_5 + 120°) + \hat{I}_7\sin(7\omega_1 t - 7\psi - \theta_7 - 120°)$$

$$i_c(t) = \hat{I}_1\sin(\omega_1 t - \psi - \phi - 240°) + \hat{I}_5\sin(5\omega_1 t - 5\psi - \theta_5 - 120°) + \hat{I}_7\sin(7\omega_1 t - 7\psi - \theta_7 - 240°)$$

Where the amplitudes are $\hat{I}_1 = \frac{\hat{V}_{An1}}{\sqrt{R^2+(\omega_1 L)^2}}$, $\hat{I}_5 = \frac{\hat{V}_{An5}}{\sqrt{R^2+(5\omega_1 L)^2}}$, $\hat{I}_7 = \frac{\hat{V}_{An7}}{\sqrt{R^2+(7\omega_1 L)^2}}$

And from the power balance:

$$V_d.i_{dc}(t) = i_A(t).v_{An}(t) + i_B(t).v_{Bn}(t) + i_c(t).v_{cn}(t) =$$
$$i_{A_1}.v_{An1} + i_{B_1}v_{Bn1} + i_{C_1}v_{Cn1} +$$
$$i_{A_5}v_{An5} + i_{B_5}v_{Bn5} + i_{C_5}v_{Cn5} +$$
$$i_{A_7}v_{An7} + i_{B_7}v_{Bn7} + i_{C_7}v_{Cn7} +$$
$$i_{A_1}v_{An5} + i_{A_5}v_{An1} + i_{B_1}v_{Bn5} + i_{B_5}v_{Bn1} + i_{C_1}v_{Cn5} + i_{C_5}v_{Cn1}$$
$$i_{A_7}v_{An5} + i_{A_5}v_{An7} + i_{B_7}v_{Bn5} + i_{B_5}v_{Bn7} + i_{C_7}v_{Cn5} + i_{C_5}v_{Cn7}$$
$$i_{A_1}v_{An7} + i_{A_7}v_{An1} + i_{B_1}v_{Bn7} + i_{B_7}v_{Bn1} + i_{C_1}v_{Cn7} + i_{C_7}v_{Cn1}$$

The direct component contribution from the multiplication of voltages and currents of the same harmonic

The dc current ripple production

Thus the dc current ripple

$$V_d.i_r(t) = i_{A_1}v_{An5} + i_{A_5}v_{An1} + i_{B_1}v_{Bn5} + i_{B_5}v_{Bn1} + i_{C_1}v_{Cn5} + i_{C_5}v_{Cn1} + i_{A_7}v_{An5} + i_{A_7}v_{An1} + i_{B_7}v_{Bn5} + i_{B_7}v_{Bn1} +$$
$$i_{C_7}v_{Cn5} + i_{C_7}v_{Cn1} + i_{A_1}v_{An7} + i_{A_5}v_{An7} + i_{B_1}v_{Bn7} + i_{B_5}v_{Bn7} + i_{C_1}v_{Cn7} + i_{C_5}v_{Cn7}$$

Interaction between the first and Fifth harmonics

$$\frac{i_{A_1}v_{An_5}}{V_d} = \left[\frac{1}{V_d}\right]\left[\hat{I}_1\sin((\omega_1 t - \psi) - \phi)\right] * \left[\frac{2V_d}{5\pi}\sin 5 * (\omega_1 t - \psi)\right] = \frac{\hat{I}_1}{5\pi}.(\cos(4\omega_1 t - 4\psi + \phi) - \cos(6\omega_1 t - 6\psi - \phi))$$

$$\frac{i_{B_1}v_{Bn_5}}{V_d} = \frac{\hat{I}_1}{5\pi}.2.\sin(\omega_1 t - \psi - \phi - 120°)\sin(5\omega_1 t - 5\psi + 120°) = \frac{\hat{I}_1}{5\pi}(\cos(4\omega_1 t - 4\psi + \phi + 240) - \cos(6\omega_1 t - 6\psi - \phi))$$

$$\frac{i_{C_1}v_{Cn_5}}{V_d} = \frac{\hat{I}_1}{5\pi}.2.\sin(\omega_1 t - \psi - \phi - 240°)\sin(5\omega_1 t - 5\psi - 120°) = \frac{\hat{I}_1}{5\pi}(\cos(4\omega_1 t - 4\psi + \phi + 120°) - \cos(6\omega_1 t - 6\psi - \phi))$$

$$\frac{i_{A_5}v_{An_1}}{V_d} = \frac{\widehat{2.I_5}V_d}{V_d\pi}\sin(5(\omega_1 t - \psi) - \theta_5)\sin(\omega_1 t - \psi) = \frac{\hat{I}_5}{\pi}.(\cos(4\omega_1 t - 4\psi - \theta_5) - \cos(6\omega_1 t - 6\psi - \theta_5))$$

$$\frac{i_{B_5}v_{Bn_1}}{V_d} = \frac{2\hat{I}_5}{\pi}\sin(5(\omega_1 t - \psi - 120) - \theta_5)\sin(\omega_1 t - \psi - 120) = \frac{\hat{I}_5}{\pi}(\cos(4\omega_1 t - 4\psi - \theta_5 + 240°) - \cos(6\omega_1 t - 6\psi - \theta_5))$$

$$\frac{i_{C_5}v_{Cn_1}}{V_d} = \frac{2\hat{I}_5}{\pi}\sin(5(\omega_1 t - \psi - 240) - \theta_5)\sin(\omega_1 t - \psi - 240)$$
$$= \frac{\hat{I}_5}{\pi}(\cos(4\omega_1 t - 4\psi - \theta_5 + 120) - \cos(6\omega_1 t - 6\psi - \theta_5))$$

$$\sum = \begin{matrix} i_{r4}(t) = 0 \\ i_{r6}(t) = \frac{-3I_1}{5\pi}\cos(6\omega_1 t - 6\psi - \phi) - \frac{3I_5}{\pi}\cos(6\omega_1 t - 6\psi - \theta_5) \end{matrix}$$

Interaction between the first and seventh harmonics

$$\frac{i_{a_1}v_{an_7}}{V_d} = \frac{\hat{I}_1.2V_d}{7\pi\, V_d}\sin(\omega_1 t-\psi-\phi)\sin(7\omega_1 t-7\psi) = \frac{\hat{I}_1}{7\pi}(\cos(6\omega_1 t-6\psi+\phi) - \cos(8\omega_1 t-8\psi-\phi))$$

$$\frac{i_{b_1}v_{bn_7}}{V_d} = \frac{\hat{I}_1}{7\pi}.2.\sin(\omega_1 t-\psi-\phi-120°)\sin(7\omega_1 t-7\psi-120°) = \frac{\hat{I}_1}{7\pi}(\cos(6\omega_1 t-6\psi+\phi) - \cos(8\omega_1 t-8\psi-\phi-240°))$$

$$\frac{i_{c_1}v_{cn_7}}{V_d} = \frac{\hat{I}_1}{7\pi}.2.\sin(\omega_1 t-\psi-\phi-240°)\sin(7\omega_1 t-7\psi-240°) = \frac{\hat{I}_1}{7\pi}(\cos(6\omega_1 t-6\psi+\phi) - \cos(8\omega_1 t-8\psi-\phi-120°))$$

$$\frac{i_{a_7}v_{an_1}}{V_d} = \frac{\hat{I}_7.2V_d}{\pi}\sin(7\omega_1 t-7\psi-\theta_7)\sin(\omega_1 t-\psi) = \frac{\hat{I}_7}{\pi}(\cos(6\omega_1 t-6\psi-\theta_7) - \cos(8\omega_1 t-8\psi-\theta_7))$$

$$\frac{i_{b_7}v_{bn_1}}{V_d} = \frac{\hat{I}_7}{\pi}.2.\sin(7\omega_1 t-7\psi-\theta_7-120°)\sin(\omega_1 t-\psi-120°) = \frac{\hat{I}_7}{\pi}(\cos(6\omega_1 t-6\psi-\theta_7) - \cos(8\omega_1 t-8\psi-\theta_7-240°))$$

$$\frac{i_{c_7}v_{cn_1}}{V_d} = \frac{\hat{I}_7}{\pi}.2.\sin(7\omega_1 t-7\psi-\theta_7-240°)\sin(\omega_1 t-\psi-240°) = \frac{\hat{I}_7}{\pi}(\cos(6\omega_1 t-6\psi-\theta_7) - \cos(8\omega_1 t-8\psi-\theta_7-120°))$$

$$\sum = \quad i_{r8}(t) = 0$$

$$i_{r6}(t) = \frac{3I_1}{7\pi}cos(6\omega_1 t-6\psi+\phi) + \frac{3I_7}{\pi}cos(6\omega_1 t-6\psi-\theta_7)$$

Interaction between the fifth and seventh harmonics

$$\frac{i_{a_7}v_{an_5}}{V_d} = \frac{\hat{I}_7.2V_d}{V_d\,5\pi}\sin(7\omega_1 t-7\psi-\theta_7)\sin(5\omega_1 t-5\psi) = \frac{\hat{I}_7}{5\pi}(\cos(2\omega_1 t-2\psi-\theta_7) - \cos(12\omega_1 t-12\psi-\theta_7))$$

$$\frac{i_{b_7}v_{bn_5}}{V_d} = \frac{2\hat{I}_7}{5\pi}\sin(7\omega_1 t-7\psi-\theta_7-120°)\sin(5\omega_1 t-5\psi+120°) = \frac{\hat{I}_7}{5\pi}\big(\cos(2\omega_1 t-2\psi-\theta_7-240°) - \cos((12\omega_1 t-12\psi-\theta_7))\big)$$

$$\frac{i_{c_7}v_{cn_5}}{V_d} = \frac{2\hat{I}_7}{5\pi}\sin(7\omega_1 t-7\psi-\theta_7-240°)\sin(5\omega_1 t-5\psi-120°) = \frac{\hat{I}_7}{5\pi}\big(\cos(2\omega_1 t-2\psi-\theta_7-120°) - \cos((12\omega_1 t-12\psi-\theta_7))\big)$$

$$\frac{i_{a_5}v_{an_7}}{V_d} = \frac{\hat{I}_5.2V_d}{7\pi\, V_d}\sin(5\omega_1 t-5\psi-\theta_5)\sin(7\omega_1 t-7\psi) = \frac{\hat{I}_5}{7\pi}\big(\cos(2\omega_1 t-2\psi+\theta_5) - \cos((12\omega_1 t-12\psi-\theta_5))\big)$$

$$\frac{i_{b_5}v_{bn_7}}{V_d} = \frac{2\hat{I}_5}{7\pi}\sin(5\omega_1 t-5\psi-\theta_5+120°)\sin(7\omega_1 t-7\psi-120°) = \frac{\hat{I}_5}{7\pi}\big(\cos(2\omega_1 t-2\psi+\theta_5-240°) - \cos((12\omega_1 t-12\psi-\theta_5))\big)$$

$$\frac{i_{c_5}v_{cn_7}}{V_d} = \frac{2\hat{I}_5}{7\pi}\sin(5\omega_1 t-5\psi-\theta_5-120°)\sin(7\omega_1 t-7\psi-240°) = \frac{\hat{I}_5}{7\pi}\big(\cos(2\omega_1 t-2\psi+\theta_5-120°) - \cos((12\omega_1 t-12\psi-\theta_5))\big)$$

$$\sum = \quad i_{r2}(t) = 0$$

$$i_{r12}(t) = \frac{3I_7}{5\pi}cos(12\omega_1 t-12\psi-\theta_7) - \frac{3I_5}{7\pi}cos(12\omega_1 t-12\psi-\theta_5)$$

Thus the overall equation

$$i_r(t) = -\frac{3\hat{I}_7}{5\pi}\cos(12\omega_1 t-\theta_7-12\psi) - \frac{3\hat{I}_5}{7\pi}\cos(12\omega_1 t-\theta_5-12\psi) - \frac{3\hat{I}_1}{5\pi}\cos(6\omega_1 t-\phi-6\psi) - \frac{3\hat{I}_5}{\pi}\cos(6\omega_1 t-\theta_5-6\psi)$$
$$+\frac{3\hat{I}_1}{7\pi}\cos(6\omega_1 t+\phi-6\psi) + \frac{3\hat{I}_7}{\pi}\cos(6\omega_1 t-\theta_7-6\psi)$$

A-1.2: Pulse width modulation:

Bessel Function:

$$J_n(x) = \sum_{k=0}^{\infty} \frac{(-1)^k (x/2)^{n+2k}}{k!\,(n+k)!} = \frac{(1)(x/2)^n}{(1)(n)!} + \frac{(-1)(x/2)^{n+2}}{(1)(n+1)} + \frac{(1)(x/2)^{n+4}}{2(n+1)(n+2)} + \cdots$$

It can be simplified to the first three terms, taking the argument $x = m\frac{\pi}{2}M$:

$$J_n\left(m\frac{\pi}{2}M\right) = \frac{(m\frac{\pi}{2})^n M^n}{2^n n!} \cdot \left[1 - \frac{\left(m\frac{\pi}{2}\right)^2 M^2}{2^2(n+1)} + \frac{\left(m\frac{\pi}{2}\right)^4 M^4}{2^4(n+1)(n+2)} + \cdots\right]$$

Results of Bessel Function:

$\boldsymbol{m = 1}$	
$J_0(x) = \frac{512 - 32\,\pi^2M^2 + \pi^4M^4}{512}$	
$J_1(x) = \frac{\pi M}{4}\left(\frac{1536-48\,\pi^2M^2+\pi^4M^4}{1536}\right)$	$J_{-1}(x) = -\frac{\pi M}{4}\left(\frac{1536-48\,\pi^2M^2+\pi^4M^4}{1536}\right)$
$J_2(x) = \frac{(\pi M)^2}{32}\left(\frac{3072-64\,\pi^2M^2+\pi^4M^4}{3072}\right)$	$J_{-2}(x) = \frac{(\pi M)^2}{32}\left(\frac{3072-64\,\pi^2M^2+\pi^4M^4}{3072}\right)$
$J_3(x) = \frac{(\pi M)^3}{384}\left(\frac{5120-80\,\pi^2M^2+\pi^4M^4}{5120}\right)$	$J_{-3}(x) = -\frac{(\pi M)^3}{384}\left(\frac{5120-80\,\pi^2M^2+\pi^4M^4}{5120}\right)$

$\boldsymbol{m = 2}$	
$J_0(x) = \frac{32 - 8\,\pi^2M^2 + \pi^4M^4}{32}$	
$J_1(x) = \frac{\pi M}{2}\left(\frac{96-12\,\pi^2M^2+\pi^4M^4}{96}\right)$	$J_{-1}(x) = \frac{-\pi M}{2}\left(\frac{96-12\,\pi^2M^2+\pi^4M^4}{96}\right)$
$J_2(x) = \frac{(\pi M)^2}{8}\left(\frac{192-16\,\pi^2M^2+\pi^4M^4}{192}\right)$	$J_{-2}(x) = \frac{(\pi M)^2}{8}\left(\frac{192-16\,\pi^2M^2+\pi^4M^4}{192}\right)$
$J_3(x) = \frac{(\pi M)^3}{48}\left(\frac{320-20\,\pi^2M^2+\pi^4M^4}{320}\right)$	$J_{-3}(x) = \frac{-(\pi M)^3}{48}\left(\frac{320-20\,\pi^2M^2+\pi^4M^4}{320}\right)$

$\sin\left((m+n)\,\pi/2\right)$				
m = 1	n = 0	1		
	n = 1	0	n = -1	0
	n = 2	-1	n = -2	-1
	n = 3	0	n = -3	0
m = 2	n = 0	0		
	n = 1	-1	n = -1	1
	n = 2	0	n = -2	0
	n = 3	1	n = -3	-1

Calculating the harmonic voltage and current amplitudes:

For (h = 1)

$\hat{I}_1 = \frac{V'}{Z_1}\cos(\omega_t - \phi)$

$\phi = \tan^{-1}\left(\frac{\omega_1 L}{R}\right) - \tan^{-1}\left(\frac{E\sin\delta}{VAn - E\cos\delta}\right)$

$V' = \sqrt{(VAn_1 - E\cos\delta)^2 + (E\sin\delta)^2}$

$z_1 = \sqrt{R^2 + (\omega_1 L)^2}$

Voltage Amplitudes

$\hat{V}_1 = \frac{V_d * M}{2}$	$\hat{V}_{mf} = \frac{2V_d}{\pi}\left(\frac{512 - 32\pi^2M^2 + \pi^4M^4}{512}\right)$	$m = 1$
$\hat{V}_{mf-2} = \frac{-2V_d}{\pi}\left(\frac{(\pi M)^2}{32}.\frac{3072 - 64\pi^2M^2 + \pi^4M^4}{3072}\right)$	$\hat{V}_{mf+2} = \frac{-2V_d}{\pi}\left(\frac{(\pi M)^2}{32}.\frac{3072 - 64\pi^2M^2 + \pi^4M^4}{3072}\right)$	
$\hat{V}_{2mf+1} = \frac{-V_d}{2\pi}\left(\frac{\pi M}{2}.\frac{96 - 12\pi^2M^2 + \pi^4M^4}{96}\right)$	$\hat{V}_{2mf-1} = \frac{-V_d}{2\pi}\left(\frac{\pi M}{2}.\frac{96 - 12\pi^2M^2 + \pi^4M^4}{96}\right)$	$m = 2$
$\hat{V}_{2mf+3} = \frac{V_d}{2\pi}\left(\frac{(\pi M)^3}{48}.\frac{320 - 20\pi^2M^2 + \pi^4M^4}{320}\right)$	$\hat{V}_{2mf+3} = \frac{V_d}{2\pi}\left(\frac{(\pi M)^3}{48}.\frac{320 - 20\pi^2M^2 + \pi^4M^4}{320}\right)$	

Current Amplitudes:

$\hat{I}_1 = \frac{\sqrt{(VAn - E\cos\delta)^2 + (E\sin\delta)^2}}{\sqrt{R^2 + (\omega L)^2}}$ (see table 4.1)	$\phi = \tan^{-1}\left(\frac{\omega_o L}{R}\right) - \tan^{-1}\left(\frac{E\sin\delta}{vAn - E\cos\delta}\right)$
$\hat{I}_{mf} = \frac{\hat{V}mf}{\sqrt{R^2 + (mf\,\omega_o L)^2}}$	$\theta_{mf} = \tan^{-1}\left(mf\,\frac{\omega_o L}{R}\right)$
$\hat{I}_{mf-2} = \frac{Vmf-2}{\sqrt{R^2 + ((mf-2)\,\omega_o L)^2}}$	$\theta_{mf-2} = \tan^{-1}\left(\frac{(mf-2)\,\omega_o L}{R}\right)$
$\hat{I}_{mf+2} = \frac{\hat{V}mf+2}{\sqrt{R^2 + ((mf-2)\,\omega_o L)^2}}$	$\theta_{mf+2} = \tan^{-1}\left(\frac{(mf+2)\,\omega_o L}{R}\right)$
$\hat{I}_{2mf+1} = \frac{\hat{V}2mf+1}{\sqrt{R^2 + ((2mf+1)\,\omega_o L)^2}}$	$\theta_{2mf+1} = \tan^{-1}\left(\frac{(2mf+1)\,\omega_o L}{R}\right)$
$\hat{I}_{2mf-1} = \frac{\hat{V}2mf-1}{\sqrt{R^2 + ((2mf-1)\,\omega_o L)^2}}$	$\theta_{2mf-1} = \tan^{-1}\left(\frac{(2mf-1)\,\omega_o L}{R}\right)$
$\hat{I}_{2mf+3} = \frac{\hat{V}2mf+3}{\sqrt{R^2 + ((2mf+3)\,\omega_o L)^2}}$	$\theta_{2mf+3} = \tan^{-1}\left(\frac{(2mf+3)\,\omega_o L}{R}\right)$
$\hat{I}_{2mf-3} = \frac{\hat{V}2mf-3}{\sqrt{R^2 + ((2mf-3)\,\omega_o L)^2}}$	$\theta_{2mf-3} = \tan^{-1}\left(\frac{(2mf-3)\,\omega_o L}{R}\right)$

General expression for voltages:

$$\boldsymbol{v_{az}}(t) = \hat{V}_1\cos(\omega_o t + \xi) + \hat{V}_{mf-2}\cos(\omega_c t + \psi_c - 2\omega_o t - 2\xi) + \hat{V}_{mf}\cos(\omega_c t + \psi_c) + \hat{V}_{mf+2}\cos(\omega_c t + \psi_c + 2\omega_o t + 2\xi)$$
$$+ \hat{V}_{2mf-3}\cos(2\omega_c t + 2\psi_c - 3\omega_o t - 3\xi) + \hat{V}_{2mf-1}\cos(2\omega_c t + 2\psi_c - \omega_o t - \xi)$$
$$+ \hat{V}_{2mf+1}\cos(2\omega_c t + 2\psi_c + \omega_o t + \xi) + \hat{V}_{2mf+3}\cos(2\omega_c t + 2\psi_c + 3\omega_o t + 3\xi)$$

$$\boldsymbol{v_{bz}}(t) = \hat{V}_1\cos\left(\omega_o t + \xi - \frac{2\pi}{3}\right) + \hat{V}_{mf-2}\cos\left(\omega_c t + \psi_c - 2\omega_o t - 2\xi + \frac{4\pi}{3}\right) + \hat{V}_{mf}\cos(\omega_c t + \psi_c)$$
$$+ \hat{V}_{mf+2}\cos\left(\omega_c t + \psi_c + 2\omega_o t + 2\xi - \frac{4\pi}{3}\right) + \hat{V}_{2mf-3}\cos(2\omega_c t + 2\psi_c - 3\omega_o t - 3\xi)$$
$$+ \hat{V}_{2mf-1}\cos\left(2\omega_c t + 2\psi_c - \omega_o t - \xi + \frac{2\pi}{3}\right) + \hat{V}_{2mf+1}\cos\left(2\omega_c t + 2\psi_c + \omega_o t + \xi - \frac{2\pi}{3}\right)$$
$$+ \hat{V}_{2mf+3}\cos(2\omega_c t + 2\psi_c + 3\omega_o t + 3\xi)$$

$$\boldsymbol{v_{cz}}(t) = \hat{V}_1 cos\left(\omega_o\, t + \xi + \frac{2\pi}{3}\right) + \hat{V}_{mf-2}\, cos\left(\omega_c t + \psi_c - 2\,\omega_o\, t - 2\xi - \frac{4\pi}{3}\right) + \hat{V}_{mf}\, cos(\omega_c t + \psi_c)$$
$$+ \hat{V}_{mf+2}\, cos\left(\omega_c t + \psi_c + 2\,\omega_o t + 2\xi + \frac{4\pi}{3}\right) + \hat{V}_{2mf-3}\, cos(2\omega_c t + 2\psi_c - 3\omega_o\, t - 3\xi)$$
$$+ \hat{V}_{2mf-1}\, cos\left(2\omega_c t + 2\psi_c - \omega_o\, t - \xi - \frac{2\pi}{3}\right) + \hat{V}_{2mf+1}\, cos\left(2\omega_c t + 2\psi_c + \omega_o\, t + \xi + \frac{2\pi}{3}\right)$$
$$+ \hat{V}_{2mf+3}\, cos\,(2\omega_c t + 2\psi_c + 3\omega_o\, t + 3\xi)$$

Due to the neutral point of the load some of the currents are not present in the current ripple expression

$$\boldsymbol{v_{an}}(t) = \frac{2}{3}v_{az} - \frac{v_{bz}}{3} - \frac{v_{cz}}{3} = v_{az} - \frac{v_{az} + v_{bz} + v_{cz}}{3}$$

$$\boldsymbol{v_{bn}}(t) = \frac{2}{3}v_{bz} - \frac{v_{az}}{3} - \frac{v_{cz}}{3} = v_{bz} - \frac{v_{az} + v_{bz} + v_{cz}}{3}$$

$$\boldsymbol{v_{cn}}(t) = \frac{2}{3}v_{cz} - \frac{v_{az}}{3} - \frac{v_{bz}}{3} = v_{cz} - \frac{v_{az} + v_{bz} + v_{cz}}{3}$$

The voltages $V_{mf}, V_{2mf-3}, V_{2mf+3}$ will cancel out due to the neutral point "n". That means the corresponding currents for these harmonics $I_{mf}, I_{2mf-3}, I_{2mf+3}$ will not flow and will not be present in the harmonic equation of the current.

The current harmonic equation

$$\boldsymbol{i_a}(t) = \hat{\boldsymbol{I_1}}\, \boldsymbol{cos}\,(\boldsymbol{\omega_o t} + \boldsymbol{\xi} - \boldsymbol{\phi}) + \hat{\boldsymbol{I}}_{\boldsymbol{mf-2}}\, \boldsymbol{cos}(\boldsymbol{\omega_c t} + \boldsymbol{\psi_c} - \boldsymbol{2\,\omega_o t} - \boldsymbol{2\xi} - \boldsymbol{\theta_{mf-2}})$$
$$+ \hat{\boldsymbol{I}}_{\boldsymbol{mf+2}}\, \boldsymbol{cos}(\boldsymbol{\omega_c t} + \boldsymbol{\psi_c} + \boldsymbol{2\,\omega_o t} + \boldsymbol{2\xi} - \boldsymbol{\theta_{mf+2}}) + \hat{\boldsymbol{I}}_{\boldsymbol{2mf-1}}\, \boldsymbol{cos}(\boldsymbol{2\omega_c t} + \boldsymbol{2\psi_c} - \boldsymbol{\omega_o t} - \boldsymbol{\xi} - \boldsymbol{\theta_{2mf-1}})$$
$$+ \hat{\boldsymbol{I}}_{\boldsymbol{2mf+1}}\, \boldsymbol{cos}(\boldsymbol{2\omega_c t} + \boldsymbol{2\psi_c} + \boldsymbol{\omega_o t} + \boldsymbol{\xi} - \boldsymbol{\theta_{2mf+1}})$$

$$\boldsymbol{i_b}(t) = \hat{\boldsymbol{I_1}}\, \boldsymbol{cos}\,(\boldsymbol{\omega_o t} + \boldsymbol{\xi} - \boldsymbol{\phi} - \frac{\boldsymbol{2\pi}}{\boldsymbol{3}}) + \hat{\boldsymbol{I}}_{\boldsymbol{mf-2}}\, \boldsymbol{cos}\left(\boldsymbol{\omega_c t} + \boldsymbol{\psi_c} - \boldsymbol{2\,\omega_o t} - \boldsymbol{2\xi} - \boldsymbol{\theta_{mf-2}} + \frac{\boldsymbol{4\pi}}{\boldsymbol{3}}\right)$$
$$+ \hat{\boldsymbol{I}}_{\boldsymbol{mf+2}}\, \boldsymbol{cos}\left(\boldsymbol{\omega_c t} + \boldsymbol{\psi_c} + \boldsymbol{2\,\omega_o t} + \boldsymbol{2\xi} - \boldsymbol{\theta_{mf+2}} - \frac{\boldsymbol{4\pi}}{\boldsymbol{3}}\right)$$
$$+ \hat{\boldsymbol{I}}_{\boldsymbol{2mf-1}}\, \boldsymbol{cos}(\boldsymbol{2\omega_c t} + \boldsymbol{2\psi_c} - \boldsymbol{\omega_o t} - \boldsymbol{\xi} - \boldsymbol{\theta_{2mf-1}} + \frac{\boldsymbol{2\pi}}{\boldsymbol{3}})$$
$$+ \hat{\boldsymbol{I}}_{\boldsymbol{2mf+1}}\, \boldsymbol{cos}(\boldsymbol{2\omega_c t} + \boldsymbol{2\psi_c} + \boldsymbol{\omega_o t} + \boldsymbol{\xi} - \boldsymbol{\theta_{2mf+1}} - \frac{\boldsymbol{2\pi}}{\boldsymbol{3}})$$

$$\boldsymbol{i_c}(t) = \hat{I}_1\, cos\,(\omega_o t + \xi - \phi + \frac{2\pi}{3}) + \hat{I}_{mf-2}\, cos\left(\omega_c t + \psi_c - 2\,\omega_o t - 2\xi - \theta_{mf-2} - \frac{4\pi}{3}\right)$$
$$+ \hat{I}_{mf+2}\, cos\left(\omega_c t + \psi_c + 2\,\omega_o t + 2\xi - \theta_{mf+2} + \frac{4\pi}{3}\right) + \hat{I}_{2mf-1}\, cos(2\omega_c t + 2\psi_c - \omega_o t - \xi - \theta_{2mf-1} - \frac{2\pi}{3})$$
$$+ \hat{I}_{2mf+1}\, \cos(2\omega_c t + 2\psi_c + \omega_o t + \xi - \theta_{2mf+1} + \frac{2\pi}{3})$$

From the power balance

$$V_d.\, i_{dc}(t) = V_d[\, I_{dc} + i_r(t)] = i_A(t).\, v_{An}(t) + i_B(t).\, v_{Bn}(t) + i_c(t).\, v_{cn}(t)$$

Interaction between the fundamental voltage and currents of the rest of the harmonics for phases a, b, c respectively

$\boldsymbol{V_1 \hat{I}_{mf-2}}$

a: $\frac{V_1 \hat{I}_{mf-2}}{2V_d}\left(cos\,(\omega_c t + \psi_c - \omega_o\, t - \xi - \theta_{mf-2}) + cos(\omega_c t + \psi_c - 3\,\omega_o\, t - 3\xi - \theta_{mf-2})\right)$

b: $\frac{V_1 \hat{I}_{mf-2}}{2V_d}\left(cos\,(\omega_c t + \psi_c - \omega_o\, t - \xi - \theta_{mf-2} + \frac{2\pi}{3}) + cos(\omega_c t + \psi_c - 3\,\omega_o\, t - 3\xi - \theta_{mf-2})\right)$

c: $\frac{V_1 \hat{I}_{mf-2}}{2V_d}\left(cos\,(\omega_c t + \psi_c - \omega_o\, t - \xi - \theta_{mf-2} - \frac{2\pi}{3}) + cos(\omega_c t + \psi_c - 3\,\omega_o\, t - 3\xi - \theta_{mf-2})\right)$

$$\sum = \quad i_{r(mf-1)}(t) = 0$$
$$i_{r(mf-3)}(t) = \frac{3V_1 \hat{I}_{mf-2}}{2V_d} cos\big((mf-3)\omega_o t + \psi_c - 3\xi - \theta_{mf-2}\big)$$

$V_1\hat{I}_{mf+2}$

a: $\frac{V_1\hat{I}_{mf+2}}{2V_d}\left(cos\ (\omega_c t+\ \psi_c+3\omega_o\ t+3\xi-\theta_{mf+2})+cos(\omega_c t+\ \psi_c+\ \omega_o\ t+\xi-\theta_{mf+2})\right)$

b: $\frac{V_1\hat{I}_{mf+2}}{2V_d}\left(cos\ (\omega_c t+\ \psi_c+3\omega_o\ t+3\xi-\theta_{mf+2})+cos\left(\omega_c t+\ \psi_c+\ \omega_o\ t+\xi-\theta_{mf+2}-\frac{2\pi}{3}\right)\right)$

c: $\frac{V_1\hat{I}_{mf+2}}{2V_d}\left(cos\ (\omega_c t+\ \psi_c+3\omega_o\ t+3\xi-\theta_{mf+2})+cos\left(\omega_c t+\ \psi_c+\ \omega_o\ t+\xi-\theta_{mf+2}+\frac{2\pi}{3}\right)\right)$

$$\sum = \quad i_{r(mf+1)}(t)=0$$

$$i_{r(mf+3)}(t)=\frac{3V_1\hat{I}_{mf+2}}{2V_d}cos\left((mf+3)\omega_o t+\ \psi_c+3\xi-\theta_{mf+2}\right)$$

$V_1\hat{I}_{2mf-1}$

a: $\frac{V_1\hat{I}_{2mf-1}}{2V_d}\left(cos\ (2\omega_c t+\ 2\psi_c-\theta_{2mf-1})+cos(2\omega_c t+\ 2\psi_c-2\ \omega_o t-2\xi-\theta_{2mf-1})\right)$

b: $\frac{V_1\hat{I}_{2mf-1}}{2V_d}\left(cos\ (2\omega_c t+\ 2\psi_c-\theta_{2mf-1})+cos\left(2w_c t+2\psi_c-2\ w_o t-2\xi-\theta_{2mf-1}-\frac{4\pi}{3}\right)\right)$

c: $\frac{V_1\hat{I}_{2mf-1}}{2V_d}\left(cos\ (2\omega_c t+\ 2\psi_c-\theta_{2mf-1})+cos\left(2\omega_c t+2\psi_c-2\ \omega_o\ t-2\xi-\theta_{2mf-1}+\frac{4\pi}{3}\right)\right)$

$$\sum = \quad i_{r(2mf-2)}(t)=0$$

$$i_{r(2mf)}(t)=\frac{3V_1\hat{I}_{2mf-1}}{2V_d}cos\left((2mf)\omega_o t+\ 2\psi_c-\theta_{2mf-1}\right)$$

$V_1\hat{I}_{2mf+1}$

a: $\frac{V_1\hat{I}_{2mf+1}}{2V_d}\left(cos(2\omega_c t+2\psi_c+2\omega_o\ t+2\xi-\theta_{2mf+1})\quad+cos(2\omega_c t+2\psi_c-\theta_{2mf+1})\right)$

b: $\frac{V_1\hat{I}_{2mf+1}}{2V_d}\left(cos\left(2\omega_c t+2\psi_c+2\omega_o\ t+2\xi-\theta_{2mf+1}-\frac{4\pi}{3}\right)+cos(2\omega_c t+2\psi_c-\theta_{2mf+1})\right)$

c: $\frac{V_1\hat{I}_{2mf+1}}{2V_d}\left(cos\left(2\omega_c t+2\psi_c+2\omega_o\ t+2\xi-\theta_{2mf+1}+\frac{4\pi}{3}\right)+cos(2\omega_c t+2\psi_c-\theta_{2mf+1})\right)$

$$\sum = \quad i_{r(2mf+2)}(t)=0$$

$$i_{r(2mf)}(t)=\frac{3V_1\hat{I}_{2mf-1}}{2V_d}cos\left((2mf)\omega_o t+\ 2\psi_c-\theta_{2mf+1}\right)$$

Interaction between the voltage of harmonic order mf-2 and currents of the rest of the harmonics for phases a, b, c respectively

$V_{mf-2}I_1$

a: $\frac{V_{mf-2}I_1}{2V_d}\left(cos\ (\omega_c t+\psi_c-\omega_o\ t-\xi-\phi)\quad+cos(\omega_c t+\psi_c-3\omega_o\ t-3\xi+\phi)\right)$

b: $\frac{V_{mf-2}I_1}{2V_d}\left(cos\left(\omega_c t+\psi_c-\omega_o\ t-\xi-\phi+\frac{2\pi}{3}\right)+cos(\omega_c t+\psi_c-3\omega_o\ t-3\xi+\phi)\right)$

c: $\frac{V_{mf-2}I_1}{2V_d}\left(cos\left(\omega_c t+\psi_c-\omega_o\ t-\xi-\phi-\frac{2\pi}{3}\right)+cos(\omega_c t+\psi_c-3\omega_o\ t-3\xi+\phi)\right)$

$$\sum = \quad i_{r(mf-1)}(t)=0$$

$$i_{r(mf-3)}(t)=\frac{3V_{mf-2}I_1}{2V_d}cos((mf-3)\omega_o t+\ \psi_c-3\xi+\phi)$$

$\boldsymbol{V_{mf-2}I_{mf+2}}$

$a: \frac{V_{mf-2}I_{mf+2}}{2V_d}\left(cos(2\omega_c t + 2\psi_c - \theta_{mf+2}) + cos(4\omega_c t + 4\xi - \theta_{mf+2})\right)$

$b: \frac{V_{mf-2}I_{mf+2}}{2V_d}\left(cos(2\omega_c t + 2\psi_c - \theta_{mf+2}) + cos\left(4\omega_c t + 4\xi - \theta_{mf+2} - \frac{2\pi}{3}\right)\right)$

$c: \frac{V_{mf-2}I_{mf+2}}{2V_d}\left(cos(2\omega_c t + 2\psi_c - \theta_{mf+2}) + cos\left(4\omega_o\, t + 4\xi - \theta_{mf+2} + \frac{2\pi}{3}\right)\right)$

$$\sum = \quad i_{r(2mf+2)}(t) = 0$$

$$i_{r(2mf)}(t) = \frac{3V_{mf-2}I_{mf+2}}{2V_d} cos\left((2mf)\omega_o t + 2\psi_c - \theta_{mf+2}\right)$$

$\boldsymbol{V_{mf-2}I_{2mf-1}}$

$a: \frac{V_{mf-2}I_{2mf-1}}{2V_d}\left(cos(3\omega_c t + 3\psi_c - 3\omega_o\, t - 3\xi - \theta_{2mf-1}) + cos(\omega_c t + 4\psi_c + \omega_o\, t + \xi - \theta_{2mf-1})\right)$

$b: \frac{V_{mf-2}I_{2mf-1}}{2V_d}\left(cos(3\omega_c t + 3\psi_c - 3\omega_o\, t - 3\xi - \theta_{2mf-1}) + cos\left(\omega_c t + \psi_c + \omega_o\, t + \xi - \theta_{2mf-1} - \frac{2\pi}{3}\right)\right)$

$c: \frac{V_{mf-2}I_{2mf-1}}{2V_d}\left(cos(3\omega_c t + 3\psi_c - 3\omega_o\, t - 3\xi - \theta_{2mf-1}) + cos\left(\omega_c t + \psi_c + \omega_o\, t + \xi - \theta_{2mf-1} + \frac{2\pi}{3}\right)\right)$

$$\sum = \quad i_{r(mf+4)}(t) = 0$$

$$i_{r(3mf-3)}(t) = \frac{3V_{mf-2}I_{2mf-1}}{2V_d} cos\left((3mf-3)\omega_o t + 3\psi_c - 3\xi - \theta_{2mf-1}\right)$$

$\boldsymbol{V_{mf-2}I_{2mf+1}}$

$a: \frac{V_{mf-2}I_{2mf+1}}{2V_d}\left(cos(3\omega_c t + 3\psi_c - \omega_o\, t - \xi - \theta_{2mf+1}) + cos(\omega_c t + \psi_c + 3\omega_o\, t + 3\xi - \theta_{2mf+1})\right)$

$b: \frac{V_{mf-2}I_{2mf+1}}{2V_d}\left(cos\left(3\omega_c t + 3\psi_c - \omega_o\, t - \xi - \theta_{2mf+1} + \frac{2\pi}{3}\right) + cos(\omega_c t + \psi_c + 3\omega_o\, t + 3\xi - \theta_{2mf+1})\right)$

$c: \frac{V_{mf-2}I_{2mf+1}}{2V_d}\left(cos\left(3\omega_c t + 3\psi_c - \omega_o\, t - \xi - \theta_{2mf+1} - \frac{2\pi}{3}\right) + cos(\omega_c t + \psi_c + 3\omega_o\, t + 3\xi - \theta_{2mf+1})\right)$

$$\sum = \quad i_{r(3mf-1)}(t) = 0$$

$$i_{r(mf+3)}(t) = \frac{3V_{mf-2}I_{2mf+1}}{2V_d} cos\left((mf+3)\omega_o t + \psi_c + 3\xi - \theta_{2mf+1}\right)$$

Interaction between the voltage of harmonic order mf+2 and currents of the rest of the harmonics for phases a, b, c respectively

$\boldsymbol{V_{mf+2}I_1}$

$a: \frac{V_{mf+2}I_1}{2V_d}\left(cos(\omega_c t + \psi_c + 3\omega_o\, t + 3\xi - \phi) + cos(\omega_c t + \psi_c + \omega_o\, t + \xi + \phi)\right)$

$b: \frac{V_{mf+2}I_1}{2V_d}\left(cos(\omega_c t + \psi_c + 3\omega_o\, t + 3\xi - \phi) + cos\left(\omega_c t + \psi_c + \omega_o\, t + \xi + \phi - \frac{2\pi}{3}\right)\right)$

$c: \frac{V_{mf+2}I_1}{2V_d}\left(cos(\omega_c t + \psi_c + 3\omega_o\, t + 3\xi - \phi) + cos\left(\omega_c t + \psi_c + \omega_o\, t + \xi + \phi + \frac{2\pi}{3}\right)\right)$

$$\sum = \quad i_{r(mf+1)}(t) = 0$$

$$i_{r(mf+3)}(t) = \frac{3V_{mf+2}I_1}{2V_d} cos\left((mf+3)\omega_o t + \psi_c + 3\xi - \phi\right)$$

$\boldsymbol{V_{mf+2}I_{mf-2}}$

a: $\frac{V_{mf+2}I_{mf-2}}{2V_d}\left(cos(2\omega_c t + 2\psi_c - \theta_{mf-2}) + cos\ (4\omega_o\, t + 4\xi + \theta_{mf-2})\right)$

b: $\frac{V_{mf+2}I_{mf-2}}{2V_d}\left(cos(2\omega_c t + 2\psi_c - \theta_{mf-2}) + cos\left(4\omega_o\, t + 4\xi + \theta_{mf-2} - \frac{2\pi}{3}\right)\right)$

c: $\frac{V_{mf+2}I_{mf-2}}{2V_d}\left(cos(2\omega_c t + 2\psi_c - \theta_{mf-2}) + cos\left(4\omega_o\, t + 4\xi + \theta_{mf-2} + \frac{2\pi}{3}\right)\right)$

$$\sum = \quad i_{r(4)}(t) = 0$$

$$i_{r(2mf)}(t) = \frac{3V_{mf+2}I_{mf-2}}{2V_d} cos\left((2mf)\omega_o t + 2\psi_c - \theta_{mf-2}\right)$$

$\boldsymbol{V_{mf+2}I_{2mf-1}}$

a: $\frac{V_{mf+2}I_{2mf-1}}{2V_d}\left(cos(3\omega_c t + 3\psi_c + \omega_o\, t + \xi - \theta_{2mf-1}) + cos(\omega_c t + \psi_c - 3\omega_o\, t - 3\xi - \theta_{2mf-1})\right)$

b: $\frac{V_{mf+2}I_{2mf-1}}{2V_d}\left(cos\left(3\omega_c t + 3\psi_c + \omega_o\, t + \xi - \theta_{2mf-1} - \frac{2\pi}{3}\right) + cos(\omega_c t + \psi_c - 3\omega_o\, t - 3\xi - \theta_{2mf+1})\right)$

c: $\frac{V_{mf+2}I_{2mf-1}}{2V_d}\left(cos\left(3\omega_c t + 3\psi_c + \omega_o\, t + \xi - \theta_{2mf-1} + \frac{2\pi}{3}\right) + cos(\omega_c t + \psi_c - 3\omega_o\, t - 3\xi - \theta_{2mf+1})\right)$

$$\sum = \quad i_{r(3mf+1)}(t) = 0$$

$$i_{r(mf-3)}(t) = \frac{3V_{mf+2}I_{2mf-1}}{2V_d} cos\left((mf-3)\omega_o t + \psi_c - 3\xi - \theta_{2mf-1}\right)$$

$\boldsymbol{V_{mf+2}I_{2mf+1}}$

a: $\frac{V_{mf+2}I_{2mf+1}}{2V_d}\left(cos(3\omega_c t + 3\psi_c + 3\omega_o\, t + 3\xi - \theta_{2mf+1}) + cos(\omega_c t + \psi_c - \omega_o\, t - \xi - \theta_{2mf+1})\right)$

b: $\frac{V_{mf+2}I_{2mf+1}}{2V_d}\left(cos(3\omega_c t + 3\psi_c + 3\omega_o\, t + 3\xi - \theta_{2mf+1}) + cos\left(\omega_c t + \psi_c - \omega_o\, t - \xi - \theta_{2mf+1} + \frac{2\pi}{3}\right)\right)$

c: $\frac{V_{mf+2}I_{2mf+1}}{2V_d}\left(cos(3\omega_c t + 3\psi_c + 3\omega_o\, t + 3\xi - \theta_{2mf+1}) + cos\left(\omega_c t + \psi_c - \omega_o\, t - \xi - \theta_{2mf+1} - \frac{2\pi}{3}\right)\right)$

$$\sum = \quad i_{r(mf-1)}(t) = 0$$

$$i_{r(3mf+3)}(t) = \frac{3V_{mf+2}I_{2mf+1}}{2V_d} cos\left((3mf+3)\omega_o t + 3\,\psi_c + 3\xi - \theta_{2mf+1}\right)$$

Interaction between the voltage of harmonic order 2mf-1 and currents of the rest of the harmonics for phases a, b, c respectively

$\boldsymbol{V_{2mf-1}I_1}$

a: $\frac{V_{2mf-1}I_1}{2V_d}\left(cos(2\omega_c t + 2\psi_c - \phi) + cos(2\omega_c t + 2\psi_c - 2\omega_o\, t - 2\xi + \phi)\right)$

b: $\frac{V_{2mf-1}I_1}{2V_d}\left(cos(2\omega_c t + 2\psi_c - \phi) + cos\left(2\omega_c t + 2\psi_c - 2\omega_o\, t - 2\xi + \phi - \frac{2\pi}{3}\right)\right)$

c: $\frac{V_{2mf-1}I_1}{2V_d}\left(cos(2\omega_c t + 2\psi_c - \phi) + cos\left(2\omega_c t + 2\psi_c - 2\omega_o\, t - 2\xi + \phi + \frac{2\pi}{3}\right)\right)$

$$\sum = \quad i_{r(2mf-2)}(t) = 0$$

$$i_{r(2mf)}(t) = \frac{3V_{2mf-1}I_1}{2V_d} cos\left((2mf)\omega_o t + \psi_c - \phi\right)$$

$\boldsymbol{V_{2mf-1}I_{mf-2}}$

a: $\frac{V_{2mf-1}I_{mf-2}}{2V_d}\left(cos\left(3\omega_c t+3\psi_c-3\omega_o\, t-3\xi-\theta_{mf-2}\right)+cos\left(\omega_c t+\psi_c+\omega_o\, t+\xi+\theta_{mf-2}\right)\right)$

b: $\frac{V_{2mf-1}I_{mf-2}}{2V_d}\left(cos\left(3\omega_c t+3\psi_c-3\omega_o\, t-3\xi-\theta_{mf-2}\right)+cos\left(\omega_c t+\psi_c+\omega_o\, t+\xi+\theta_{mf-2}+\frac{2\pi}{3}\right)\right)$

c: $\frac{V_{2mf-1}I_{mf-2}}{2V_d}\left(cos\left(3\omega_c t+3\psi_c-3\omega_o\, t-3\xi-\theta_{mf-2}\right)+cos\left(\omega_c t+\psi_c+\omega_o\, t+\xi-\theta_{mf-2}-\frac{2\pi}{3}\right)\right)$

$$\sum = \quad i_{r(mf+1)}(t)=0$$

$$i_{r(3mf-3)}(t)=\frac{3V_{2mf-1}I_{mf-2}}{2V_d}cos\left((3mf-3)\omega_o t+3\,\psi_c-3\xi-\theta_{mf-2}\right)$$

$\boldsymbol{V_{2mf-1}I_{mf+2}}$

a: $\frac{V_{2mf-1}I_{mf+2}}{2V_d}\left(cos\left(3\omega_c t+3\psi_c+\omega_o\, t+\xi-\theta_{mf+2}\right)\quad+cos\left(\omega_c t+\psi_c-3\omega_o\, t-3\xi+\theta_{mf+2}\right)\right)$

b: $\frac{V_{2mf-1}I_{mf+2}}{2V_d}\left(cos\left(3\omega_c t+3\psi_c+\omega_o\, t+\xi-\theta_{mf+2}-\frac{2\pi}{3}\right)+cos\left(\omega_c t+\psi_c-3\omega_o\, t-3\xi+\theta_{mf+2}\right)\right)$

c: $\frac{V_{2mf-1}I_{mf+2}}{2V_d}\left(cos\left(3\omega_c t+3\psi_c+\omega_o\, t+\xi-\theta_{mf+2}+\frac{2\pi}{3}\right)+cos\left(\omega_c t+\psi_c-3\omega_o\, t-3\xi+\theta_{mf+2}\right)\right)$

$$\sum = \quad i_{r(3mf+1)}(t)=0$$

$$i_{r(mf-3)}(t)=\frac{3V_{2mf-1}I_{mf+2}}{2V_d}cos\left((mf-3)\omega_o t+\psi_c-3\xi+\theta_{mf+2}\right)$$

$\boldsymbol{V_{2mf-1}I_{2mf+1}}$

a: $\frac{V_{2mf-1}I_{2mf+1}}{2V_d}\left(cos\left(4\omega_c t+4\psi_c-\theta_{2mf+1}\right)+cos\left(2\omega_o\, t+2\xi-\theta_{2mf+1}\right)\right)$

b: $\frac{V_{2mf-1}I_{2mf+1}}{2V_d}\left(cos\left(4\omega_c t+4\psi_c-\theta_{2mf+1}\right)+cos\left(2\omega_o t+2\xi-\theta_{2mf+1}-\frac{4\pi}{3}\right)\right)$

c: $\frac{V_{2mf-1}I_{2mf+1}}{2V_d}\left(cos\left(4\omega_c t+4\psi_c-\theta_{2mf+1}\right)+cos\left(2\omega_o\, t+2\xi-\theta_{2mf+1}+\frac{4\pi}{3}\right)\right)$

$$\sum = \quad i_{r(2)}(t)=0$$

$$i_{r(4mf)}(t)=\frac{3V_{2mf-1}I_{2mf+1}}{2V_d}cos\left((4mf)\omega_o t+4\psi_c-\theta_{2mf+1}\right)$$

Interaction between the voltage of harmonic order 2mf+1 and currents of the rest of the harmonics for phases a, b, c respectively

$\boldsymbol{V_{2mf+1}I_1}$

a: $\frac{V_{2mf+1}I_1}{2V_d}\left(cos(2\omega_c t+2\psi_c+2\omega_o\, t+\xi-\phi)\quad+cos(2\omega_c t+2\psi_c+\phi)\right)$

b: $\frac{V_{2mf+1}I_1}{2V_d}\left(cos\left(2\omega_c t+2\psi_c+2\omega_o\, t+\xi-\phi-\frac{4\pi}{3}\right)+cos(2\omega_c t+2\psi_c+\phi)\right)$

c: $\frac{V_{2mf+1}I_1}{2V_d}\left(cos\left(2\omega_c t+2\psi_c+2\omega_o\, t+\xi-\phi+\frac{4\pi}{3}\right)+cos(2\omega_c t+2\psi_c+\phi)\right)$

$$\sum = \quad i_{r(2mf+2)}(t)=0$$

$$i_{r(2mf)}(t)=\frac{3V_{2mf+1}I_1}{2V_d}cos\left((2mf)\omega_o t+2\psi_c+\phi\right)$$

$\boldsymbol{V_{2mf+1}I_{mf-2}}$

a: $\frac{V_{2mf+1}I_{mf-2}}{2V_d}\left(cos(3\omega_c t + 3\psi_c - \omega_o\, t - \xi - \theta_{mf-2}) + cos(\omega_c t + \psi_c + 3\omega_o\, t + 3\xi + \theta_{mf-2})\right)$

b: $\frac{V_{2mf+1}I_{mf-2}}{2V_d}\left(cos\left(3\omega_c t + 3\psi_c - \omega_o\, t - \xi - \theta_{mf-2} + \frac{2\pi}{3}\right) + cos(\omega_c t + \psi_c + 3\omega_o\, t + 3\xi + \theta_{mf-2})\right)$

c: $\frac{V_{2mf+1}I_{mf-2}}{2V_d}\left(cos\left(3\omega_c t + 3\psi_c - \omega_o\, t - \xi - \theta_{mf-2} - \frac{2\pi}{3}\right) + cos(\omega_c t + \psi_c + 3\omega_o\, t + 3\xi + \theta_{mf-2})\right)$

$$\sum = \quad i_{r(3mf-1)}(t) = 0$$

$$i_{r(mf+3)}(t) = \frac{3V_{2mf+1}I_{mf-2}}{2V_d} cos\left((mf+3)\omega_o t + \psi_c + 3\xi + \theta_{mf-2}\right)$$

$\boldsymbol{V_{2mf+1}I_{mf+2}}$

a: $\frac{V_{2mf+1}I_{mf+2}}{2V_d}\left(cos(3\omega_c t + 3\psi_c + 3\omega_o\, t + 3\xi - \theta_{mf+2}) + cos(\omega_c t + \psi_c - \omega_o\, t - \xi + \theta_{mf+2})\right)$

b: $\frac{V_{2mf+1}I_{mf+2}}{2V_d}\left(cos(3\omega_c t + 3\psi_c + 3\omega_o\, t + 3\xi - \theta_{mf+2}) + cos\left(\omega_c t + \psi_c - \omega_o\, t - \xi + \theta_{mf+2} + \frac{2\pi}{3}\right)\right)$

c: $\frac{V_{2mf+1}I_{mf+2}}{2V_d}\left(cos(3\omega_c t + 3\psi_c + 3\omega_o\, t + 3\xi - \theta_{mf+2}) + cos\left(\omega_c t + \psi_c - \omega_o\, t - \xi + \theta_{mf+2} - \frac{2\pi}{3}\right)\right)$

$$\sum = \quad i_{r(mf-1)}(t) = 0$$

$$i_{r(3mf+3)}(t) = \frac{3V_{2mf+1}I_{mf+2}}{2V_d} cos\left((3mf+3)\omega_o t + 3\psi_c + 3\xi - \theta_{mf+2}\right)$$

$\boldsymbol{V_{2mf+1}I_{2mf-1}}$

a: $\frac{V_{2mf+1}I_{2mf-1}}{2V_d}\left(cos(4\omega_c t + 4\psi_c - \theta_{2mf-1}) + cos(2\omega_o\, t + 2\xi + \theta_{2mf-1})\right)$

b: $\frac{V_{2mf+1}I_{2mf-1}}{2V_d}\left(cos(4\omega_c t + 4\psi_c - \theta_{2mf-1}) + cos\left(2\omega_o\, t + 2\xi + \theta_{2mf-1} - \frac{4\pi}{3}\right)\right)$

c: $\frac{V_{2mf+1}I_{2mf-1}}{2V_d}\left(cos(4\omega_c t + 4\psi_c - \theta_{2mf-1}) + cos\left(2\omega_o\, t + 2\xi + \theta_{2mf-1} + \frac{4\pi}{3}\right)\right)$

$$\sum = \quad i_{r(2)}(t) = 0$$

$$i_{r(4mf)}(t) = \frac{3V_{2mf+1}I_{2mf-1}}{2V_d} cos\left((4mf)\omega_o t + 4\psi_c - \theta_{2mf-1}\right)$$

Thus the expression for the instantaneous current ripple on the dc side is

$$
\begin{aligned}
i_r(t) = {} & \frac{3V_1 I_{mf-2}}{2V_d}\cos\left((mf-3)\omega_o\,t+\psi_c-3\xi-\theta_{mf-2}\right)+\frac{3V_1 I_{mf+2}}{2V_d}\cos\left((mf+3)\omega_o\,t+\psi_c+3\xi-\theta_{mf+2}\right)\\
& +\frac{3V_1 I_{2mf-1}}{2Vd}\cos\left((2mf)\omega_o\,t+2\psi_c-\theta_{2mf-1}\right)+\frac{3V_1 I_{2mf+1}}{2V_d}\cos\left((2mf)\omega_o\,t+2\psi_c-\theta_{2mf+1}\right)\\
& +\frac{3V_{mf-2} I_1}{2V_d}\cos\left((mf-3)\omega_o\,t+\psi_c-3\xi+\phi\right)+\frac{3V_{mf-2} I_{mf+2}}{2V_d}\cos\left((2mf)\omega_o\,t+2\psi_c-3\xi-\theta_{mf+2}\right)\\
& +\frac{3V_{mf-2} I_{2mf-1}}{2V_d}\cos\left((3mf-3)\omega_o\,t+3\psi_c-3\xi-\theta_{2mf-1}\right)\\
& +\frac{3V_{mf-2} I_{2mf+1}}{2V_d}\cos\left((3mf+3)\omega_o\,t+\psi_c+3\xi-\theta_{2mf+1}\right)\\
& +\frac{3V_{mf+2} I_{\wedge}}{2V_d}\cos\left((mf+3)\omega_o\,t+\psi_c+3\xi-\phi\right)+\frac{3V_{mf+2} I_{mf-2}}{2V_d}\cos\left((2mf)\omega_o\,t+2\psi_c-\theta_{mf-2}\right)\\
& +\frac{3V_{mf+2} I_{2mf-1}}{2V_d}\cos\left((3mf-3)\omega_o\,t+\psi_c-3\xi-\theta_{2mf-1}\right)\\
& +\frac{3V_{mf+2} I_{2mf+1}}{2V_d}\cos\left((3mf+3)\omega_o\,t+3\psi_c+3\xi-\theta_{2mf+1}\right)+\frac{3V_{2mf-1} I_1}{2V_d}\cos\left((2mf)\omega_o\,t+2\psi_c-\phi\right)\\
& +\frac{3V_{2mf-1} I_{mf-2}}{2V_d}\cos\left((3mf-3)\omega_o\,t+3\psi_c-3\xi-\theta_{mf-2}\right)\\
& +\frac{3V_{2mf-1} I_{mf+2}}{2V_d}\cos\left((mf-3)\omega_o\,t+\psi_c-3\xi+\theta_{mf+2}\right)\\
& +\frac{3V_{2mf-1} I_{2mf+1}}{2V_d}\cos\left((4mf)\omega_o\,t+4\psi_c-\theta_{2mf+1}\right)+\frac{3V_{2mf+1} I_1}{2V_d}\cos\left((2mf)\omega_o\,t+2\psi_c+\phi\right)\\
& +\frac{3V_{2mf+1} I_{mf-2}}{2V_d}\cos\left((mf+3)\omega_o\,t+\psi_c+3\xi+\theta_{mf-2}\right)\\
& +\frac{3V_{2mf+1} I_{mf+2}}{2V_d}\cos\left((3mf+3)\omega_o\,t+3\psi_c+3\xi-\theta_{mf+2}\right)\\
& +\frac{3V_{2mf+1} I_{2mf-1}}{2V_d}\cos\left((4mf)\omega_o\,t+4\psi_c-\theta_{2mf-1}\right)
\end{aligned}
$$

Appendix A-2

Data of 1 module of an axial flux modular PM machine:

Rating of one module:
Rated power: 1000 kW
rated speed: 17 rpm
N° of poles: 104 (➔ rated frequency: f_n = 14.73 Hz)
rated current: I_n = 925 A_{rms}

Parameters of one module:
Line-to-neutral EMF, at rated speed: E_0 = 495 V_{rms} (sinusoidal waveform)
Synchronous inductance: L = 3.276 mH
Phase resistance: R = 14.3 mOhm
Almost no cogging
Magnetic saturation negligible (due to the very wide equivalent air-gap: 10 mm in air + 30 mm PM height)

N.B.:
1) the field winding is absent: so, the transient inductance is the same of the synchronous inductance; moreover, no damping cage exists nor significant damping equivalent effect, thus, also the sub-transient inductance coincides with the synchronous inductance;
2) the machine is completely isotropic: so d and q axis parameters have the same values.

Main sizes and other quantities concerning one module:
rotor inertia (1 module): J = $3.7 \cdot 10^4$ kg·m^2
axial length (1 module): L_{ax} = 300 mm
external diameter: D_{ext} = 5000 mm
copper mass: M_{cu} = 2650 kg
stator core lamination mass: M_{fes} = 4415 kg
PM mass: M_{PM} = 3360 kg

One Module losses in rated conditions:
Three-phase Copper losses at rated current: P_{cun} = 36.7 kW
Stator core losses: P_{fen} = 9.3 kW
PM eddy current losses (at rated speed, with stator rated current): P_{PM} = 3.6 kW
Mechanical losses (mainly friction, in the bearings): P_{fr} = 20 kW

Appendix A-3

```
% Design of two PI controllers: current and speed loops
% The outputs are: kpI kiI kpW kiW
clear all
close all
Rs = 14.3E-3; Ls = 3.276E-3;  % circuit parameters [ohms % henry ]
f=14.73; %rated frequency [Hz]
wrated=2*pi*f;
E_ph= 495; %phase emf [V]
psiPM= sqrt(3)*E_ph/wrated;
I_rated= 925; %rated current
Prated=1.E6; %rated power in [W]
p=104; %number of poles
Wmrated=4*pi*f/p; %rated mechanical speed [mec.rad/sec]
J=3*37.E3; %moment of inertia [kg*m^2]
B=3*1250; %[kg*m^2/s]
mf=678;
fc=f*mf;
%Tsw=1/fc;
Tsw=1/fc;
s = tf('s'); % define s as the complex frequency

% 1) CURRENT LOOP
% Transfer functions
% inverse of the machine impedance + Inverter: as for the current loop, it is
the  system under control
GI = 1/((1+s*Tsw)*(s*Ls+ Rs));

figure(1);
w = logspace(-1,4,100); % w ranges between 1E-1 and 1E4 rad/s with 100 points
bode(GI,'r',w);   grid; % frequency response
title('Transfer Function of the GI(s) system regarding the current loop');

% Determination of kpI and kiI with the variation of phase margin, assigned
% critical pulse wcI
wcI = 300;  % Critical pulse [rad/s]
[magI,csI] = bode(GI,wcI); %amplitude and phase in correspondence to wc
phiI = 10:1:90; % phase margin [deg]
theta = -180 + phiI - csI;
kpI = cos(theta*pi/180)/magI;    kiI = -wcI*sin(theta*pi/180)/magI;
figure(2);
subplot(2,1,1); plot(phiI,kpI); grid; xlabel('phiI [deg]'); ylabel('kpI');
title('kpI [p.u.] and kiI [1/s] with variation of phase phi [deg]');
subplot(2,1,2); plot(phiI,kiI); grid; xlabel('phiI [deg]'); ylabel('kiI');


% Design of kpI and kiI as a function of the phase margine phiI, once the
% cross-over frequency wcI has been set up ( from the figure 300 rad/sec
% should be the maximum frequency
%wcI = ;  % The cross-over frequency wcI is set up <<<<<<<<--------------
phimI = 70;       % The phase margin is set up           <<<<<<<<----------
---
[magI,csI] = bode(GI,wcI); % magnitude and phase of GI at wcI
magdb=20*log10(magI);    theta = -180 + phimI - csI;
```

```
kpI = cos(theta*pi/180)/magI;    kiI = -wcI*sin(pi*theta/180)/magI;
PID_I = kpI + kiI/s; % current PI controller
LI = PID_I*GI; % open loop transfer function
KI = LI/(1 + LI); % closed loop transfer function

% Frequency response of the open loop and closed loop transfer functions
figure(3);
bode(LI,'b',KI,'r',w); grid;
title('Open loop LI(s) and closed loop KI(s) transfer functions');
legend('LI(s)','KI(s)');

 % ****************************************************************
% 2) Speed Loop
% Transfer functions
Fc = 1 / (J*s+B);       % transfer function of the machine ( mechanical POV )
GW = Fc*KI; % process to be controlled (KI: current loop)

figure(4);
w = logspace(-1,3,100); % w ranges between 1E-1 and 1E3 rad/s, with 100
points
bode(GW,'b',w);   grid;
title('Transfer function of the process GW(s) regarding the mechanical
loop');
% Determination of kpI and kiI with the variation of phase margin, assigned
% critical pulse wcI
wcW = 10;  % critical angular frequency [rad/s]
[magW,csw] = bode(GW,wcW); %amplitude and phase corresponding to wc
phiW = 10:1:90; % phase margin [deg]
theta = -180 + phiW - csw;
kpW = cos(theta*pi/180)/magW;    kiW = -wcW*sin(theta*pi/180)/magW;
figure(5);
subplot(2,1,1); plot(phiW,kpW); grid; xlabel('phiW [deg]'); ylabel('kpW');
title('kpW [p.u.] and kiW [1/s] varying with the phase margin phi [deg]');
subplot(2,1,2); plot(phiW,kiW); grid; xlabel('phiW [deg]'); ylabel('kiW');

% Design of kpV and kiV as a function of the phase margine phiV, once the
% cross-over frequency wcV is given
%wcV = 2*pi*10;  % The cross-over frequency wcV is set up    <<<<<<<<--------
------
phimW = 70;       % phase margin                              <<<<<<<<---------
-----
[magW,csw] = bode(GW,wcW); % magnitude and phase at wcV
magdb=20*log10(magW);    theta = -180 + phimW - csw;
kpW = cos(theta*pi/180)/magW;    kiW = -wcW*sin(pi*theta/180)/magW;
PID_W = kpW + kiW/s; % voltage PI controller
LW = PID_W*GW; % open loop transfer function
KW = LW/(1 + LW); % closed loop transfer function

% Frequency response of the open loop and closed loop transfer functions
figure(4);    bode(LW,'b',KW,'r',w); grid;
title('Open loop LW(s) and closed loop KW(s) transfer functions');
legend('LW(s)','KW(s)');

Kpi_reg  = [kpW kiW kpW kiW];
```

Appendix A-4

```
% Machine Parameters
m=1;%number of modules
Pn = m*1E6; %[W] rated power
Rs = 14.3e-3; %[ohm]
Ls = 3.276e-3; % [H]
Ld =Ls;     Lq = Ls;
frated = 14.73; %[Hz] rated frequency
wrated = 2*pi*frated;
% psiPM = 0.07147*1.5;
E_phase = 495; % phase voltage at rated speed
psiPM = sqrt(3)*E_phase / wrated; %PM flux in a dq frame
Vrated=E_phase;
%Vrated = wrated*psiPM;
p = 104; % number of poles
Wmrated = wrated*2/p; % mechanical rated speed;
i_rated = 925; % [A] rated current

% Remember : Simpower System blockset use a differt Park Transform
J = 37000*m; % moment of inertia [kg*m2]
B = 1250*m;
Trated = Pn/Wmrated; %rated torque
Tload = 0.4*Trated;
psi_rated = psiPM;

% PWM Parameters
Vdc=1600;
%Vdc=808;
f=14.73;
mf=15;
fc=mf*f;
wc=2*pi*fc;
tc=1/fc;
Vm=1;
tc1=tc/4;
tc2=tc/2;
tc3=3*tc/4;

%PI
%Constants for mf=15
Ccurr.Kp=0.3563;
Ccurr.Ki=5.1016;
%1Module
Cmecc.Kp=3.1836E+5;
Cmecc.Ki=1.6486E+6;
%2Modules
%Cmecc.Kp=6.3673E+5;
%Cmecc.Ki=3.2971E+6;
%3Modules
%Cmecc.Kp=9.5509E+5;
%Cmecc.Ki=4.9457E+6
```

```
%Constants for mf=678
%Ccurr.Kp=0.9291;
%Ccurr.Ki=96.5939;
%1Module
%Cmecc.Kp=3.1911E+5;
%Cmecc.Ki=1.8491E+6;
%2Modules
%Cmecc.Kp=6.3821E+5;
%Cmecc.Ki=3.6982E+6;
%3Modules
%Cmecc.Kp=9.5732E+5;
%Cmecc.Ki=5.5474E+6

%low cutoff frequency 20 rad/s and mf=15
%Ccurr.Kp=0.0537;
%Ccurr.Ki=0.8131;
%1Module
%Cmecc.Kp=9.2116E+6;
%Cmecc.Ki=1.5239E+6;
```

Appendix A-5

```
%Validating equation 4-4 developed to the current ripple of the dc side
%current
clc
R = 14.3E-3;
L = 3.276E-3;
f=14.73; %rated frequency [Hz]
w=2*pi*f;
mf=15;
Vd=1600;
E=495;
psiPM=(sqrt(3)*E)/w;
Pn=1e+6;
p=104;
Trated=(Pn*p)/(w*2);
Iq=(Trated*2)/(psiPM*p);
I1_peak=sqrt(2)*(Iq/sqrt(3));
I1=Iq/sqrt(3);
X=2*pi*f*L;
delta=atan((X*I1/(E-R*I1)));
Delta_deg=delta*180/pi;
V1=(E-R*I1)/(cos(delta));
V1_peak=V1*sqrt(2);
M=2*V1_peak/Vd;

%Voltage Amplitudes
V_mf=Vd*besselj(0,M*(pi/2))*(2/pi);
V_mf2=Vd*besselj(2,M*(pi/2))*(-2/pi);
V_mf_2=Vd*besselj(-2,M*(pi/2))*(-2/pi);
V_2mf1=Vd*besselj(1,2*M*(pi/2))*(-1/pi);
V_2mf_1=Vd*besselj(-1,2*M*(pi/2))*(1/pi);
V_2mf3=Vd*besselj(3,2*M*(pi/2))*(1/pi);
V_2mf_3=Vd*besselj(-3,2*M*(pi/2))*(-1/pi);

%Impedences
Z_1=sqrt((R^2)+((w*L)^2));
Z_mf=sqrt((R^2)+((mf)*w*L)^2);
Z_mf2=sqrt((R^2)+((mf+2)*w*L)^2);
Z_mf_2=sqrt((R^2)+((mf-2)*w*L)^2);
Z_2mf1=sqrt((R^2)+((2*mf+1)*w*L)^2);
Z_2mf_1=sqrt((R^2)+((2*mf-1)*w*L)^2);
Z_2mf3=sqrt((R^2)+((2*mf+3)*w*L)^2);
Z_2mf_3=sqrt((R^2)+((2*mf-3)*w*L)^2);

%Currents
I_mf=V_mf/Z_mf;
I_mf2=V_mf2/Z_mf2;
I_mf_2=V_mf_2/Z_mf_2;
I_2mf1=V_2mf1/Z_2mf1;
I_2mf_1=V_2mf_1/Z_2mf_1;
I_2mf3=V_2mf3/Z_2mf3;
I_2mf_3=V_2mf_3/Z_2mf_3;
```

```
Theta_mf=atan(((mf)*w*L)/R);
Theta_mf2=atan(((mf+2)*w*L)/R);
Theta_mf_2=atan(((mf-2)*w*L)/R);
Theta_2mf1=atan(((2*mf+1)*w*L)/R);
Theta_2mf_1=atan(((2*mf-1)*w*L)/R);
Theta_2mf3=atan(((2*mf+3)*w*L)/R);
Theta_2mf_3=atan(((2*mf-3)*w*L)/R);

phi=(180-Delta_deg)*pi/180;

%DC component of the dc side current
Idc=(3/Vd)*((V1*I1*cos(phi))+(V_mf_2*I_mf_2*cos(Theta_mf_2))+(V_mf2*I_mf2*cos
(Theta_mf2))+(V_2mf_1*I_2mf_1*cos(Theta_2mf_1))+(V_2mf_1*I_2mf_1*cos(Theta_2m
f_1)));

%Ripple component
t = (0:1999)/2000;
psi=0;
f1=(mf-3)*f;
Ir_mf_3=(3/2)*(1/Vd)*((V1*sqrt(2)*I_mf_2*cos((2*pi*f1*t)+psi-
Theta_mf_2))+(V_mf_2*I1*sqrt(2)*cos((2*pi*f1*t)+psi+phi))+(V_2mf_1*I_mf2*cos(
(2*pi*f1*t)+psi-
Theta_2mf_1))+(V_mf2*I_2mf_1*cos((2*pi*f1*t)+psi+Theta_mf2)))*(1/Idc);
f2=(mf+3)*f;
Ir_mf3=(3/2)*(1/Vd)*((V1*sqrt(2)*I_mf2*cos((2*pi*f2*t)+psi-
Theta_mf2))+(V_mf_2*I_2mf1*cos((2*pi*f2*t)+psi-
Theta_2mf1))+(V_mf2*I1*sqrt(2)*cos((2*pi*f2*t)+psi-
phi))+(V_2mf1*I_mf_2*cos((2*pi*f2*t)+psi+Theta_mf_2)))*(1/Idc);
f3=(3*mf-3)*f;
Ir_3mf_3=(3/2)*(1/Vd)*((V_mf_2*I_2mf_1*cos((2*pi*f3*t)+3*psi-
Theta_2mf_1))+(V_2mf_1*I_mf_2*cos((2*pi*f3*t)+3*psi-Theta_mf_2)))*(1/Idc);
f4=(3*mf+3)*f;
Ir_3mf3=(3/2)*(1/Vd)*((V_mf2*I_2mf1*cos((2*pi*f4*t)+3*psi-
Theta_2mf1))+(V_2mf1*I_mf2*cos((2*pi*f4*t)+3*psi-Theta_mf2)))*(1/Idc);
f5=(2*mf)*f;
Ir_2mf=(3/2)*(1/Vd)*((V1*sqrt(2)*I_2mf_1*cos((2*pi*f5*t)+2*psi-
Theta_2mf_1))+(V_2mf_1*sqrt(2)*I1*cos((2*pi*f5*t)+2*psi-
phi))+(V1*sqrt(2)*I_2mf1*cos((2*pi*f5*t)+2*psi-
Theta_2mf1))+(V_2mf1*sqrt(2)*I1*cos((2*pi*f5*t)+2*psi+phi))+(V_mf_2*I_mf2*cos
((2*pi*f5*t)+2*psi-Theta_mf2))+(V_mf2*I_mf_2*cos((2*pi*f5*t)+2*psi-
Theta_mf_2)))*(1/Idc);
f6=(4*mf)*f;
Ir_4mf=(3/2)*(1/Vd)*((V_2mf_1*I_2mf1*cos((2*pi*f6*t)+4*psi-
Theta_2mf1))+(V_2mf1*I_2mf_1*cos((2*pi*f6*t)+4*psi-Theta_2mf_1)))*(1/Idc);

Ir=Ir_mf_3+Ir_mf3+Ir_3mf_3+Ir_3mf3+Ir_2mf+Ir_4mf;

y = fft(Ir)   ;
m = abs(y)  ;
fs = 0:999;% Half the sampling time
m = m(1:1000);% must be the same length of fs
stem(fs/f,m/10,'filled')% Normalizing fs over the switching frequency and
magnitude over percent.
ylabel 'Ripple magnitude % of Idc'
xlabel 'Harmonic order'
grid on
```


POLITECNICO
MILANO

Single Module PMSG:

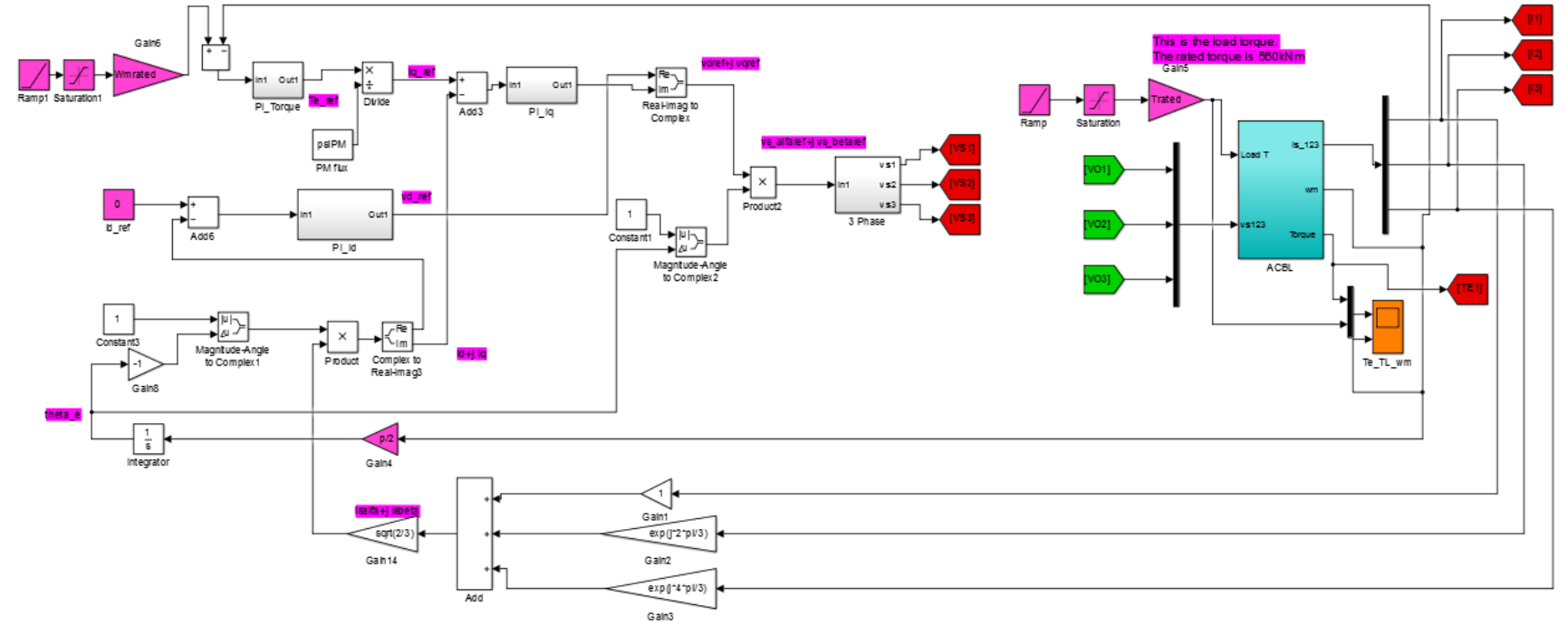

Overall Control Scheme of 1 module PMSG

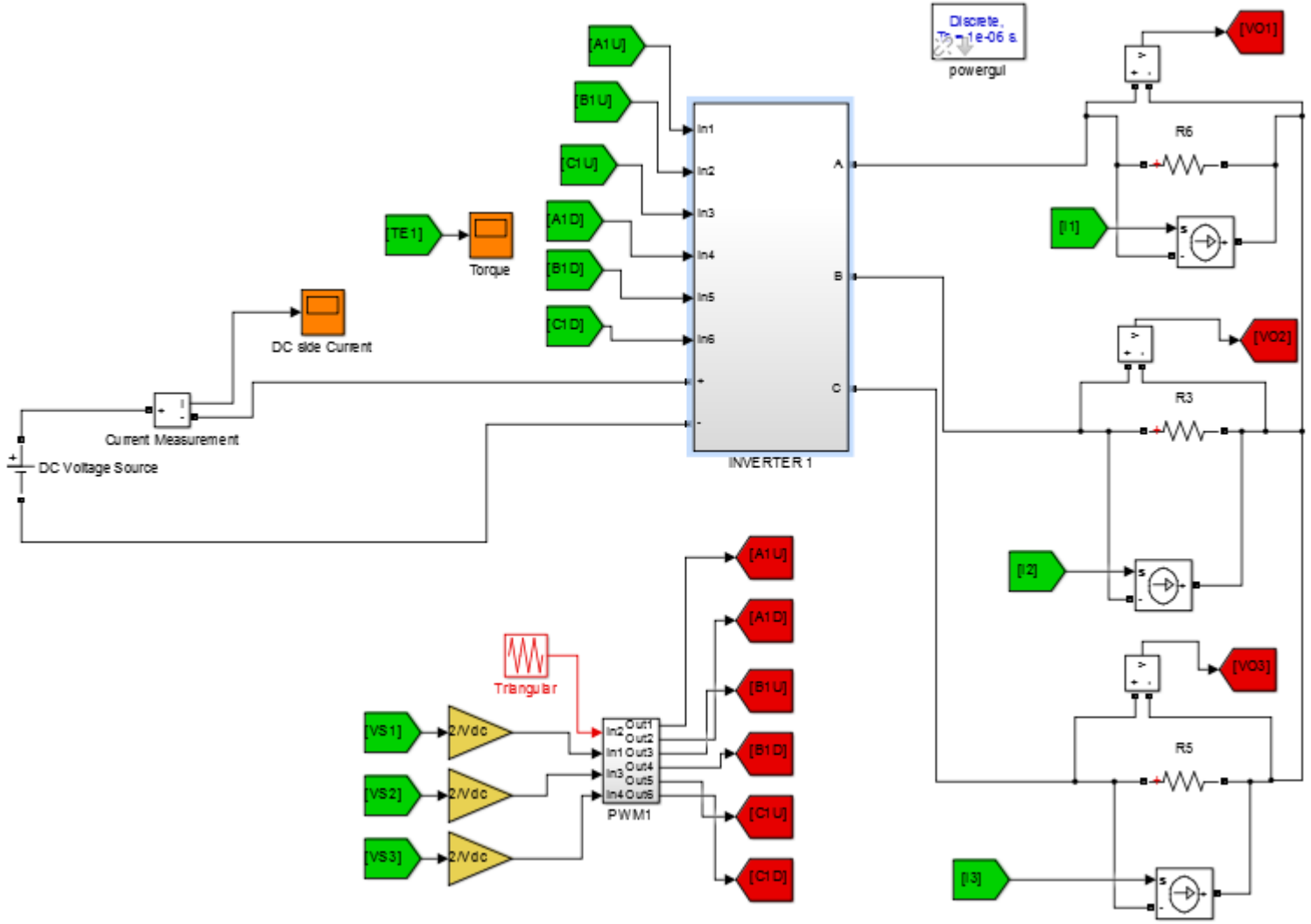

Inverter model for single module PMSG machine

Two Modules PMSG:

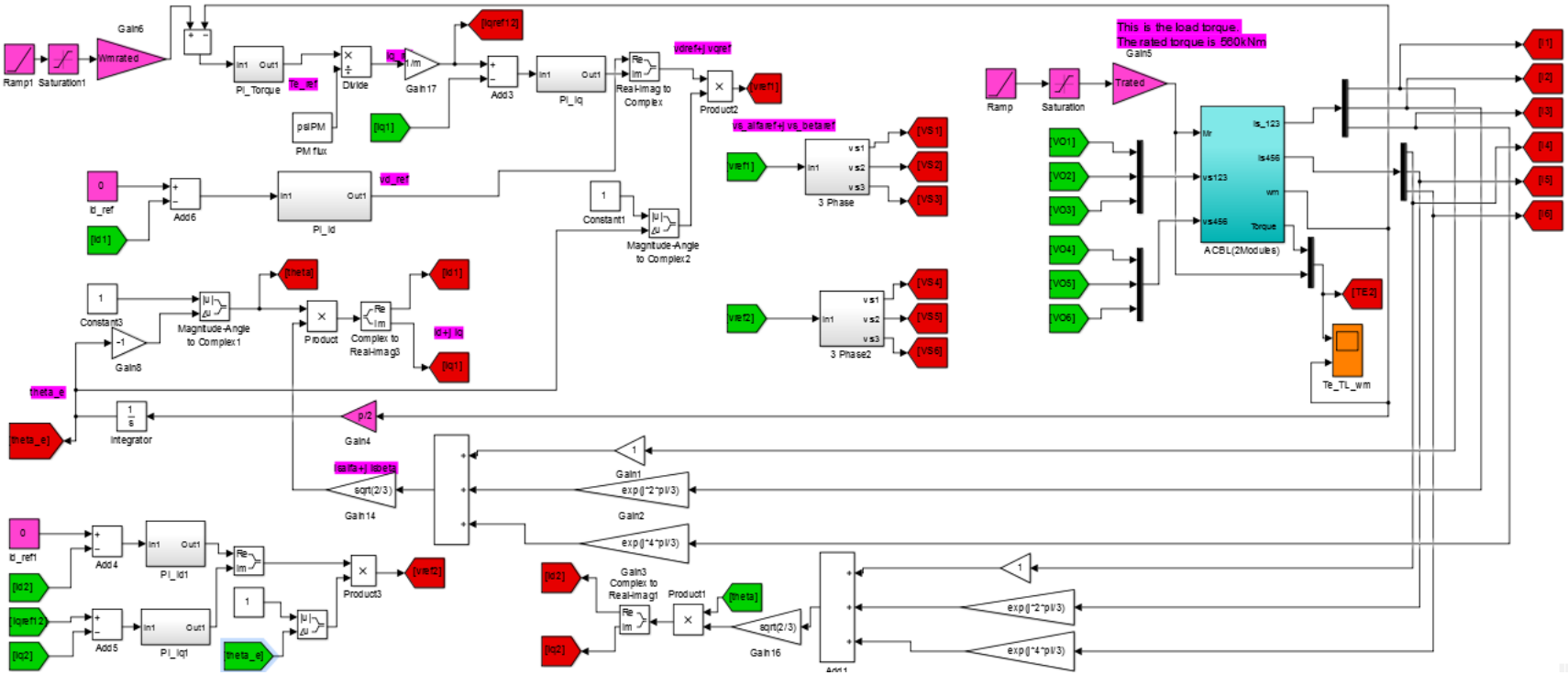

Overall Control Scheme of 2 modules PMSG


POLITECNICO
MILANO